Bolt Load Retention Response and Creep of AS41 Mg-Alloy

Vom Promotionsausschuss der
Technischen Universität Hamburg-Harburg
zur Erlangung des akademischen Grades
Doktor-Ingenieur (Dr.-Ing)
genehmigte Dissertation

von
Okechukwu Anopuo

aus
Lagos-Nigeria

2010

Erster Gutachter: Prof. Dr. Karl Ulrich Kainer

Zweiter Gutachter: Prof. Dr. Karl Schulte

Tag der mündlichen Prüfung

12.07.2010

Table of contents

1 Introduction

It is generally believed that threaded fasteners have been in use for at least half of a millennium [1]. Their simplicity and ease of application makes them preferentially used when generation and maintenance of a specific clamping force is required in a joint. In situation where joints or part are needed to be regularly disassemble and reassemble for routine check, simple bolts and nuts are readily preferred. This is of course because of the ease of loosening and tightening of the joint without causing any damage on the parts or joint. However, the complexity of a simple nut and bolt is often underestimated.

Joints respond to external stimuli (forces, temperatures and environmental conditions) in which they are subjected to. When fastener clamp loads are exceedingly high or drastically reduced under service conditions in an engineering design, the result is failure of the engineering parts or possibly the bolts. In most cases the failure are catastrophic in nature. The adaptation of various names in trying to explain this phenomenon in the open literature makes it a little difficult in expressly dealing with the subject: It is often referred to as compressive stress retention characteristics [2], stress relaxation in bolted joints [3], bolt load compressive stress retention [4] or bolt load retention behaviour [5, 6]. In this work, the term bolt load retention is used. As at present, there is no internationally adopted standard for bolt load retention (BLR) measurement for materials. This generally makes comparison of BLR data from various research groups increasingly difficult. This is largely due to the adoption of variegated BLR testing techniques and partly because of not fully understanding the factors influencing the same. It becomes more challenging when dealing with light materials such as magnesium alloys due to its crystal structure and deformation mechanisms especially at elevated temperature. At high temperature (above 200 °C), there is activation of more slip systems on magnesium alloys and this influences the deformation behaviour of these alloys.

The possibilities of application of magnesium alloys in certain demanding areas in automobiles such as power train components, makes this engineering parameter an issue of utmost importance. This is because of the prevalence of bolted joints present in power train parts. Several prediction have been made on the increase of magnesium alloys in automobile application in the future [7, 8].

Power train component is expected to play important role because of its possible compound weight reduction in automobile when Mg-alloys are used. The aim of this weight saving is to reduce significantly the CO_2 emission in our environment.

The tendency to reach this desired goal calls for concentrated effort in terms of research and development of new magnesium alloys, improvement in production processes and modification of design processes. In the bid to develop new high performance magnesium alloys that will withstand the challenges of automobile application, effort is needed to develop along side suitable testing techniques that can be used to adequately characterise these magnesium alloys. There is need therefore to understand the deformation processes observable at elevated temperature BLR of Mg-alloys. Important also is development of standard experimental set-up and model that can accurately predict the behaviour of magnesium alloys at bolted joints.

2 State of the art

2.1 Creep of metallic materials

Creep is a slow but progressive permanent deformation over a period of time that is associated with materials under constant stress at elevated temperature. It is usually carried out at constant load or stress and at constant temperature condition. Creep strain (ε) is a function of stress (σ), temperature (T) and time (t) expressed as $\varepsilon = f(\sigma, T, t)$. Creep deformation is normally represented using a plot of strain (ε) against time or creep rate ($\dot{\varepsilon}$) with respect to strain (ε). Figure 1(a, b) show a typical tensile creep curve and Figure 1(c, d) represent a typical compressive creep curve.

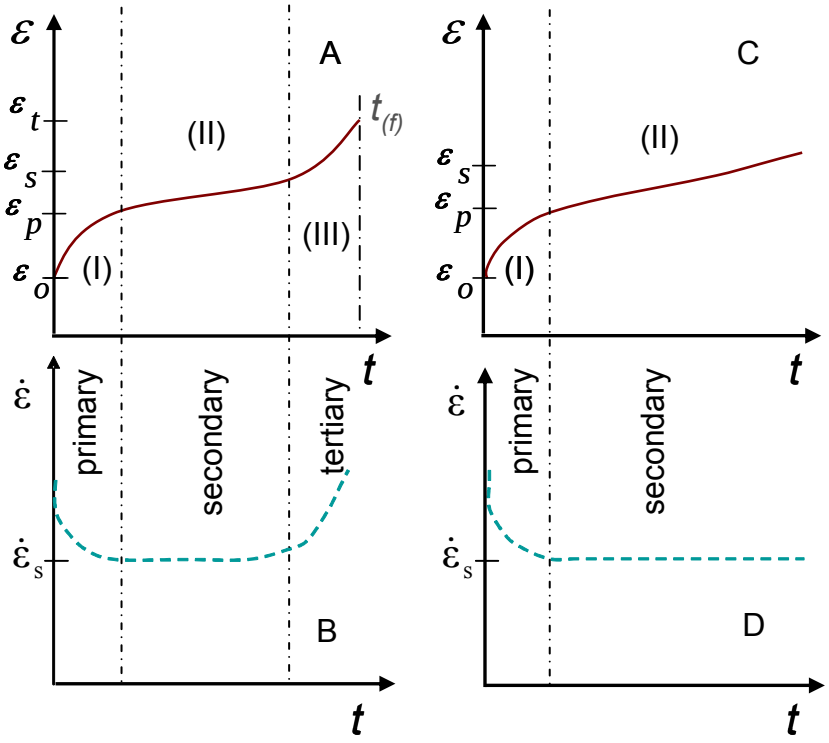

Figure 1: (a). Typical tensile creep curve and (b) its creep rate against strain. (c). Typical compressive creep curve and (d) its creep rate with respect to strain

From tensile creep curve in Figure 1(a, b), three conspicuous sections which characterized the creep curve of metallic materials above $0.4T_m$ are observed. This comprises the stage (I) often referred to as the transient or primary creep, stages (II) and (III) also known as steady state creep and tertiary creep respectively. As can be seen from Figure 1(c, d), the compressive creep curve

show only the primary and secondary creep stages. This is because the tertiary stage is not usually reached under compressive creep test. The total creep strain $\varepsilon_{(t)}$ under tensile mode is then given as equation 1.

$$\varepsilon_{(t)} = \varepsilon_o + \varepsilon_p + \varepsilon_s + \varepsilon_t \qquad \text{Equation 1}$$

ε_o, ε_p, ε_s and ε_t are the instantaneous strain, primary strain, secondary strain and tertiary strain respectively. For compressive creep, the total creep strain is the sum of instantaneous, primary and secondary strain. This is shown in equation 2. From Figure 1, $\dot{\varepsilon}_S$ and t_f are secondary creep rate and time to fracture respectively.

$$\varepsilon_{(t)} = \varepsilon_o + \varepsilon_p + \varepsilon_s \qquad \text{Equation 2}$$

Early work on transient creep was carried out by Andrade [9] with his postulation of equation 3. Cottrell modified Andrade's work to include the instantaneous deformation ε_o and the steady state creep rate $\dot{\varepsilon}_S$ [10]. The transient creep equation by Cottrell is given as equation 4. β in equation 3 and 4 are constants while $\varepsilon_{(T)}$ is transient creep.

$$\varepsilon_{(T)} = \beta t^{1/3} \qquad \text{Equation 3}$$

$$\varepsilon_{(T)} = \varepsilon_o + \beta t^{1/3} + \dot{\varepsilon}_S t \qquad \text{Equation 4}$$

$$\varepsilon_{(T)} = \varepsilon_o + \varepsilon_t \left[1 - \exp(-mt)\right] + \dot{\varepsilon}_S t \qquad \text{Equation 5}$$

Garofalo adopted an approach that includes parameters that accounts for physical interpretation and this leads to equation 5. In Garofalo`s work [11], ε_t represents the length of the primary regime while the reciprocal of the value m is the time constant of the transient creep. The exponential function in equation 5 shows that transient creep is an exhaustion process. The deforming material past ε_o experiences resistance in creep as deformation becomes increasingly difficult as a result of strain hardening. This causes change in strain with respect to time and creep deformation approaches a standstill (Figure 1). The end of transient creep ushers in the secondary or steady state creep stage which is usually the creep stage with the longest duration. It must be mentioned here that the deformation in the transient regime of most metals are determined by similar creep law as deformation within the secondary regime.

The secondary or steady state creep is usually reduced to two variables: Stress and temperature dependence of the steady state creep. The stress dependence of the steady state creep is usually expressed using Norton's law [12]. This is shown as equation 6. The temperature dependence of the steady state creep obeys an Arrhenius relationship expressed as equation 7. The combination of stress and temperature dependence of the steady state creep gives equation 8.

$$\dot{\varepsilon}_s \propto \sigma^n \qquad \text{Equation 6}$$

$$\dot{\varepsilon}_S \propto \exp\left(\frac{-Q_C}{RT}\right) \qquad \text{Equation 7}$$

$$\dot{\varepsilon}_S = A\sigma^n \exp\left(\frac{-Q_C}{RT}\right) \qquad \text{Equation 8}$$

From equation 8, stress exponent *n* and activation energy of creep *(Q_c)* can be evaluated. *A* in equation 8 is a material dependent constant, *(R)* is the gas constant (8.31 $Jmol^{-1}K^{-1}$), *(T)* the temperature and $\dot{\varepsilon}_s$ the secondary creep rate. σ is the applied stress. For very high stresses, the hyperbolic sine equation 9 is used [11, 13]. β in equation 9 is a stress dependent constant.

$$\dot{\varepsilon}_S \propto \sinh(\beta\sigma)^n \qquad \text{Equation 9}$$

The n values for metallic materials fall mostly between 3 and 5. For n values equal to 1, equation 9 describes diffusion creep and for n=2 grain boundary sliding. It is generally believed that values of n>4 has no physical explanation but represents empirical information [14].

The magnitude of the activation energy of creep gives insight as to the nature of the active mechanism controlling the creep process of such metallic material within a set of established stress and temperature ranges. For pure metals at high temperature, the application of this relationship has been found to yield an activation energy of creep (Q_c) that is close to the activation energy for lattice self diffusion (Q_{sd}). Sherby and Burke investigated the activation energy of creep and compared it to that of self diffusion for pure metals [12]. Figure 2 shows a plot of the relationship between the activation energy of creep (Q_c) and the activation energy of self diffusion (Q_{sd}) for some pure metallic materials at elevated temperature.

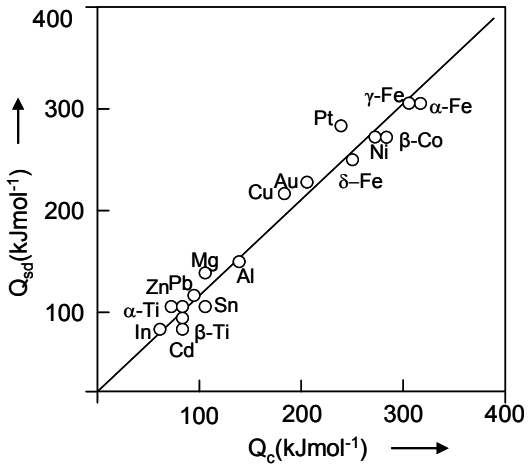

Figure 2: Activation energy of creep and that of self diffusion for pure metals [12]

The end of the steady state creep marks the initiation of the tertiary creep in metallic materials. This starts by appearance of micro cracks and micro pores. Monkman and Grant [15], came up with an empirical relationship that describes the fracture strain (ε_f) and the time to fracture (t_f). This is expressed as equation 10. The parameter (*C*) is a temperature and stress independent constant. Equation 10 is used in the prediction of sample lifetime.

$$t_f = \frac{C}{\dot{\varepsilon}_s} \qquad \text{Equation 10}$$

2.2 Creep mechanism in metallic materials

Creep process in metallic materials comprises of different mechanisms operating at various stages of creep deformation depending on the applied stress, operating temperature and nature of the material among other things. The nature of the dislocation structure present during creep deformation plays active role in determining the overall creep process of the alloy under investigation. Usually, three major mechanisms are associated with creep deformation in metallic materials. These processes in reality overlap each other but always exhibiting one dominant mechanism while others appear recessive in nature during creep deformation. These mechanisms include: (a) Diffusion flow, (b) Dislocation creep, and (c) Grain boundary sliding. It is however important to mention that creep processes are independent of each other and

as such the total creep deformation of the material is the sum of all the processes. Hence the overall steady state creep in metallic materials is given by equation 11. In equation 11, ε_T is total creep deformation, ε_{diff} represents diffusion creep while ε_{disl} and ε_{gb} are the dislocation creep and grain boundary sliding creep respectively.

$$\varepsilon_T = \varepsilon_{diff.} + \varepsilon_{disl.} + \varepsilon_{gb} \qquad \text{Equation 11}$$

2.2.1 Diffusion controlled process

Early works on diffusion controlled processes were carried out by Nabarro, Herring and Coble [16-18]. Nabarro and Herring in their work represented diffusional creep as occurring only through crystal lattice. The relationship between the steady state creep rate and the flux of vacancy (J_v) diffusing from the source regions to the sink regions is given by equation 12. d is the average grain diameter.

$$\dot{\varepsilon}_s = \frac{J_v}{d} \qquad \text{Equation 12}$$

$$J_v = 2Dv\frac{C_o}{d'}\frac{\Omega\sigma}{kT} \qquad \text{Equation 13}$$

$$D_{sd} = D_v.C_o.\Omega \qquad \text{Equation 14}$$

In equation 13, (D_v) is the vacancy diffusion coefficient, (d') is the average distance a vacancy moves from area of high concentration to area of lower concentration. C_o is the equilibrium concentration of vacancies in a crystal lattice, Ω is the volume of a vacancy produced at the source region. σ is the applied stress while (k,T) are Boltzmann's constant and temperature respectively. Substitution of equation 13 and 14 into equation 12 yields equation 15 which is consistent with the power law relationship of equation 8. $\dot{\varepsilon}_s$ is the secondary creep rate, A_{NH} is constant and D_{sd} represents the diffusion coefficient of lattice self diffusion.

$$\dot{\varepsilon}_s = A_{NH}\frac{D_{sd}}{d^2}\frac{\Omega\sigma}{kT} \qquad \text{Equation 15}$$

Coble [18] proposed a slightly different approach to Nabarro and Herring by saying that vacancy transport can be effected not only within the crystal lattices

but also along the grain boundaries. Coble's work is represented using equation 16.

$$\dot{\varepsilon}_s = A_C \frac{D_{gb}}{d^2}\frac{\delta}{d}\frac{\Omega\sigma}{kT} = A_C \frac{D_{gb}}{d^3}\frac{\delta\Omega\sigma}{kT} \qquad \text{Equation 16}$$

A_C and D_{gb} in equation 16 are constant and diffusion coefficient due to grain boundary respectively. The parameter (δ/d) represents the area of the grain boundary region close to the grain with average grain diameter (d). In the Coble equation 16, as also in Nabarro-Herring equation, the secondary creep rate ($\dot{\varepsilon}_s$) varies linearly with stress (σ). This means that (n~1) with respect to the power law equation 8, it then follows that the activation energy for creep in this case is that for grain boundary self diffusion with the result that (Q_c is less than Q_{sd}). In general when experimental creep are carried out on metallic materials at temperature around ($0.4T_m$) and low stress condition, if the application of power law equation yields an n value equal to unity and activation energy less than that of self diffusion. It is believed that the metallic material is obeying Coble creep.

2.2.2 Dislocation controlled process

Several creep models have been proposed which tries to elucidate microscopic creep in terms of dislocation control processes. Pioneer works in this area were those of Weertman [19], Barrett and Nix [20]. Other works include those of Nabarro and Harper-Dorn [21, 22]. Weertman's model was based on the glide and climb movement of dislocations. The fundamental assumption for his model was that, dislocation movement involves slow climbing and fast gliding activities during creep process. Weertman was of the opinion that dislocations overcome obstructions basically by climbing of edge dislocations and that deformation are consequence of slip. He sees climbing as a non-conservative movement of dislocation during which vacancies are emitted. The dynamics of deformation are controlled by the rate of climbing. Weertman's steady state creep rate equation is given by equation 17.

$$\dot{\varepsilon}_s = A_{wtm}\frac{DGb}{kT}\left(\frac{\sigma}{G}\right)^4 \qquad \text{Equation 17}$$

Equation 17 makes reasonable prediction for low stress conditions. The Weertman's steady state creep rate varies proportionally to the 4th power of stress as is often observed experimentally in metallic materials. It is also proportional to the diffusion coefficient *D* as expected. A_{wtm}, b and G are constant, burgers vector and shear modulus respectively.

The dislocation creep model of Barrett and Nix sees the movement of dislocation as constantly opposed by frictional forces. The dislocation witnesses a steady and uniform resistance as it cuts across the material and overcomes the frictional forces by thermal activation process. Barrett and Nix in their "jogged screw dislocation model" assumed that dislocations are a consequence of gliding of screw dislocations. In their work, the screw dislocations are made up of jogs which serve as positive and negative points for emitting and absorbing vacancies. The steady state creep equation according to Barrett and Nix were derived from the basic dislocation equation. This is expressed as equation 18.

$$\dot{\varepsilon}_s = A_{BN}\frac{D}{b^2}\left(\frac{\sigma}{G}\right)^2 \sinh\frac{b^2\lambda\sigma}{kT} \qquad \text{Equation 18}$$

In equation 18, A_{BN}, b, λ and G are the constant, burgers vector, wave length and shear modulus respectively. The work of Barrett and Nix made reasonable prediction of the steady state creep rate ($\dot{\varepsilon}_s$) with respect to small and large stress values. It is observed from equation 18 that ($\dot{\varepsilon}_s$) is directly proportional to the 3rd power of stress for small stress level and for larger stresses, it varies proportionally to the exponential stress. This infers that the transition from power law at lower stresses to exponential law at higher stresses is reasonably predicted.

2.2.3 Grain boundary sliding controlled process

Grain boundary sliding is one of the deformation processes that is often associated with creep of polycrystalline materials at elevated temperature. This is believed to occur as a result of the concurrent movement of the neighbouring grains along their common boundary. Grain boundary sliding is classified as "Pure" when they occur at the boundary surfaces and "Zone" when observed at zones adjacent to the boundary surfaces. Pure grain boundary sliding (GBS) is necessitated as a result of the movement of dislocation through the grain

boundary and this can be accommodated by either diffusion creep or climb and glide of dislocation creep. GBS maybe accounting for between 10 to 60% of the total creep strain in polycrystalline materials. The type of material and the combination of stress and temperature influences GBS. GBS are favoured in most cases by increasing temperature and stress with small grain sizes. For most polycrystalline metals above 0.6 homologous temperatures, the shear strength was observed to be low. It is believe that this could be as a result of loose atomic arrangement at the grain boundary region

2.3 Creep of magnesium and its alloys

2.3.1 Deformation behaviour of hexagonal close packed crystals

As a hexagonal closed packed metal, magnesium has restricted slip systems at room temperature. This ordinarily means that at low temperature and high loading rates, magnesium is susceptible to mechanical twinning. Figure 3 shows principle directions while Figure 4 show major planes of magnesium crystallite.

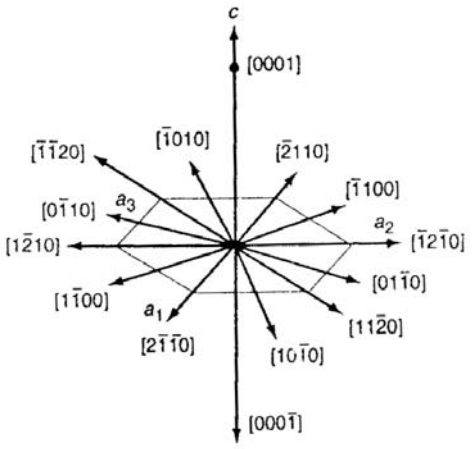

Figure 3: Principal direction of magnesium crystallite [31]

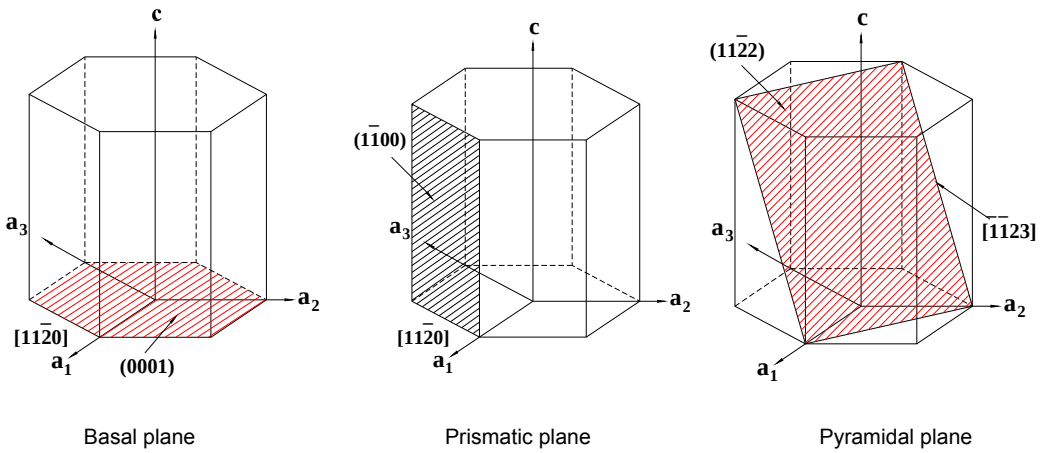

Figure 4: Major planes of magnesium crystallite [23]

Table 1: Slip systems of hexagonal metals [24]

Slip system	Burgers vector	Slip direction	Slip plane		No of slip systems	
					Total	Independent
1	a	$\langle 11\bar{2}0 \rangle$	Basal	$\{0001\}$	3	2
2	a	$\langle 11\bar{2}0 \rangle$	Prismatic	$\{10\bar{1}0\}$	3	2
3	a	$\langle 11\bar{2}0 \rangle$	Pyramidal	$\{10\bar{1}1\}$	6	4
4	c+a	$\langle 11\bar{2}3 \rangle$	Pyramidal	$\{11\bar{2}2\}$	6	5
5	c	$\langle 0001 \rangle$	Prismatic	$\{10\bar{1}0\}$	3	2
6	c	$\langle 0001 \rangle$	Prismatic	$\{11\bar{2}0\}$	3	2

Table 1 shows the slip systems in hexagonal close packed metals. The dominant slip systems in magnesium alloys are the basal $\{0001\}\langle 11\bar{2}0 \rangle$, prismatic $\{10\bar{1}0\}\langle 11\bar{2}0 \rangle$ and pyramidal $\{10\bar{1}1\}\langle 11\bar{2}0 \rangle$ systems including pyramidal twinning. At room temperature, plastic deformation occurs predominantly by basal slip and pyramidal twinning [25, 26]. The critical resolved shear stress (crss) for slip on $\{0001\}$ basal planes and the prismatic $\{10\bar{1}0\}$ or pyramidal $\{10\bar{1}1\}$ planes differ considerably. Previous works [27, 28] show that the (crss) of either prismatic or pyramidal slip at 25 °C is several orders of magnitude higher than that of basal slip. This means that the probability of basal slip occurring even at grains unfavourably oriented for basal slip is high at room temperature.

At elevated temperature (above 200 °C), other slip systems are activated. The pyramidal $\{10\bar{1}1\}\langle 11\bar{2}0 \rangle$ becomes active. The $\{10\bar{1}1\}$ planes are the next most closely packed planes after the basal plane. The work of Reed-Hill and Roberts [29] on single crystal up to 286 °C show prismatic and pyramidal slip together with basal slip. Bakarian and Matthewson [27] observed also pyramidal slip between temperatures of 225 °C and 330 °C together with the basal slip on single crystal. For Mg-alloys in compression, twinning readily occurs when the applied stress is parallel to the basal plane. In contrast, under tensile load, twinning occurs when the stress is parallel to the c-axis. Small shear is sufficient to cause the necessary atomic movement to produce twin in magnesium [30].

Figure 5 shows $\{10\bar{1}2\}$ twinning in magnesium which is typical at room temperature [24]. Secondary twinning has been observed across the $\{30\bar{3}4\}$ planes [29]. At elevated temperature, twinning has also been found to occur across the $\{10\bar{1}3\}$ planes. Other reported twinning planes in magnesium include $\{10\bar{1}1\}$, $\{11\bar{2}4\}$, $\{11\bar{2}1\}$ and $\{10\bar{1}5\}$ [28, 29, 31,]. The possibility of retwinning and detwinning has been reported in Mg-alloys [28]. From the reviewed work, major deformation mode observed in Mg and it alloys are basal slip $\{0001\}\langle 11\bar{2}0\rangle$ at room temperature condition. Prismatic $\{10\bar{1}0\}$ and pyramidal $\{10\bar{1}1\}$ both with $\langle 11\bar{2}0\rangle$ direction are predominant at elevated temperature in combination with the basal slip.

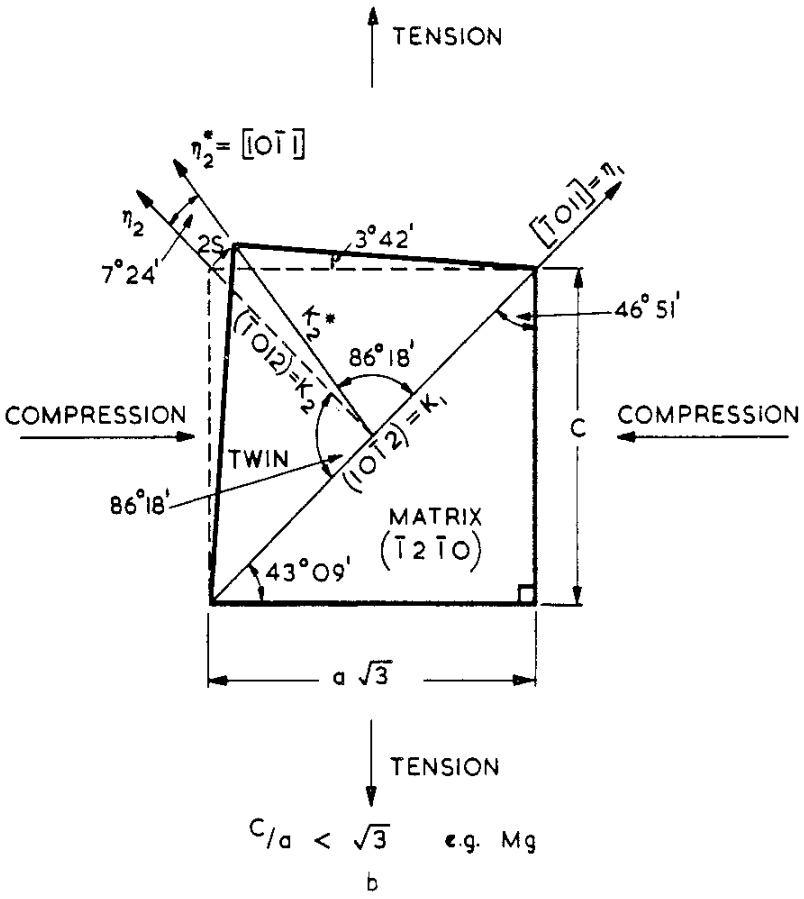

Figure 5: Twinning in magnesium {10-12} [24]

2.3.2 Creep of pure Mg

Early work in creep deformation of pure magnesium single crystal was carried out by Trozera et al. [32]. Creep experiment was performed between temperatures of -196 °C to 427 °C and the activation energy for basal creep was determined. According to reference [32], the apparent activation energy for creep over the range from -196 °C to -73 °C was found to increase linearly with the absolute temperature according to the relation Q=36 RT (R= Gas constant, T= Absolute temperature). It was concluded that creep within this region is controlled by intersection mechanism. Over the temperature range of between -23 °C and 427 °C, the apparent activation energy for creep increased with temperature according to Q=50 RT. Trozera and co worker attributed this to dislocation mechanism due to jogged screw dislocations.

The studies as documented in reference [33] covered stresses of up to 69 MPa in tensile mode and temperatures of between 93 °C and 316 °C. Roberts [34] in an attempt to correlate primary and steady state creep in polycrystalline magnesium with the deformation mechanisms used a fine-grained extruded magnesium stock. It was observed that at lower temperatures, deformation at grain boundaries play less role in the creep process than deformation within the grains. This becomes different as the temperature increases. Grain boundary deformation process becomes dominant. Reference [34], related the transient creep stage to the deformation within the grains and the steady state creep to the grain boundary deformation.

Chaudhuri et al [35] investigated polycrystalline magnesium of grain diameter 2-3 mm at temperature of 371 °C. It was observed that basal slip was active during the initial loading corresponding to high strain rate. Non-basal slip was found to progressively develop during the creep experiment and accounted for the greater part of the total strain.

From the reviewed work, it was observed that creep at low temperature for magnesium was dominated by basal slip within the grain including formation of sub-grain structures and twinning. At higher temperature, diffusion dependent grain boundary deformation becomes the dominant creep mechanism. At low temperature approaching that of liquid nitrogen, the prismatic $\{10\bar{1}0\}$ planes are important. The prismatic $\{10\bar{1}0\}$ and pyramidal $\{10\bar{1}1\}$ planes are involved in elevated temperature deformation. The controlling creep process in magnesium

at any giving condition will depend on the stress, temperature, strain rate and creep time.

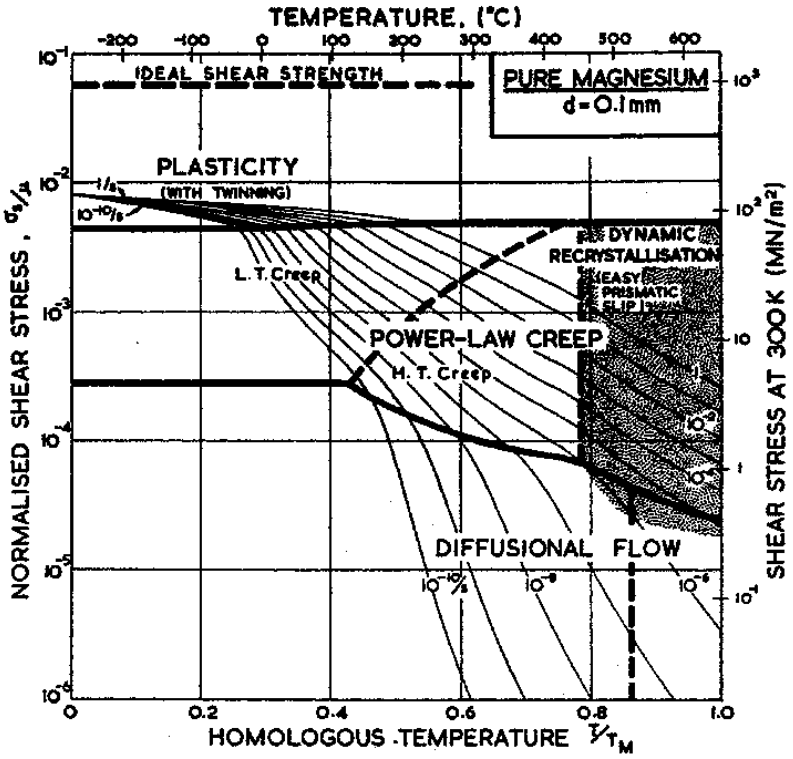

Figure 6: Deformation map of pure Mg with grain size of 0.1 mm [36]

Figure 6 shows the deformation map of polycrystalline magnesium with grain size of 0.1 mm. Frost and Ashby [36] summarized the deformation mechanisms with respect to the normalized shear stress and homologous temperature of polycrystalline magnesium. It covers the range of plasticity and twinning at lower temperature and higher stresses (lower temperature creep). The region of high temperature creep and diffusional flow is seen at between moderate to low stress regions. Dynamic recrystallization at high temperature and stresses with prismatic slip is also present in the deformation map.

2.3.3 Creep of Mg-alloys

The presence of alloying elements in Mg-alloys influences the overall creep deformation behaviour of the alloys. The solidification process during casting, the volume fraction and distribution of the second phases depending on the casting technique all play roles in the final dominant creep mechanism within specified stress and temperature ranges. For most die cast Mg-alloys, because of the high solidification rates, the grain sizes are small and the matrix are supersaturated with alloying elements. The possibilities of formation of stable or metastable intermetalic phases during creep deformation, dislocation reaction, stacking fault energies and so on could complicate creep behaviour of Mg-alloys.

Lövold [37] studied the transient creep of die cast AS21, AS41 and AZ81 in tensile mode. Stress levels of between 34 to 67 MPa and temperatures of 100 °C to 175 °C was investigated. It was found that the creep properties of silicon containing Mg-alloys are far better than that of AZ81 especially at 150 °C. The activation energy for creep was found to be approximately 37 kJ/mol, this is independent of the applied stress. Stress exponent n was found to be 2.6 for all the investigated alloys. Lövold concluded that the rate controlling creep mechanism is the formation of jogs in undissociated dislocations. The high value of the constant A for the AZ81 was believed to be as a result of high dislocation density around the β-$Mg_{17}Al_{12}$ precipitate which reveals itself as a result of the difference in Young's moduli.

Die cast AZ91 was observed to creep at room temperature through a dislocation climb mechanism [38]. It has been suggested that strain induced precipitation could be responsible for this room temperature behaviour. Gjestland et al. [39] investigated the influence of grain size on the creep of AZ91 alloy. AZ91 with grain sizes of 1.5 µm and 11.6 µm were used for the creep experiment. It was found that the alloy with smaller grain size has creep rate of 2 orders of magnitude higher than that of larger grain. The enhanced creep rate in the smaller grains is believed to be as a result of grain boundary sliding due to more grain boundaries available in the solidified alloy. When Ca was added to the AZ91, the creep property of the Ca modified alloy improved considerably. This improvement in the creep property of the modified alloy was

attributed to the formation of Al_2Ca intermetallic phase which is a high temperature stable phase.

Dargusch and co-workers [40] studied the creep behaviour of die cast AZ91, AE42 and AS21. It was found that the creep strengths of die cast AS21 and AE42 are superior to that of die cast AZ91. This is as a result of the lower volume fraction of supersaturated α-Mg in these alloys and the thermal stable intermetallics that are additionally present at the grain boundary regions. The stress exponents as observed by [40] are ~2 at lower stress regions and ~5 at high stress regions. The apparent activation energy for creep was between 30 – 40 kJ/mol when n~2. Higher creep deformation at grain boundaries was observed than within dendrite regions. This they concluded must have been caused by the dynamic precipitation of the inter-dendritic $Mg_{17}Al_{12}$ phase during creep deformation of Mg-Al alloys. Han et al. reported a similar observation as Dargusch but however suggested that the inhomogeneous deformation was as a result of the enhanced deformation in the matrix phase and the eutectic adjacent to the grain/dendritic regions [41].

The presence of Al_4(RE) intermetallics for AE42 reinforces the grain boundary region of these alloys and provide opposition to creep deformation. More work is needed to clarify the exact mechanism for the creep deformation behaviour of AS41 alloy. It is widely believed that the presence of Mg_2Si phase was responsible for the improved creep response on AS21 [40, 42] by pinning the grain boundary regions. This Mg_2Si phase with a density of (1.9 g/cm^3) and melting point of (1085 °C) is relatively stable at elevated temperature. A different creep mechanism was suggested to be responsible for creep of AS41 below 150 °C, although no work has been done to verify this assumption [43]. It is important to mention here that extensive creep investigation in both compressive and tensile mode is necessary to clear this point.

2.4 Stress relaxation compression test

Stress relaxation is simply the time-dependent decrease in stress in a solid material under specified constraints. This is generally carried out under constant temperature applying a force to a specimen with fixed amount of constraint. It could be carried out under different loading conditions: Compression, bending or tension loading. Stress relaxation experiments are necessary for obtaining useful design information on materials for specific conditions. This is also employed in the analysis of the level of stress concentration at cracks, inclusions and etc. Information of the materials stress relaxation behaviour gives insight on things like activation volume and internal stresses [44].

The methods for conducting compressive stress relaxation test are outlined in the ASTM standard E 328 [45]. A handful of research activities have been carried out on stress relaxation of magnesium alloys. In their work [46], Watzinger et al. focused on AZ91, AM60, AE42 and AS21 Mg-alloys produced using high pressure die casting techniques. Stress relaxation samples used in this research work measures 6.2 mm length and cross section of 5 mm with loading direction being parallel to the transverse direction of the original cast plate from where the specimens were machined. The authors of reference [46] carried out their experiment between stresses of 90-250 MPa. Temperatures of 70, 100, 135 and 150 °C were also used in the experiment. Considering the result for AS21 and that of AZ91 presented in reference [46], it show similarities to the work of Aune and Ruden [47]. The AS21 and AZ91 alloys in both experiments exhibited the same kind of behaviour with AS21 showing better stress relaxation properties than AZ91 alloy.

Aune and Ruden in their work, “High temperature properties of magnesium die-casting alloys” [47] investigated among other things the compressive stress relaxation behaviour of rare earth and silicon containing magnesium alloys. It is observed that the choice of rare earth addition as alloying element to aluminum containing magnesium alloy improves the stress relaxation property of these alloys. One sees here that increase in test temperature affects negatively the degree of stress relaxation. That is to say, the higher the temperature, the lesser the amount of stress retained in these die cast magnesium alloys.

At temperature of 150 °C and 50 MPa, AE42 and AS41 show better stress relaxation properties. When the stress was increased to 100 MPa and the

temperature reduced to 100 °C, AE42 and AS21 were a little better than others [47]. On the deformation mechanism that is associated with the stress relaxation of the investigated alloys, the authors of reference [46] suggested that there is no indication to assume that deformation is governed by sliding along grain or phase boundaries. But that the overall macroscopic behaviour is quite normal for metallic solid solution deforming by dislocation glide. Taking into consideration the high cooling rate and seemingly small grain sizes associated with (HPDC) alloys, more investigations is needed to clarify the deformation mechanism that is associated with the stress relaxation behaviour of die cast magnesium alloys.

In another work of Albright and Aune [48], the stress relaxation behaviour of traditional AZ91 was further compared with that of AE based (AE21, AE61, AE91) magnesium alloys. Stresses between 30 MPa to 100 MPa were used as initial stresses while constant temperature ranges covering 100 °C to 200 °C were employed. Inferences from this work show that the higher the initial stresses and temperature, the more the relaxation. The authors of reference [48] also show the influence of sample materials and specimen dimensions on stress relaxation at 150 °C for magnesium alloys. It is observed that at very large stress of 200 MPa, the diameter of the test specimen played a very significant role on the stress relaxation behaviour of extruded ZK30 and that of AZ91. It is seen that the higher the sample thickness and the smaller the samples diameter, the more the amount of stress loss during relaxation.

Riehemann and co-workers used stress relaxation measurement for detection of internal stresses in metal matrix composites [49]. This was done with the aid of electronic balance on saffil-fibre reinforced Mg-alloys (Mg -22 % Al_2O_3 and QE22 -22 % Al_2O_3). It was found that ageing of stress relaxation strength are substantially higher in light metal matrix composites than in corresponding matrix materials. The authors concluded that the thermal mismatch of the metal matrix phase and reinforcing ceramic particles are instrumental to internal stresses and mobile dislocation segments. The same conclusion was also reached by Kiehn et al. on the stress relaxation of short fiber reinforced AZ91 and QE22 with 96 % Al_2O_3 and 4 % SiO_2 [50].

Based on the work as presented in [48], a standard specimen configuration of 12 mm diameter and 5 mm thickness was suggested. Xu et al. [51] however

observed that the result as presented by Albright and Aune is not consistent with the intent of stress relaxation analysis as stress relaxation data should not depend on specimen configuration if it is performed according to standard. Owing to the higher stress level that is employed in this analysis which is way above the normal stresses used in stress relaxation, such results maybe possible. It must be mentioned here that a more extensive stress relaxation test is needed to clarify this controversy. Such test should cover a wide range of specimen configurations, stresses and temperature.

2.5 Bolting and joint fundamentals

A classical joint in an engineering assembly is made up of a bolt, washer, nut and the clamped material. When clamped together, both the bolt and joint members function as a stiff spring. As long as enough clamped force is maintained in the joint, it performs its expected task. When the force is removed, the spring relaxes and as such loses the energy to clamp the joint together. The concept of stiffness is therefore very important as long as creating and maintaining force in a joint is concern. Figure 7 shows a bolt and nut assembly.

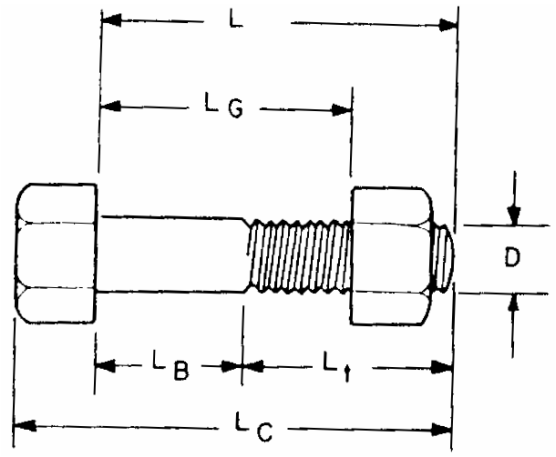

Figure 7: A typical bolt and nut assembly

Where L is the nominal shank length and L_G represents the grip length. D is the nominal bolt diameter, L_B denotes the length of the unthreaded bolt and L_t is the threaded length. L_C represents the combined length of the bolt.

The stiffness of a bolt K_B is therefore given by equation 19 [1].

$$k_B = \frac{F_P}{\Delta L_C} \qquad \text{Equation 19}$$

The quantity F_P is the axial force and ΔL_C, the change in length of the bolt. Since the joint is never clamped by the bolt alone but by the combination of a given bolt-nut-washer system, the total stiffness of the system is given by K_T as expressed in equation 20 [1, 51].

$$\frac{1}{K_T} = \frac{1}{K_B} + \frac{1}{K_N} + \frac{1}{K_W} \qquad \text{Equation 20}$$

The stiffness of the nut and washer are given as K_N and K_W respectively.

A bolted joint is usually represented using a joint diagram [1]. For a clamped joint such as the one shown in Figure 8(a), a corresponding joint diagram for such a preloaded couple is shown in Figure 8(b).

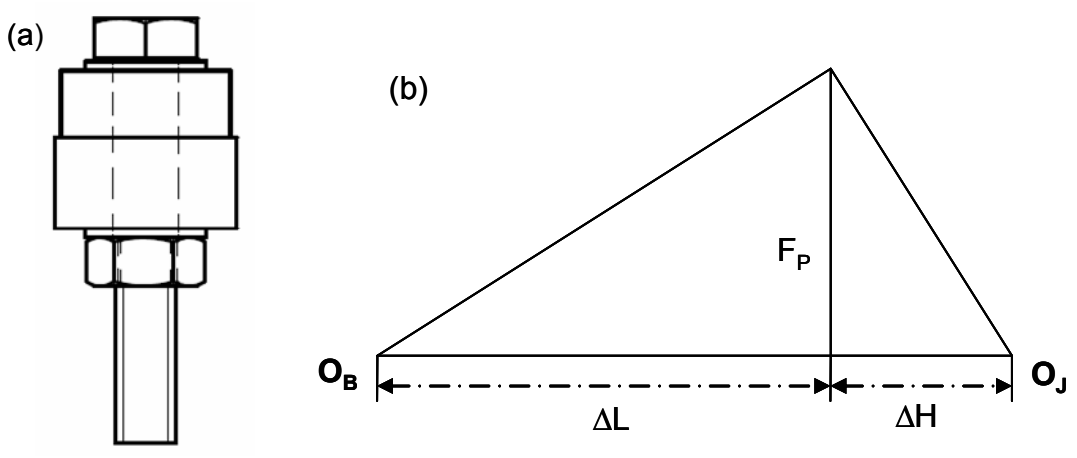

Figure 8: (a). A bolted joint, (b). A preloaded joint diagram

In Figure 8(b), the point O_B is equal to the bolt length when stress is zero. Conversely, O_J is equal to the reference point for the joint height when the stress acting on it is zero. The change in bolt length and joint deflection are equal to ΔL and ΔH respectively.

Application of external load to an already preloaded couple influences the joint behaviour. In the same way, change of the stiffness of the bolt or joint has a direct influence on the joint diagram. For a preloaded joint with an additional external tensile load, the corresponding joint diagram is shown in Figure 9.

The diagram shows L_x which is the external tension load. The change in bolt load and joint are ΔF_B, and ΔF_J respectively. The bolt elongation before and after application of external load are given as ΔL, and $\Delta L'$ respectively. The compressions of joint members before and after application of external load are represented by ΔH and $\Delta H'$ respectively. Since not the entire external tensile load is experienced by the bolt, the portion that is actually felt by the bolt is a function of Φ_K as shown in equation 21 and 22. According to VDI directive 2230 [52] Φ_K is referred to as the load factor.

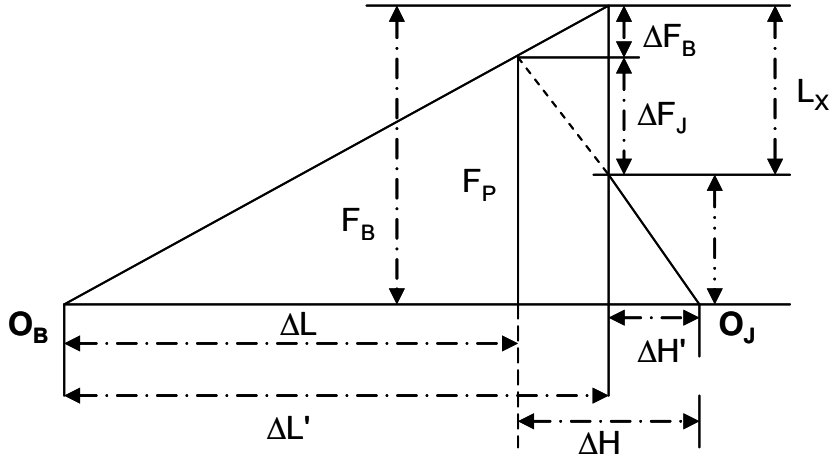

Figure 9: Preloaded joint diagram with external tensile load

$$\Delta F_B = \left(\frac{K_B}{K_B + K_J} \right) L_X \qquad \text{Equation 21}$$

$$\Phi_K = \frac{\Delta F_B}{L_X} = \frac{K_B}{K_B + K_J} \qquad \text{Equation 22}$$

K_B and K_J are bolt stiffness and joint stiffness respectively

The load absorbed by the joint, which is the remaining external load is given as

$$\Delta F_J = L_X - \Delta F_B = (1 - \Phi_K) L_X \qquad \text{Equation 23}$$

Extended treatment on this subject is given in reference [1].

2.6 Bolt load retention of Mg-alloys

The quest to increase the amount of magnesium components use in automotive industry has continued to drive research activities involving magnesium alloys. Generally speaking, the pressure that is generated within the engine blocks of an automobile when gases combined with air are ignited is really enormous. This pressure, when divided by the area of the piston gives an approximate value of the force operational within the system. The real challenge is how to keep and maintain this force so that everything will function effectively without the failure of the magnesium alloy in service. Many of the components in automobiles are joined with bolts and are under compressive load. These include transmission casings, engine blocks, oil filter housings, cam bearing straps, flywheel to clutch assemble, vibration damper, etc. The loaded components are in most cases subjected to thermo-cyclic service conditions; the result is tremendous loss of fastener clamp load. In some cases this leads to noise and vibration, leaking of oil and if unchecked could lead to a catastrophic failure.

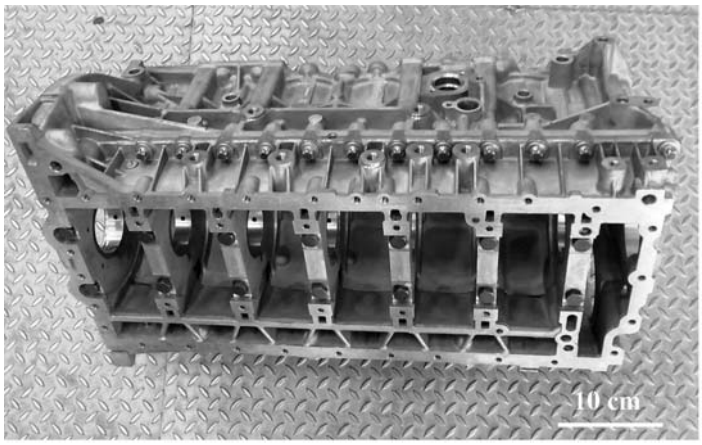

Figure 10: Mg-alloy crankcase with Al-alloy insert

The issue here is not how to measure the real time bolt load loss in magnesium components under service condition because that can be really tedious. The idea is to take care of this during materials selection and design by determining the extent of bolt load retained or loss as a result of creep of magnesium alloy under service condition. Figure 10 shows a Mg-alloy crankcase with an Al-alloy insert.

2.6.1 Typical BLR behaviour

A bolted joint is formed when two or more parts are bolted together with a predetermined force high enough to do a specific job in an engineering assembly. The application of torque in a bolt generates a clamping load on the members of the bolted joint. The tightening of the bolt causes it to be strained in tension from the head bolt to the nut area, while the component parts in-between the bolt and nut are strained in compression. Figure 11 shows a typical bolted joint.

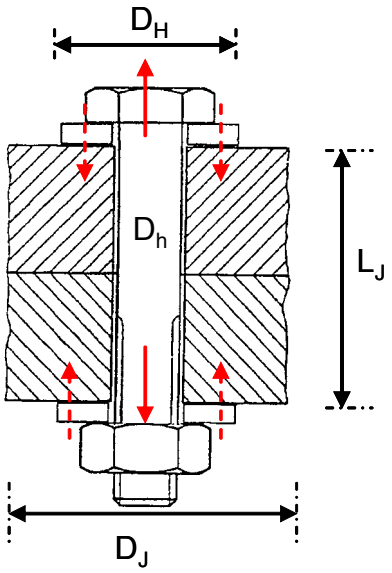

Figure 11: A flange and base through hole bolted joint

D_H represents the washer diameter, D_h - joint hole diameter, L_J - joint length and D_J - joint diameter. The strain produced on the bolt is strongly dependent on the Young's modulus and the stressed area of the component since only part of the component carries the load. With force *(F)* applied on the couple, the components are strained according to equation 24.

$$\varepsilon = \frac{F}{EA_{Sec}} \qquad \text{Equation 24}$$

Where ε is strain, E represents the Young's modulus and A_{sec} is the stressed area calculated from the jointed couple. The stressed area A_{sec} could be estimated using equation 25.

$$A_{Sec} = \frac{\pi}{4}\left(D_H^2 - D_h^2\right) + \frac{\pi}{8}\left(\frac{D_J}{D_H} - 1\right)\left(\frac{D_H L_J}{5} + \frac{L_J^2}{100}\right) \qquad \text{Equation 25}$$

Equation 25 was derived from the cross sectional area of a substitute cylinder taking cognisance of the cylindrical geometry approximate of a bolted joint [1, 53].

For a specimen of 20 mm external diameter, 10 mm internal diameter and 15 mm height, a 10 kN load according to equation 24 for magnesium alloy AS41 will yield a deformation of approximately 0.1 %. This of course increases with higher load values. The comparisons of deflection sustained by AS41 magnesium alloy at various load in relationship to Al ($AlMg_3$) and steel (S235JR) are shown in Figure 12. Deflection δ was calculated using equation 26.

$$\delta = \frac{Fl}{EA_{\text{sec}}} \qquad \text{Equation 26}$$

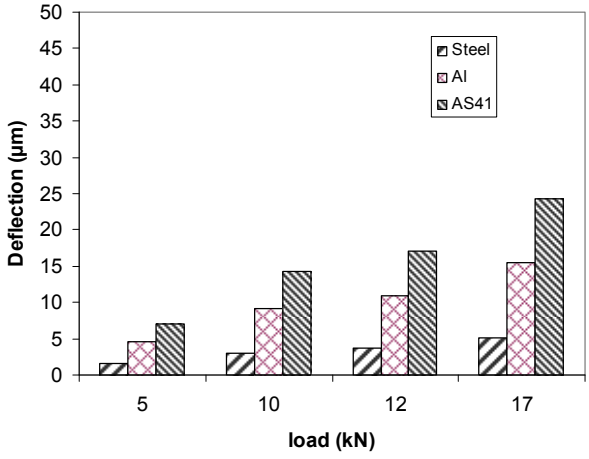

Figure 12: Comparative deflection of materials at room temperature

It is clear to see from Figure 12 that under the same loading condition and specimen configuration, AS41 magnesium alloy will sustain more strain than either aluminium or steel. This is understandable since, the elastic moduli of aluminium and steel are higher than that of AS41 alloy.

For the calculation of Figure 12, the Young's moduli used were 45 GPa for AS41, 70 GPa for pure aluminium and 210 GPa for steel. In bolted joint members, deformation within the components invariably means load relaxation within the couple. This is usually higher for magnesium alloys than other

engineering materials. For AS41 magnesium alloy loaded at room temperature and between stresses of 20 MPa and 70 MPa, deflection of between 0.05 and 4 % was observed after 150 hrs. Figure 13 shows a comparative plot of bolt load loss for some selected Mg-alloys at room temperature.

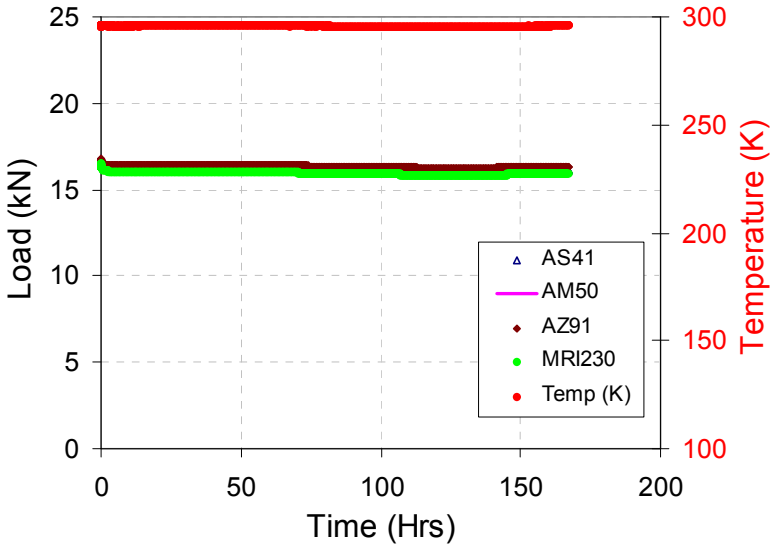

Figure 13: Bolt load behaviour of selected Mg-alloys at room temperature

The bolt load retention behaviour of magnesium components at room temperature is not more of a problem. This is because the bolt load loss is not much and as such the remaining bolt load is always enough to accomplish its fastening assignment in an engineering assembly. This is however not the case at elevated temperature bolt load behaviour. At elevated temperature, a different bolt load retention profile is observed. Figure 14 shows a typical elevated temperature BLR profile of magnesium alloy. The labelled points in Figure 14 indicate the critical loads that define the elevated temperature bolt load behaviour of the alloys under investigation. P_i indicates the initial load applied to the couple at room temperature, P_k is equal to the highest load attained by the couple during heating to the test temperature. P_r is the load retained at constant temperature just before returning to room temperature. P_f is the final load retained by the couple after cooling down to room temperature.

Looking at Figure 14, it becomes evident that the bolted joint must maintain a minimum clamp load in order to prevent it from failure under service condition. The bulk of this research work focuses on the elevated temperature BLR

behaviour of AS41 magnesium alloy which is important for automotive powertrain application.

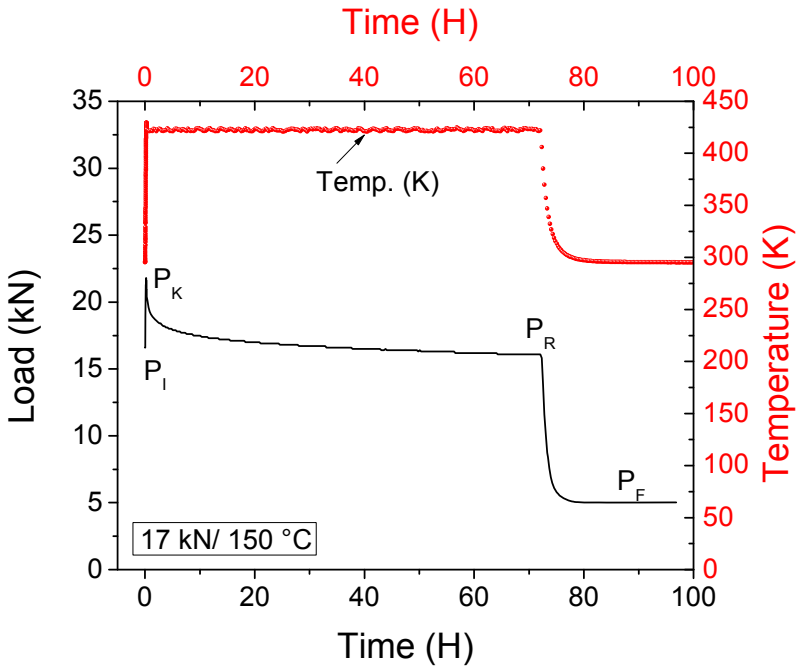

Figure 14: Elevated temperature BLR test profile

2.6.2 Research activities in BLR of Mg-alloys

Bolt load retention testing can be used to simulate the relaxation that may occur at bolted joint in service under compressive loading. The overall bolt load retention behaviour is generally believed to be a combination of two separate effects: compressive yielding and compressive creep [54, 55]. At the moment, the situation is such that research laboratories across the world use various test specifications. The experimental set-ups, specimen configurations, data representation and interpretations vary from one research laboratory to the other. In order to have an overview of research activities in this area, a critical review of the existing test procedures are carried out in this section. Several works have been carried out in this area with each employing its own method. This has basically resulted in variegated results and these data cannot be directly compared to each other.

Some of the works in this area include Pettersen and Fairchild [3]. In their work, a standard grade 8.8 steel bolt was equipped with strain gauges which was

connected in a temperature compensated full-bridge configuration such that there were two active measurement gauges and two reference gauges for temperature compensation. Two identical alloy bosses were joined using this bolt such that the magnesium coupon and the washers are stressed in compression, while the bolt is stressed in tension from the bolt head to the nut. The torqued couple was inserted into a furnace at constant temperature. The bolt load retention was afterwards calculated by taking the ratio of the final load at ambient temperature to that of the initial load. Figure 15(a) shows the BLR test fixture used by reference [3]. Figure 15(b) shows a similar BLR test set up adopted by Bettles et al. [54].

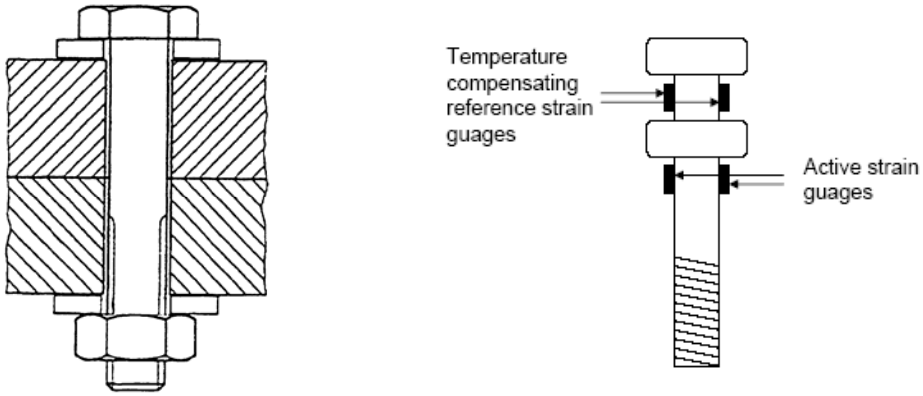

(a) (b)

Figure 15: (a). BLR test fixture used by Pettersen and Fairchild [3], (b). BLR test fixture used by Bettles [54]

Noranda used a torque-retorque set for its bolt load retention experiments [56]. In their work, Noranda used a standard M8 steel bolt and pre-loaded a 9 mm thick cylindrical die-cast sample of 25.4 mm diameter. A torque of 30 Nm (265 lb.in) was applied by using a high precision electronic torque wrench. The bolted couples were immersed in silicon oil bath at 150 °C for 48 hrs. The number of degrees required to retorque the bolt at the same load value was measured. It is important however to note that while the Noranda method can offer a clue to the bolt load retention properties of magnesium alloys, there is also the possibility of getting variegated results. Different people will probably retorque with different forces and at different torqing angles. This could influence the number of degrees. Figure 16(a) shows the BLR test system used by Noranda group. E.G. Sieracki et al. adopted the shaft-coupon-socket

procedure [2]. Figure 16(b) shows the test fixture used by Sieracki et al. The method used here is such that a steel threaded shaft was allowed to pass through the test coupon, two hardened and ground steel washers, two locating steel washers and two nuts.

This shaft was used to apply a compressive load to the entire test specimen by twisting the nuts at each end of the shaft. The ground flat washers applied the load directly on the coupon (one at each side of the centre hole) and a digital displacement gauge at the end of the shaft was used to monitor the stretch applied to threaded shaft while twisting the nuts. Considering the BLR results of the alloys studied using this test procedure, there are discrepancies in comparison with that of Pettersen and Fairchild [3].

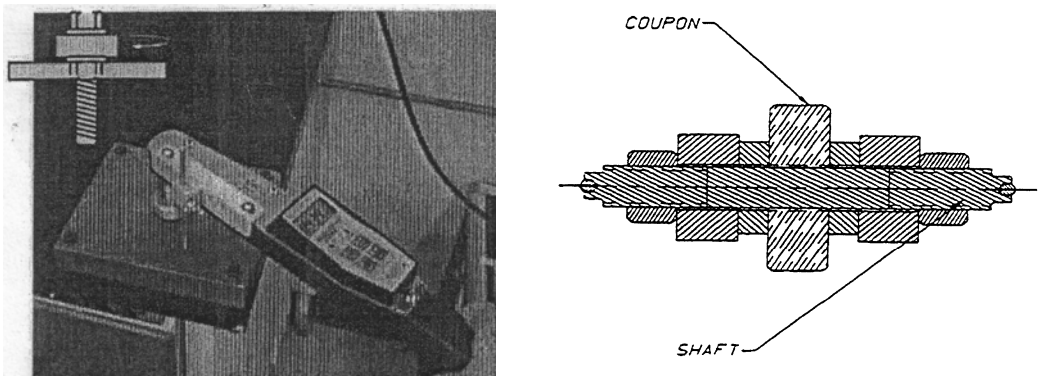

Figure 16: (a). BLR test setup used by Noranda [56], (b). BLR test setup used by Sieracki et al. [2]

Sieracki et al. investigated AZ91, AE42X1 and 380Al with respect to powertrain service condition. The influence of thickness on the remaining stress of the test coupons was studied with an initial load of 95 % of yield stress for 2000 hours. It was reported in this work that for temperature of 100 °C and sample thicknesses of 24 mm and 12 mm, that there was no apparent difference in the amount of remaining load. But at temperature of 125 °C the load loss was much higher on the 24 mm sample thickness than on 12 mm thickness. For the 380Al at 150 °C, it however showed slight difference between the two thicknesses investigated. As the load in the fastening system was determined by the stretch on the shaft: The degree of accuracy in load determination is supposedly to be established by the accuracy in length determination assuming every other considerable influence is constant. More work is needed to clear the contradictions between references [3] and [2].

For F.C. Chen et al., in trying to use for the bolt load retention test a geometrical representation of a typical boss region, made use of flange and case pieces [5]. In this bolt load retention assembly, a strain gauged standard transmission bolt is threaded and torqued to join two pieces. The flange component is a square block 10 mm thick and 40 mm on each side, with an 11 mm hole in the centre. A case component block of 30 mm thickness with sides of 40 mm, containing a machined threaded hole in its centre. This sample was designed for obtaining bolt load retention information for transmission housings of Mg alloy and was considered generally as a representation of the engine block. Case piece was fitted with cast ribs of 4 mm thickness to surround the threaded hole and link it to the outer walls. The idea is to make up for ribs find in transmission casings.

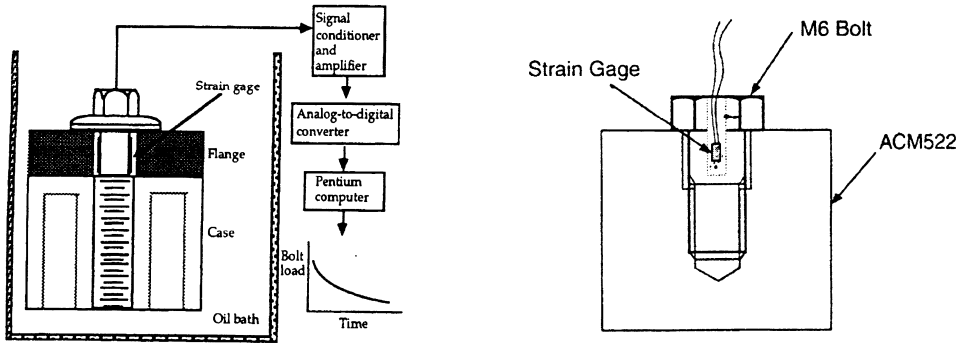

Figure 17: (a). BLR test fixture used by Chen et al. [5], (b). BLR test fixture used by Hollrigl-Rosta et al. [42]

A smooth shank was created below the M10 steel bolt used for this work to allow for the coupling of four karma-alloy strain gauges. It was observed that signal drift could be minimized by cycling the bolts several times between ambient temperature and 175 °C before the experiment. Afterwards the bolt load retention assembly was lowered into the furnace and the load displacement was monitored over a computer. This work however do not document any study on geometry parameter of specimens. It did investigate the influence of three different material configurations with respect to bolt load retention. These are either a combination of both different type of Mg alloys as either flange and case or a combination of Mg alloy flange and either stainless steel or Aluminum alloy. Figure 17(a) shows the test fixture used by Chen and his group.

In trying to simulate the bolt load retention effect in the development of Mg alloy oil pan, F. Hollrigl-Rosta et al. [42] used a different approach. In their work, the strain gauges were embedded in an M6 bolt and this was used to measure axial force during the experiment. The test specimens were extracted from the biscuit part of the die cast oil pan. However details of the method used for attaching the strain gauges to the bolts, signal drift or calibration of the instrument was not documented. The test apparatus used by Hollrigl-Rosta et al. is shown in Figure 17(b).

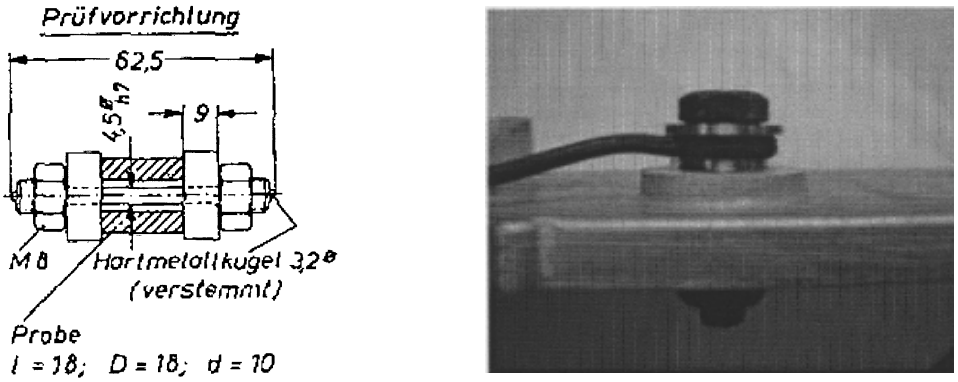

Figure 18: (a). BLR test setup used by Labelle et al. [57], (b). BLR test setup used by Druschitz and Showalter [4]

Figure 18(a) shows the BLR test assembly used by Labelle et al. [57]. This system made use of the instrumented bolt measuring techniques. Hole cylindrical specimens were machined from die cast parts. It is important to note here that the grip length which is the combined thickness of all clamped components by the bolt and nut is twice that of the sample length in this test couple. The increase of the effective length of the bolt is expected to influence the overall remaining bolt load. The 9 mm thick washers used was to eliminate any external effect coming from washer deflection during the experiment.

Druschitz and Showalter [4] used a Lebow 3718-112-8MM high temperature bolt force sensor in their work. The bolt load compressive stress retention of some selected magnesium alloys was investigated. Comparison was made with that of gray cast iron and 383Al alloy. A special large hardened 440C stainless steel washer (58-60 HRC) and an M8 Grade 10.9 bolt (7.8 mm nominal diameter) and nut were used. The hardness of the selected bolts was determined in the as-received condition and after testing to establish if there

were changes in the bolt during experiment. The bolt load sensor was separated by two washers before slipping the sample through the steel bolt and was torqued using the nut. The test set up used for this work is shown in Figure 18(b). The bolt force sensors were connected to measurement group model 2120B signal conditioner. The output from the signal conditioner was stored using a measurement computing PCI-DAS64/M2/16 data acquisition board. The bolt load compressive stress retention data obtained from this work showed that none of the magnesium alloys investigated in the as cast condition performed better than aluminum alloy 383 or gray iron. However, in the heat treated condition and at low initial stress (70 MPa); AE42 and AJ52X had much closer performance as well as gray iron. In general, magnesium alloys showed better bolt load performance after heat treatment. It must be mentioned here however, that the Lebow bolt force sensors used were not temperature compensated. It follows that apparent strain vs. temperature data was collected for each sensor and the measured strain vs. time curves were corrected. Future work involving the use of sensors is expected to address the issue of high sensitivity and temperature compensations to have a more dependable test results.

In their review, Xu et al. [51] made a survey on critical bolt joints in automobiles. This was done together with the assistance of the North American car manufacturing industries and covers the cradle of an automobile with its front and rear attachments. The cradle is usually connected to the body of automobile with steel bolts. The bolts were passed through the frame rail and through the cradle joint with the nut and washers at the lower part behind the cross member surface. The cradle to body structure rear attachment of a Corvette C6 car uses a cross member of Al, this can of course be replaced with Mg-alloy. The Al cross member has an external diameter of 40 mm, internal diameter of 19.4 mm and thickness of 39 mm. The steel bolt used for its attachment was a grade 10.9 bolt with diameter and pitch of 14 mm and 2 mm respectively, and length of greater than 270 mm. From the above illustrated information, laboratory simulated BLR experiments can be carried out by applying appropriate loading and temperature conditions.

Nyberg et al. [58, 59] also used an instrumented bolt technique to investigate thixomolded ZAX8506 and AZ91D. It was concluded in their work that the improved BLR properties exhibited by ZAX8506 was as a result of the

compositional difference in the eutectic phase and the presence of $(Zn,Al,Mg)_4Ca$ particles. Bettles et al. studied the effect of grain size on the bolt load retention behaviour of AMC-SC1 alloy [55]. The authors concluded that the overall BLR behaviour of AMC-SC1 at 8 kN/ 423 K or 11 kN/ 423 K are independent of grain size up to 536 µm. At 450 K and same preload level, reference [55] found a decrease in BLR as the grain size increases up to 536 µm. It will however be mentioned here that more work is needed to verify the influence of grain size on BLR of Mg-alloys. Creep properties of Mg-alloys are known to improve with increase in grain size. Since BLR is partly creep dependent, any action to improve creep property will also improve BLR property of Mg-alloys. The test set up used by Nyberg et al. and Bettles et al. are shown in Figure 19(a,b) respectively.

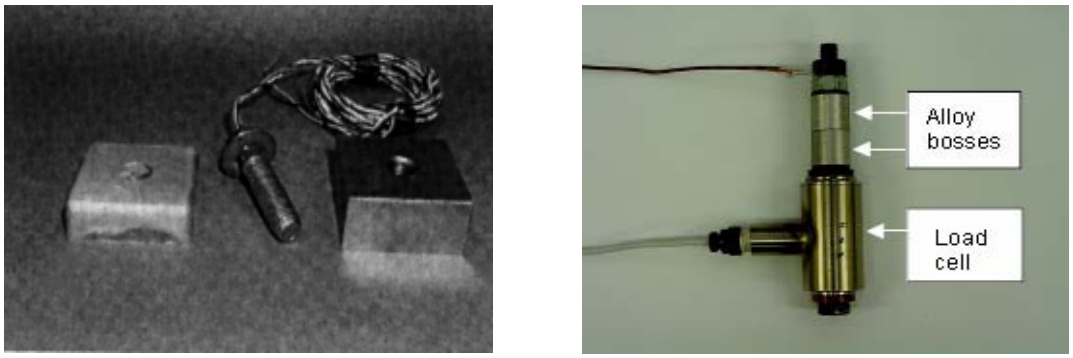

(a) (b)

Figure 19: (a) BLR test set up used by Nyberg et al. [59], (b) BLR test set up used by Bettles et al. [55]

Owing to the reviewed bolt load test procedures, it becomes very obvious that there is need to provide a basis for adoption of a common test procedure for bolt load retention testing of magnesium alloys for automotive applications. The application of variegated test procedures makes comparing of results from one research institute to the other almost impossible. This is because test equipments have specific intrinsic setup properties, and test condition varies. There is also need for a common test specimen (shape, dimension) and bolt load retention fixtures so as to make data comparison amongst research scientist and product designers more comparable. Efforts are especially made in this work to model BLR behaviour of AS41 using compressive creep information of the alloy at relevant temperatures. The influence of initial and

final load on the bolt load retention of magnesium alloys was also studied. From the reviewed work, it is clear that all the samples used for the experiments could be reduced to either a tapped cylindrical specimen or a cylindrical specimen with through hole for passage of steel bolt. In this work a cylindrical AS41 test sample with through hole was used.

2.6.3 Summary of BLR models available

Several attempts have been made in the past to model BLR behaviour of Mg-alloys using different approaches [5, 54]. Arimond [60] proposed a mechanical element model to a bolted joint. This model was later applied by Chen et al. [5] in predicting the time dependent bolt load loss as a result of creep of AE42 and AZ91D. Equation 27 shows Arimond's model.

$$F(t) = F_o \frac{C^f + C_o^b}{C^f + C^b(t)} \qquad \text{Equation 27}$$

In equation 27, F_o is the initial load, C^f is bolt compliance, C_o^b and $C^b(t)$ are the initial boss compliance and time dependent boss compliance respectively. Compliance is the inverse of stiffness and is expressed as equation 28.

$$\left[S_{ij}\right] = \left[C_{ij}\right]^{-1} \qquad \text{Equation 28}$$

S_{ij} is the stiffness matrix and C_{ij} the compliance matrix. It is reasonable to try to model bolt load retention of Mg-alloys using bolt and boss compliances since these are different materials and also should contribute to the overall bolt load. This model however, did not take into account the initial stage of bolt load retention process. There is no mention of the thermal expansion contribution in equation 27. The thermal expansion mismatch occasioned by the differences in coefficient of thermal expansion between the steel bolt and the Mg-alloys are important in determining the final bolt load.

Reference [54] applied a power law relationship to explain the time dependent BLR behaviour of MEZ and AZ91 alloy. Equation 29 shows the power law equation according to reference [54].

$$F(t) = at^n \qquad \text{Equation 29}$$

In equation 29, $F(t)$ is the time dependent bolt load loss at the bolted joint, while *a* and *n* are constants. Equation 29 is an empirical relationship and do not

consider the geometry and properties of the steel bolt, washers and Mg-alloy boss in the joint.

Pettersen and Fairchild [3] proposed equation 30 for the description of the initial stage of bolt load retention test for Mg-alloys. In equation 30, ΔF is the increase in load and ΔT the change in temperature. The coefficient of thermal expansion for Mg component, that of steel washer and bolt are given as α_{mg}, α_{washer} and α_{bolt} respectively. l_{mg}, l_{washer} and l_{bolt} are lengths of Mg sample, that of washer and bolt respectively. *K* is the spring constant.

$$\Delta F = \Delta T\left(\frac{\alpha_{mg} l_{mg} + \alpha_{washer} l_{washer} + \alpha_{bolt} l_{bolt}}{K}\right) \qquad \text{Equation 30}$$

One of the major drawbacks of equation 30 is that, it makes prediction of several orders of magnitude higher than the experimental results. A modification of equation 30 or a new approach is therefore needed for this purpose. Gerstmayr and Eichlseder [61] used a model based on Norton´s relationship to describe the time dependent drop in stress. This is expressed in equation 31.

$$\sigma(t) = \left[\sigma_O^{-n+1} - (1-n).E.B.e^{-\frac{Q}{RT}}.t\right]^{\frac{1}{1-n}} \qquad \text{Equation 31}$$

In equation 31, σ_o is the initial stress, *n* the stress exponent and *E.B* constants. *Q*, *R* and *T* are activation energy of creep, gas constant and absolute temperature respectively while *t* is time. The work of Gerstmayr and Eichlseder [61] did not include the heating up phase, the influence of thermal expansion mismatch of the bolted componets was no included in their work but concentrated only on the effect of creep at test temperature.

Other models include those applied by Longworth [62] on Mg-alloys, where neural network method was used. This was based on the Bayesian approach developed by Mackay [63]. In this model, information about the unknown is added through the use of Baye´s theorem [64]. A typical neural network is described as:

$$X \rightarrow Y\left(x^{\cdot}, w, A\right) \qquad \text{Equation 32}$$

In equation 32, the vector *x* is the parameter defining the physical problem. The vector *w* describes the weight while *A* is related to the architecture of the

network [63, 65]. It must be said that this technique is ambiguous to apply and difficult to analyse specifically what is happening inside the network. The form of relationship among variables cannot be evaluated directly from a neural network. This are however easily inferred using empirical approach. A physical based empirical relationship will be a good technique for prediction of bolt load retention of Mg-alloys.

Some other concepts on modelling BLR of materials include the application of boundary element formulation as used by Lee and Kim [66] on predicting the BLR of thermosetting polymer. Another work is also that of Jaglinski et al. [67] on modelling BLR of aluminium joint. It must be mentioned here that whereas these models attempt to predict BLR of the materials investigated, the results of the models differ with the experiments by great margin. A new approach is required. The BLR behaviour of Mg-alloy is geometry and material dependent. This means that, the configuration of the test sample, the compliance of the bolt/joint and creep response of the material under investigation play important role in determining the joint response under load and temperature.

3 Motivation and objectives

This research work was embarked on in order to address the issues as raised in the previous sections. A systematic investigation was designed to critically investigate the creep and bolt load retention behaviour of magnesium alloys. To do this, a standard AS41 magnesium alloy was used in the analysis. The need to use an already established magnesium alloy in this test is crucial as influences coming from specific factors affecting the bolt load retention behaviour of magnesium alloys can easily be inferred. The aims of this present work are therefore:

- To identify the deformation process observable for BLR deformed AS41 Mg-alloy at elevated temperature. And to clarify the creep mechanism that is associated with creep of permanent mould AS41 Mg-alloy under compressive mode.
- Identification of the factors affecting bolt load retention behaviour of AS41 Mg-alloys at bolted joint. This is with respect to temperature, initial load, final load, effective length and joint stiffness. Understanding the nature and behaviour of these influences will be helpful in material selection and designs using Mg-alloy components for elevated temperature application.
- The application of interrupted test procedure in BLR measurement, which is seemingly a “near reality” condition, will be addressed. Results from this will be compared to isothermal BLR test. This is expected to provide information that is of practical importance in characterising Mg-alloys with respect to automotive application.
- To establish a simple and suitable bolt load retention (BLR) testing equipment using continuous load cell measuring technique. Identification of the factors influencing BLR testing procedures and make recommendations based on the findings for running BLR experiments.
- There is need to provide a suitable model that can predict BLR behaviour of Mg-alloys with reasonable accuracy. Present models either do not

include the inception of the BLR process or makes prediction of several orders of magnitude higher than the experiment.

4 Experimental procedures

4.1 Material

Permanent cast AS41 Mg alloy was used in this investigation. The AS41 alloy was cast into a detachable permanent steel mould of total height 500 mm with top and bottom diameter of 210 mm and 105 mm respectively. This is shown in Figure 20. The wall thickness of the steel mould is 22.5 mm. The mould produces a cast billet of 400 mm height and 100 mm bottom diameter with average weight of 8 kg (Figure 21). The melt and mould temperature were 700 °C and 220 °C respectively. The casting was carried out under 0.2 % SF_6-argon mix cover gas and allowed to cool in air. The chemical composition of the AS41 alloy used in this investigation is measured using spectroanalysis technique. The aluminum alloy and steel that were used to produce joints with the AS41 were as delivered from the company. These materials were machined to the desired specimen configuration in each case.

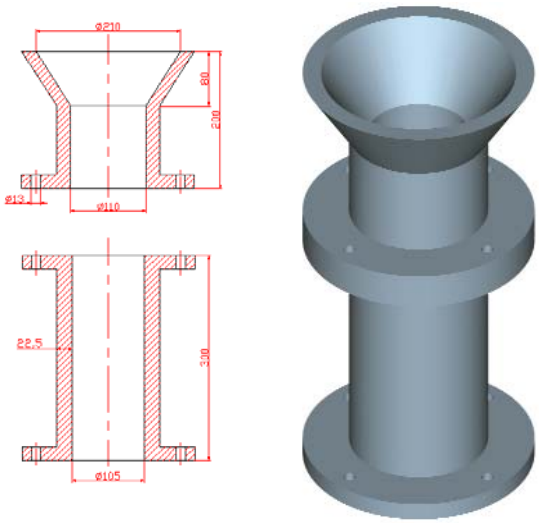

Figure 20: Diagrammatic representation of the steel mould used for casting the alloy

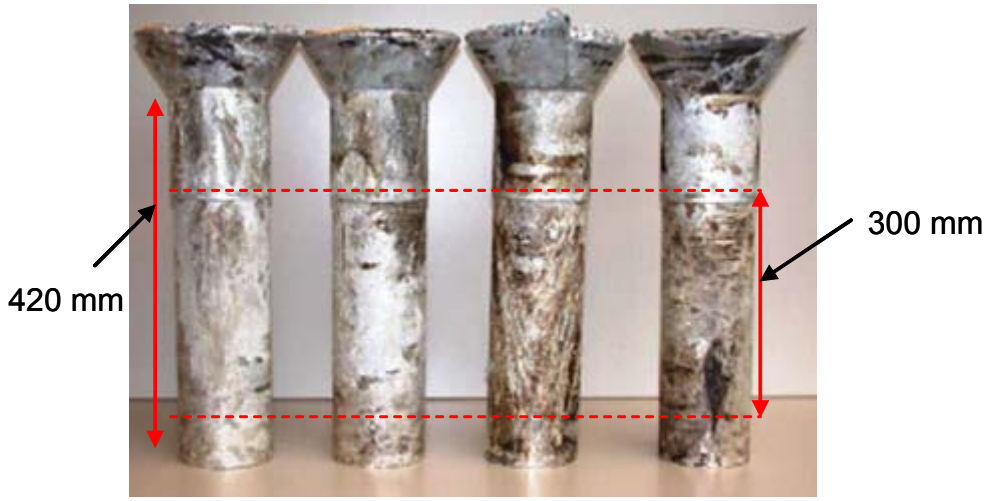

Figure 21: Cast AS41 billet showing areas within which investigated samples were taken from

The regions marked out with dashed lines with height of 300 mm constitute the section from where samples for experiments were taken.

4.2 Density measurements

In order to control the extent of porosity on the cast samples, density measurement were made on the samples before experiments. The density measurements were carried out using Archimedes principle according to ASTM standard B311-93. Specimens were weighed in air and (99%) ethanol and subsequently their densities were calculated using equation 33. Density of ethanol ($\rho_{ethanol}$) is equal to (0.789-0.001 T °C) g/cm^3.

$$\rho_{specimen} = \left(\frac{M_{air}}{M_{air} - M_{ethanol}} \right) \rho_{ethanol} \qquad \text{Equation 33}$$

The porosity was subsequently calculated using equation 34. Where ($\rho_{theoritical}$) and ($\rho_{apparent}$) are theoretical and apparent densities respectively. The theoretical density was calculated by taking the summation of the respective weight (%) of elements and their densities. Densities of Mg, Al and Si used are 1.738 g/cm^3, 2.70 g/cm^3 and 2.33 g/cm^3 respectively.

$$(\%) Porosity = \left(\frac{\rho_{theoritical} - \rho_{apparent}}{\rho_{theoritical}} \right) 100 \qquad \text{Equation 34}$$

4.3 Metallography

4.3.1 Sample preparation

In order to gain insight into the microstructure, specimens were prepared for metallographic investigations. Grinding was done using silicon carbide emery paper up to 4000 grit. Further preparation on the test specimens include, polishing using 0.05 μm colloidal silica for up to 60 seconds. Detailed information on the sample preparation is given in reference [68].

4.3.2 Microstructure investigation

The microstructures of the alloys investigated were characterized using light microscope, scanning electron microscope, transmission electron microscope and X-ray diffractometer. This is very necessary in order to have understanding of what goes on at the micro level before and after bolt load retention analysis of the investigated alloys. Creep specimens were also analyzed microstructurally after creep tests.

4.3.2.1 Optical microscopy

A Reichert-Jung MeF3 microscope was used for this investigation. The microscope is equipped with a digital camera. The whole assembly is then connected to a computer which runs an (analysis pro) software. This enables the digital pictures to be adequately analyzed using the analysis capabilities present in this software. The micrographs were taken at different magnifications revealing various stages of the microstructural development in the alloys under investigation.

4.3.2.2 Scanning electron microscopy

Scanning Electron Microscope (SEM) ZEISS DSM-962 (Germany) operating at 15 KV was used for microstructure characterization. The SEM is equipped with an Energy Dispersive X-ray analysis (EDX) to detect the composition of bulk specimens using WINEDS software. The SEM images were taken using secondary electrons (SE) and back scattered electrons (BSE). EDX was used for measuring the volume fraction of different phases and precipitates using back scattered electrons. EDX line scans were taken with a dwelling time of 30 seconds per spot to insure significant counts above the background. EDX point scans were taken with a live time of minimum 200 seconds and EDX mapping

was taken with dwelling time of 30 minutes again to ensure significant peak counts above the background.

4.3.2.3 Transmission electron microscopy

For TEM sample preparation, the specimens were cut to a thickness of 7 μm and diameter of 2.3 mm. The samples were further ground to a thickness of 120 nm and with an electrolytic polishing; a hole was made at the centre of the specimen for the passage of electron beams. The electrolyte was made up of 2.5% perchloric acid ($HClO_4$) in 97.5 % ethanol. Temperature of -45 °C was maintained in the electrolytic bath. Current and voltage of 10 μA and 20 V were used during the electrolytic polishing. Afterwards, the polished samples were washed in acetone before TEM observation.

A Philips C200 Transmission Electron Microscope (TEM) was used in the TEM investigation of the alloys. TEM micrographs were taken in bright field mode and selected area diffraction was made with average exposure time of 5 seconds and 880 mm camera lens.

4.4 Creep test

The creep investigations were carried out on a “2330 Lever Arm” Applied Test System (ATS) machine. Figure 22 shows the specimen holder that was used for the compression creep investigations.

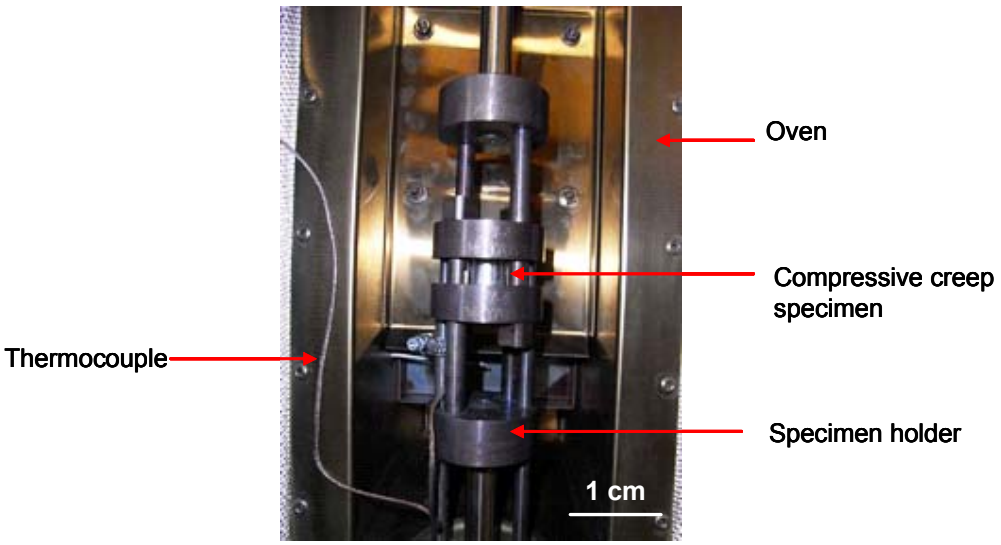

Figure 22: Specimen holder for compressive creep test

Cylindrical specimens with an outer diameter of 20 mm, an inner diameter of 10 mm and a height of 15 mm were used. The sample corresponds to a solid cylinder gauge diameter of 17.3 mm and stressed area of 235.6 mm^2. Experiments were performed in compressive mode under constant stress condition of 40 MPa, 55MPa, 70 MPa and 90 MPa. Investigated temperatures were 100 °C, 125 °C, 150 °C, 175 °C and 200 °C. At the appropriate stress level a soaking time of approximately 1 hour was observed after which the creep test starts automatically. The creep deformation was constantly measured via an extensometer.

4.5 Compression test

Compressive yield strength of the investigated alloys was tested at various temperatures using the ASTM standard E 9 [69]. The compressive test was carried out using a Zwick Z050 model machine. The major parts include: the main frame, the bearing blocks for positioning the test specimen, heating chamber for generating desired temperature and the data logger. The data

obtained from this test include yield strength, ultimate compressive strength and stress-strain curve of the investigated alloys at different temperatures.

Cylindrical samples measuring 15 mm height and 10 mm diameter was used in this investigation. Care was taken to prevent the specimen from buckling during loading. The temperature range chosen for this experiment covers between room temperature and 175 °C with a constant strain rate of 10^{-3}/s.

4.6 Hardness testing (Hv)

In order to gain more insight on the degree of deformation associated with both BLR and creep deformed AS41 specimens, the hardness of the samples were measured before and after experiments. An average of 20 points was measured with a 5 kg weight and the mean value was calculated and taken as the hardness of the specimen.

4.7 Bolt load retention test

4.7.1 Specimen configuration

In this work, three types of specimen sizes were used for the bolt load retention analysis. This selection is made based on thorough review of past research activities which invariably reduced every bolted joint to a cylindrical specimen with hole [2-6, 47, 51, 55, 56]. The BLR test specimens chosen are therefore through hole cylindrical specimens measuring for (a) 30 mm outside diameter, 10 mm inside diameter and 15 mm height. That of specimen (b) measures 20 mm outside diameter, 10 mm inside diameter and 15 mm height. Specimen (c) measures 20 mm outside diameter, 10 mm inside diameter and 30 mm height. The cast billets were carefully machined to the desired configuration, taking care that less internal stresses or deformation are induced on the samples. The specimen dimensions selected corresponds to a gauge height/diameter ratio of a=0.5, b=0.75 and c=1.5. When the specimens are considered as solid cylinder without holes, the ratio of gauge height/diameter becomes: a=0.53, b=0.87 and c=1.73. From left to right, Figure 23(a-c) shows the direct relationships of height to diameter ratio.

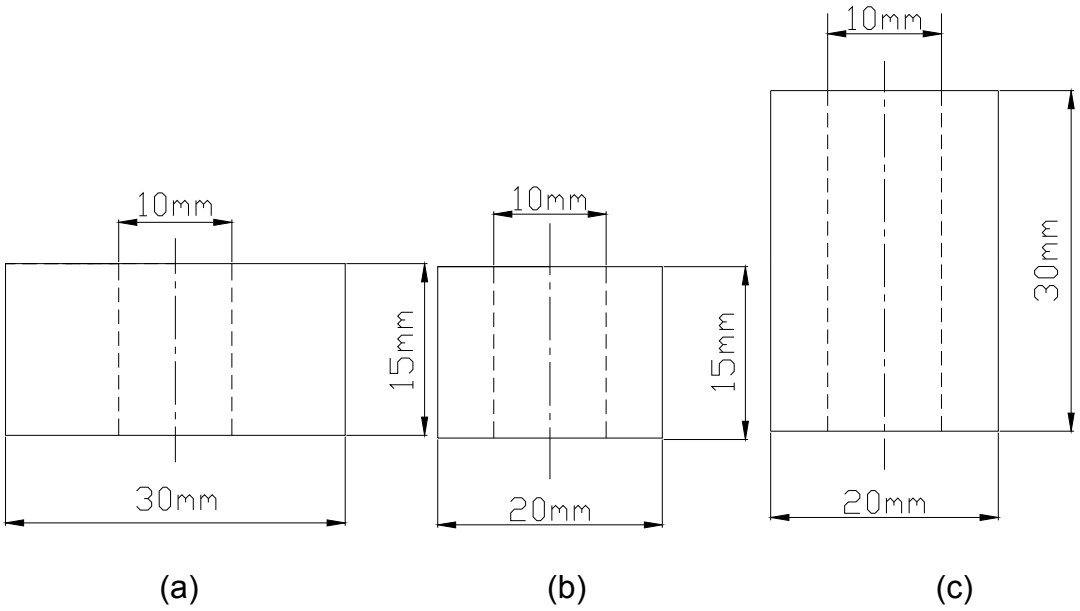

Figure 23: From left to right (a, b, and c) of specimen dimension in (mm)

4.7.2 Equipments used for BLR test

4.7.2.1 Load Cell

The load cell measuring technique was used in the measurement of bolt load retention (BLR) behaviour of the alloy investigated. Another often used method is the instrumented bolt technique. The major difference between the two methods is that strain gauges are often embedded in the bolts for the instrumented bolt technique. That of load cell system is simply coupled with the bolt during torquing to the desired load before starting the experiment. The load cell used in this investigation is shown in Figure 24.

The sensor is an F207 model load cell measuring instrument. The axial strain cylinder in weather sealed case is equipped with raised end load bearing faces and hole right through. It is used for compression or in fail-safe tensile measurement on a wide range of end-user applications. The F207 model sensor used (Figure 24), has a measuring range of between 0 and 40 kN and a stiffness of 4.44 $x10^9$ (N/m). It has an outside diameter of 28 mm, a load measuring ring of 19 mm diameter and a hole of 10.2 mm for passing M10 bolt. The sensor is calibrated so that the incoming data strings in mV are converted to the actual load readings in kN. Here the voltage measurement of the sensor

runs between 0-10.221 mV, the sensor is therefore being calibrated to reflect the range of load between 0 and 40 kN. Technical data for the load cell used in the BLR analysis are found in reference [70].

Figure 24: High precision load cell

4.7.2.2 Heating device

The heating device used in this work is a PZ 26-4 model furnace. The technical data and properties of the furnace are listed in Table 2. The heating element is a HE 245 Ni which has a stainless steel receptacle and a thermostatic sensor.

Table 2: Technical data of PZ 26-4 heating device

Technical Data	PZ 26-4
Temperature range	20 …. 400°C
Voltage	220 …240 V, 50-60 Hz
Power	1200 Watt
Overall dimension	310 mm x 310 mm x 280 mm
Weight	6.8 kg

The furnace is also equipped with a WS 16 Rocker-switch and a temperature controller. The PZ 26-4 is suitable for use as oil bath for temperatures up to 400 °C. An integrated NiCr-Ni mantle thermocouple measures the temperature in the bath container and passes on the corresponding switching command to the temperature display/control unit. The microprocessor calculates the desired heating power and releases the heating current accordingly. When operating

around temperatures under 100 °C, the rise in temperature is quicker than the microprocessors calculation capabilities and the bath will overheat by a few degrees. The overheating is however being compensated by the regulator which reduces the heating power. The set temperature point is maintained with a difference of ± 1.5 °C.

4.7.2.3 Bolts/Nuts/Washers

Steel and Al bolts were used as fasteners in this investigation. The bolts are high strength M10 steel bolts with 60 mm threaded length, DIN 933 and strength 10.9. The nuts were selected to match the bolts, a high strength M10 nut, DIN 934 is used for this work. Washers (DIN 125) with inside and outside diameters of 11 mm, 20 mm respectively were used. The bolts, nuts and washers were cycled between 150 °C and ambient temperature before using in the experiments. The thermal cycling of the bolt is to reduce drift. Considering the yield strength of the bolts, each bolt can be re-used for several times.

4.7.2.4 Silicone oil

The need to have a uniform temperature condition during the (BLR) experiment is very important as non uniformity in temperature could influence the bolt load behaviour of the alloy under investigation. Silicone oil was therefore used to stabilize the temperature within the furnace. A constant temperature within the furnace was maintained during the bolt load retention experiment. The Silicone oil has a suitable running temperature range of between +20 °C to 250 °C. It also has a flash point of 270 °C and a fire point of > 360 °C. The Silicone oil is subject to ground contamination and water damage. The silicone oil is changed as soon as its ability to homogenize and maintain a constant temperature is lost. This is determined using thermocouple that is permanently inserted in the oil bath.

4.7.3 Functional principle of the BLR testing equipment

Figure 25 shows the schematic diagram of the bolt load retention test equipment used. The four axial strain cylinders are connected to a 4 channel amplifier which works on the principle of a Wheatstone bridge.

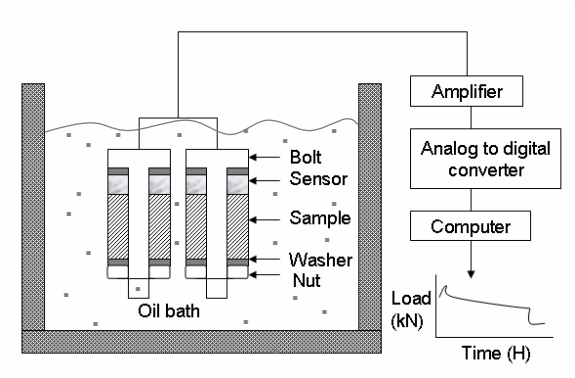

Figure 25: Experimental set up for BLR test

The variation of the load was amplified to an output value of 0 to 10 Volts. The four channels were digitized via a 24 bit sigma-delta ADC (analog digital converter) with serial interface. The ADC can be read out by the PC which runs a Labview programme. In this programme an average value was stored over an adjustable time slot. There are two graphs in the programme window; the first graph shows the values which have been processed and stored during the test. In this graph, the X-axis measures the time in hours while the Y-axis measures the load in kilo Newton (kN). The second graph reveals the actual data that has been just received so as to have the momentary overview of incoming data. The data are stored in a file that can be selected. The overall programme was developed together with the technical department of GKSS especially for this investigation. Incorporated in the programme is also the possibility of tracking the already stored data through a readback plot so that real time information could be derived when needed during the test duration.

4.7.4 Details of BLR test

The M10 bolt was passed through a 10 mm hole made on the specimen. Load measuring sensor was loaded by passing an M10 steel bolt through it so that the sensor was positioned between the head bolt/washer contact and the specimen. Sketches are shown in Figure 25 and Figure 26. The M10 steel bolt was cycled up to 5 times between room temperature and 150 °C to reduce drift. The degree of stability of the sensor output with respect to temperature effect, load effect and other factors was verified by monitoring the signal drift over 100 hours in different conditions. This was done by torquing the sensor at 150 °C to

a preload of 30 kN, another at 8 kN with one also at a preload of 30 kN and room temperature. The last was kept untorqued at 150 °C and at room temperature. In all the five observed conditions, the output remained essentially constant but with a maximum difference of between 1-3 % of the initial load measurement reading. It is also observed that the load calibration for the sensor is generally stable differing by only about 3% after running bolt load retention test with a high load of 30 kN at 150 °C. For every BLR test experiment carried out in this work, baseline tests was done by loading the sensor with a similar steel specimen and subject the loaded couple to the same test condition. In this way, the test results were effectively controlled for possible error that could emanate from test equipment.

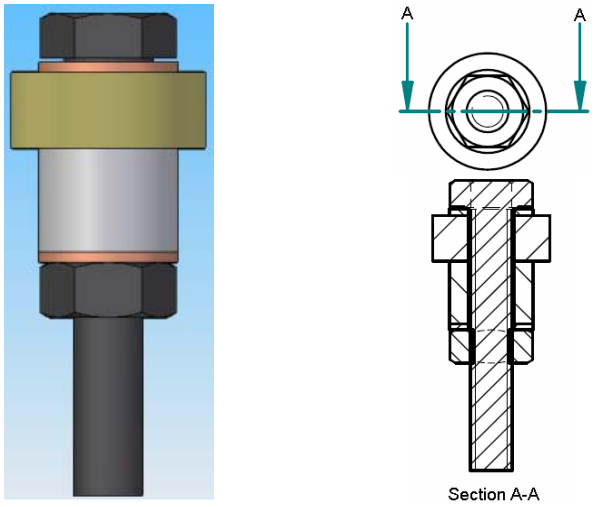

Figure 26: Bolted couple used for modelling bolted joint of AS41

Samples were torqued to the desired load, in this case 5 kN, 10 kN, 12 kN and 17 kN which corresponds to 20 MPa, 40 MPa, 50 MPa and 70 MPa respectively. In result and discussion sections comparison were mainly made using 5 kN, 10 kN and 17 kN loads since the values of 10 kN and 12 kN loads are close to each other. The bolted couples were usually torqued to about 3% above the desired preload and are held for 1 hour at ambient temperature. The extra 3 % of preload along with the waiting period prior to immersion into the oil bath is to minimize the effects of short term relaxation. This short term relaxation occurs immediately after torquing the couple and can be caused by factors such as reduction of stress concentration in thread contact surfaces.

After the waiting time, the loaded couples were inserted into the oil bath and heated to the desired temperature. The temperature covered for the BLR test were 100 °C, 125 °C, 150 °C and 175 °C. The Labview computer programme is programmed to record the data every 10 seconds for the first 20 minutes after placing the bolted couple in the oil bath. The data logging rate was manually adjusted afterwards to record the data every 15 minutes. The initial recording mode is very important so as to be able to monitor the increase in load as a result of thermal expansion mismatch as the bolted couple was heated to the test temperature. The duration of the tests were restricted to 72 hours for short term test. Long term tests were carried out for up to 350 hours. For interrupted BLR test, a programmable time switch was used to sequence the interrupted temperature condition. This allows for flexibility in temperature and time adjustments. Samples were allowed at temperature of interest for 5 hours, then cooled for 3 hours and again heated to test temperature for 5 hours. At the end of each test the bolted couple was cooled in the oil bath to room temperature.

5 Modelling of BLR

Bolt load retention behaviour of magnesium alloy AS41 was modelled in this work by using two basic approaches. The first includes numerical approach, using compliance and creep property of the magnesium alloy under investigation. The second approach involves the application of a “three-parameter creep equation” by using a commercial finite element code. In this section, the explanation of the models adopted in prediction of BLR behaviour of permanent mould AS41 was given.

5.1 Modelling BLR behaviour (compliance-creep approach)

Bolt load retention behaviour of AS41 Mg-alloy was modelled numerically using the compliance of the bolted joint and the compressive creep properties of the AS41 alloy. In a bolted assembly, individual elastic moduli of the component materials constituting the joint play important role. However, the stiffness of the bolted couple and the compressive creep behaviour of the alloy influence the joints overall BLR response. A typical BLR curve as shown in Figure 27 could further be represented as having different stages during the process.

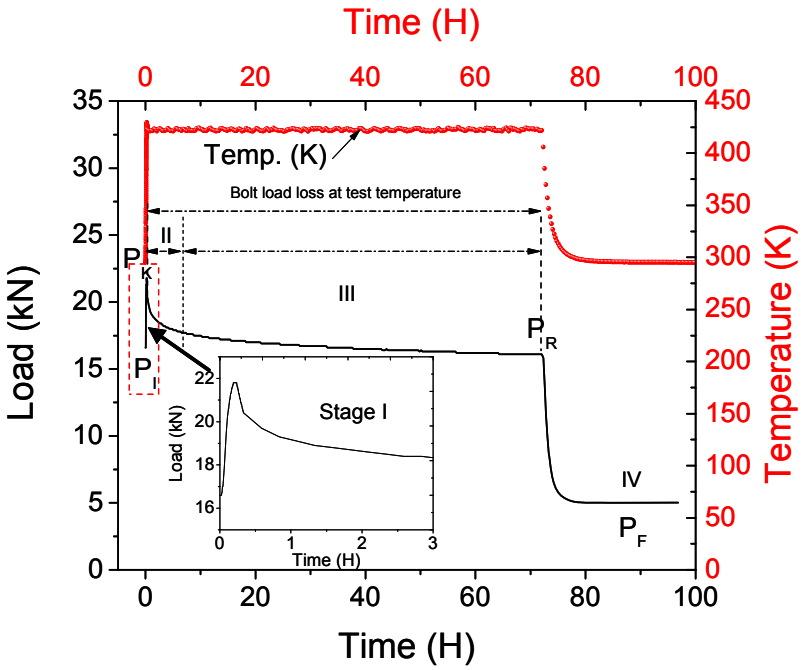

Figure 27: Stages associated with typical BLR experiment

5.1.1 Stages of BLR test procedures

Figure 27 shows different stages or phases during bolt load retention test. These four conspicuous stages characterise the thermal and load history of a bolted magnesium assembly under service condition. The first stage of BLR curve as shown in Figure 27 is associated with the increase in load. This load increase is as a result of thermal expansion mismatch between the steel components and the AS41 magnesium component. The couple torqued at room temperature indicated as point (P_i) in Figure 27 is equal to the initial clamp load P_o operational at the joint. The change in bolt load from P_o to point (P_k) in Figure 27 is computed with equation 35. P_k is the highest point attained by the couple just before relaxation begins.

$$\Delta P = \Delta T l_{mg}\left(\frac{\alpha_{mg} - \alpha_{steel}}{C_{eq}}\right) \qquad \text{Equation 35}$$

In equation 35, ΔT is the change in temperature from room temperature condition T_1 to temperature of interest T_2. The symbol l_{mg} is the thickness of the AS41 used in this work. The thermal expansion coefficient of AS41 magnesium alloy and steel components were represented as α_{mg} and α_{steel} respectively. The equivalent compliance of the couple C_{eq} is given as equation 36. The results of the measured α_{mg} are shown in Appendix D. The steel compliance C_{steel} which is the compliance of all the steel components used in this work is given by equation 37. Equation 38 shows the elements from which the equivalent compliances were calculated.

$$C_{eq} = C_{mg} + C_{steel} \qquad \text{Equation 36}$$

$$C_{steel} = C_{bolt} + C_{washer} + C_{sensor} \qquad \text{Equation 37}$$

$$C_{eq} = \left(\frac{l_{mg}}{A_{mg}E_{mg}} + \frac{l_{bolt}}{A_{bolt}E_{bolt}} + \frac{l_{washer}}{A_{washer}E_{washer}} + \frac{l_{sensor}}{A_{sensor}E_{sensor}}\right) \qquad \text{Equation 38}$$

A_{mg} in equation 38 is equal to equation 25 and that is the effective stressed area of the magnesium AS41 alloy component. The Young's moduli of AS41, steel bolt, washer and sensor were expressed as E_{mg}, E_{bolt}, E_{washer}, and E_{sensor} respectively. The steel bolt stressed area was given as A_{bolt} while l_{bolt} is the effective length of the bolt, which is defined as the sum of the engagement

length plus 0.5 of the head bolt and nut. The symbol l_{washer} and l_{sensor} are the thickness of washers and sensor.

The load operational at point P_k on the BLR curve in Figure 27 is then computed as the sum of the initial load P_o and the change in load ΔP from T_1 to T_2. This is expressed as equation 39. Note that the initial clamp load P_o is equal to the load at point P_i on the bolt load retention curve in Figure 27.

$$P(T) = P_o + \Delta P \qquad \text{Equation 39}$$

5.1.2 Evaluation of retained clamp load using creep result

Stages (II) and (III) as shown in Figure 27 represents the total bolt load loss at test temperature. This is the region between P_k and P_r. The bolt load loss in this region is due to creep of Mg-alloy AS41 sample used. This means that knowledge of the compressive creep behaviour of this alloy is needed at the temperature of interest. Stages (II) and (III) obeys the same law, the only difference is the degree of relaxation is higher at stage (II) than in (III). The compressive creep behaviour of AS41 magnesium alloy is expressed using equation 40.

$$\varepsilon_c = \beta t^{n_i} \qquad \text{Equation 40}$$

In equation 40, ε_c is the creep deformation, β is a material dependent constant and n_i is compressive creep parameter. Taking the natural logarithm of equation 40 results to equation 41 so that a plot of $\ln(\varepsilon_c)$ against $\ln(t)$ gives a straight line whose slope is n_i.

$$\ln \varepsilon_c = \ln \beta + n_i \ln t \qquad \text{Equation 41}$$

The time dependent deformation due to creep of AS41 at bolted joint is then represented using equation 42.

$$\varepsilon_{(t)} = \varepsilon_i t^{-k_i n_i} \qquad \text{Equation 42}$$

The symbol ε_i is equal to the sum of elastic and partly plastic strain sustained by the magnesium component. While t is creep time, n_i is the creep parameter computed from equation 41 and k_i is dimensionless constant that depends on the joint-to-bolt stiffness ratio of the couple and is approximately equal to $0.25\,\Phi_K$ of equation 22. The time dependent bolt load loss due to creep of the

magnesium component is expressed then as *P(t)* as shown in equation 43. *C* in equation 43 is a temperature and specimen geometry dependent material constant.

$$P(t) = C\varepsilon_i t^{-k_i n_i} \qquad \text{Equation 43}$$

Typical bolt load prediction for AS41 using this method is shown in section 6.9. Equation 43 makes reasonable prediction of the amount of bolt load retained in a magnesium alloy through hole bolted joint.

5.2 Modelling BLR behaviour (FEA approach)

The application of this approach requires the knowledge of the geometric configuration of the bolted joint in question. Important also are the material properties of the bolted couple. These include compressive creep information of the alloy (in this case AS41), thermal expansion coefficients at different temperature range of interest, compression strength, etc. The time dependent stress-strain response of magnesium alloy AS41 at bolted joint was modelled using compressive creep results obtained from typical cylindrical bolt load retention samples. A power law creep relationship coded in finite element program is used to describe this time dependent stress-strain behaviour. The total uniaxial stress-strain relationship of joint material was computed as the sum of elastic, plastic and creep strains.

5.2.1 Application of FEA on bolted joint

Torque was applied on the bolt head as shown in Figure 26. When the desired preload is reached, in this case 10 kN and 17 kN which correspond to 40 MPa and 70 MPa respectively. The end of the bolt was locked with a steel nut assuming no further displacement of the steel bolt occurred or any sliding between the steel bolt and the nut. This also allows for the assumption that the grip length is constant during simulation. Grip length is the combined length of all the members of the bolted joint clamped by the bolt head and the nut. It is important to mention that the stress distribution between the bolt head, members of the clamped couple and the nut was studied in this model. The details of the bolt and nut thread were not modelled in this investigation.

A finite element program ADINA [71] was applied in the simulation of this bolt joint. The configuration of the bolt joint consists of two steel washers of 2 mm thickness each with 20 mm external diameter and a through hole of 11 mm. The AS41 permanent mould magnesium sample measures 15 mm thickness, 20 mm external diameter and 10 mm internal diameter.

A steel load cell measuring 11 mm thickness, 30 mm external diameter and 11 mm through hole for passing M10 steel bolt was used. The load sensing part of the load cell is equal to the external diameter of the sample. The combined thickness clamped by the bolt head and the nut is 30 mm. The bolt joint was modelled axisymmetrically and was mirrored to get a complete bolt joint mesh.

5.2.2 Creep evaluation using three-parameter creep equation

The knowledge of creep behaviour of AS41 magnesium alloy in compressive mode is needed in order to adequately model the bolt load retention response of AS41. To do this, a “three-parameter creep model” coded in finite element program was used to evaluate the compressive creep of AS41. Equation 44 shows the power-law creep model that was used.

$$\frac{d\varepsilon_c}{dt} = C\sigma^m t^n \qquad \text{Equation 44}$$

where ε_c is the time dependent creep deformation, σ is the equivalent stress and t is time. The other parameters (C,m,n) are temperature dependent material constants which are evaluated using regression process. Hence equation 44 can be further expressed as equation 45 and the values of the constants could be determined.

$$\ln d\frac{\varepsilon_c}{dt} = \ln C + m\ln\sigma + n\ln t \qquad \text{Equation 45}$$

The slope of the plot of the natural logarithm of creep against that of time yields the value of n at a particular stress as shown in equation 45. The parameter n used was therefore obtained by taking the average of n values at different stress levels. For the computation of the parameter m, constant time condition was applied so that a plot of the natural logarithm of creep strain against various stress (σ) conditions yields the slope m as shown in equation 45.

5.2.3 Retained clamp load at bolted joint

Since the elevated temperature behaviour of magnesium alloy at bolted joint is influenced by the alloys compressive yield and creep properties. It follows that the overall bolt load retention behaviour of AS41 magnesium alloy, which is the time-dependent stress retained at the bolted joint should be modelled taking into consideration the stress-strain relationship of the alloy at relevant temperature. The uniaxial stress-strain behaviours of joint material are expressed as equation 46 and 47.

$$\varepsilon_T = \varepsilon_e + \varepsilon_p + \varepsilon_c \qquad \text{Equation 46}$$

$$\varepsilon_T = \frac{\sigma}{E(T)} + A(T)\sigma^N + C\sigma^m t^n \qquad \text{Equation 47}$$

The application of this model takes into account the stress-strain response of AS41 within the elastic regime just before the yield deformation was attained. The plastic and creep deformation at the investigated temperature was also included. Hence in equation 46 and 47, ε_T represents the overall strain, ε_e the elastic strain, ε_p the plastic strain and ε_c the creep strain. E is the Young's modulus, T the temperature, A and N are material constants.

6 Results

6.1 As cast microstructure of AS41

The chemical composition of the AS41 alloy measured using spectroanalysis show 4.14 wt. % Al, 1.03 wt. % Si and 0.24 wt. % Mn. The remaining elements are in the range of ppm. The presence of α-Mg matrix are clearly observed from the micrograph in Figure 28. The precipitates are the Mg-Al rich phase, Al-Mn rich phase and the Mg-Si rich phase. The inter-dendritic regions are rich in solute elements giving colour contrast within the grains under optical microscope. The presence of Mg_2Si is clearly seen in the optical micrograph of AS41 as shown in Figure 28 in form of coarse “Chinese script”.

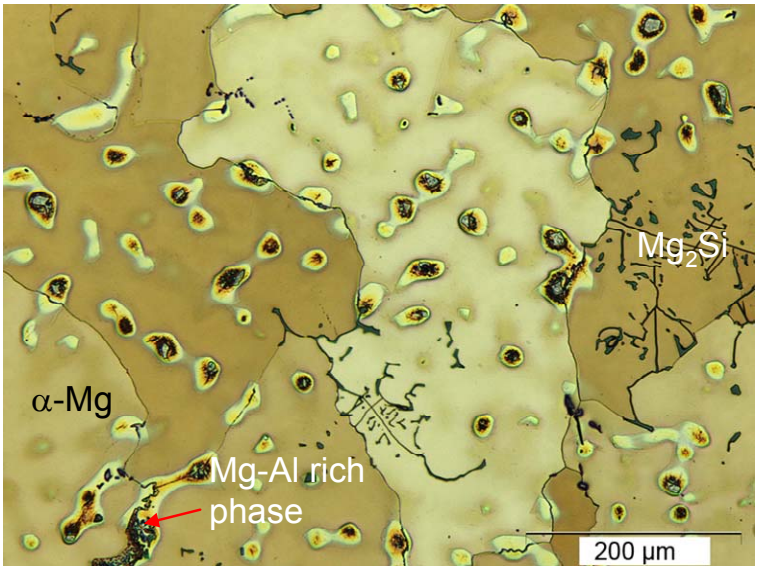

Figure 28: Optical micrograph of as cast AS41 Mg-alloy

The Mg_2Si are seen within the grains and close to the grain boundaries. The Mg-Al rich phases are observed mostly at the grain boundaries while the Al-Mn phase exist between the dendrites arms and also close to the grain boundaries. EDX analysis and SEM micrographs reveal that the Al-Mn phase exists in tiny blocky form of about 2-4 µm and in needle-like form. Figure 29 and Table 3 show SEM micrograph and quantitative EDX measurements on the as cast AS41 magnesium alloy used in this investigation. The phases present in this alloy were identified using TEM analysis. The phases include α-Mg, $Mg_{17}Al_{12}$, Mg_2Si, and Al-Mn phase.

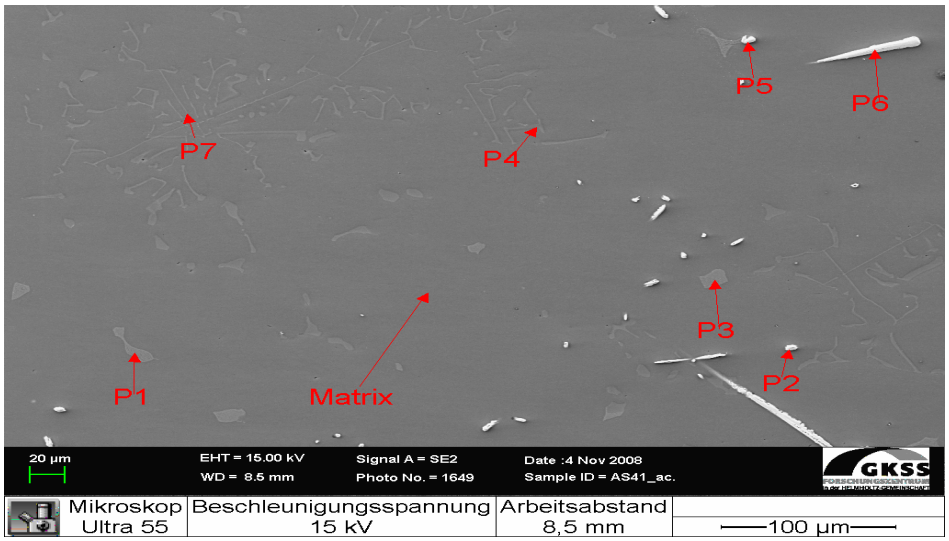

Figure 29: SEM micrograph and point analysis for AS41 Mg-alloy

Table 3: Quantitative EDX analysis for as cast AS41 Mg-alloy

Point analysis	Percentage of elements in the alloy	Mg	Al	Si	Mn	Zn	O
Matrix	Wt. %	97.51	-----	-----	-----	-----	2.49
	At. %	96.26	-----	-----	-----	-----	3.74
P1	Wt. %	62.45	35.01	-----	-----	-----	2.54
	At. %	63.82	32.23	-----	-----	-----	3.94
P2	Wt. %	-----	29.34	8.53	62.14	-----	-----
	At. %	-----	43.11	12.04	44.45	-----	-----
P3	Wt. %	67.18	31.90	-----	-----	0.92	-----
	At. %	69.79	29.86	-----	-----	0.36	-----
P4	Wt. %	69.69	-----	30.31	-----	-----	-----
	At. %	72.65	-----	27.35	-----	-----	-----
P5	Wt. %	0.32	41.56	3.19	54.94	-----	-----
	At. %	0.49	57.76	4.25	37.50	-----	-----
P6	Wt. %	1.14	37.01	5.26	56.60	-----	-----
	At. %	1.17	52.04	7.10	39.09	-----	-----
P7	Wt. %	71.02	-----	28.98	-----	-----	-----
	At. %	72.77	-----	27.23	-----	-----	-----

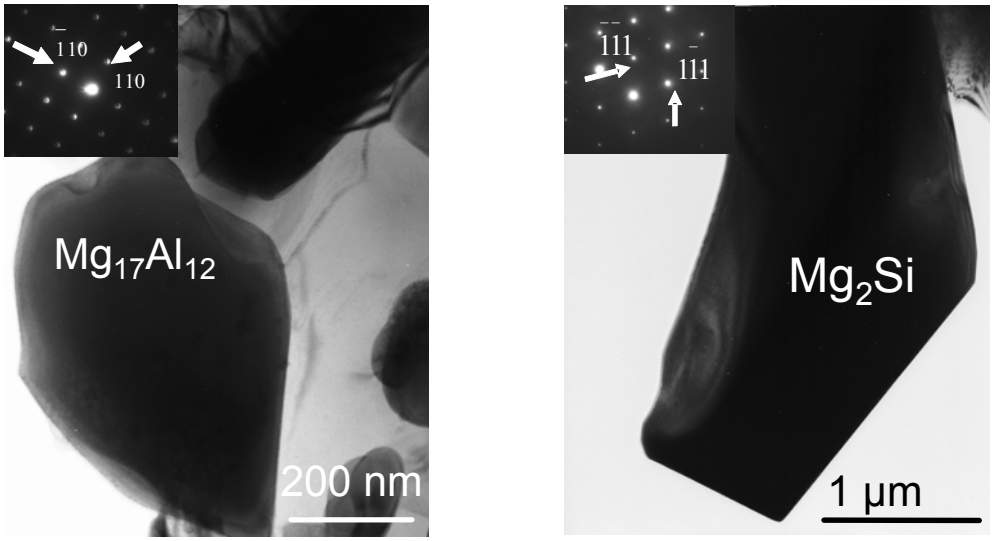

Figure 30: TEM micrograph of the ß-phase with zone axis [001] and that of Mg_2Si with zone axis $[0\bar{1}\bar{1}]$

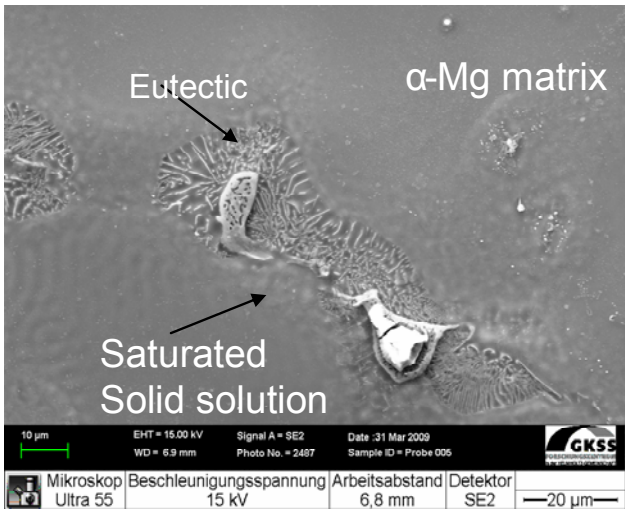

Figure 31: SEM micrograph of as cast AS41 showing primary α-Mg, eutectic and saturated solid solution

Appendix A shows the EDX mapping of the microstructure of AS41. Also shown in Appendix B are the diffraction peaks from the point analysis according to Table 3. Figure 30 show the TEM micrograph with diffraction pattern for $Mg_{17}Al_{12}$ and Mg_2Si. The magnified SEM micrograph of the as cast AS41 showing the α-Mg matrix, eutectic and saturated solid solution is also represented in Figure 31.

There are no twins visible on the as cast microstructure of AS41 under light optical micrograph and SEM micrograph. However, EBSD orientation map and EBSD image quality map of the as cast AS41 show that few twins exist on the microstructure of as cast AS41. The EBSD orientation map and EBSD image quality map of AS41 in the as cast condition are shown in Figure 32(a) and Figure 32(b) respectively.

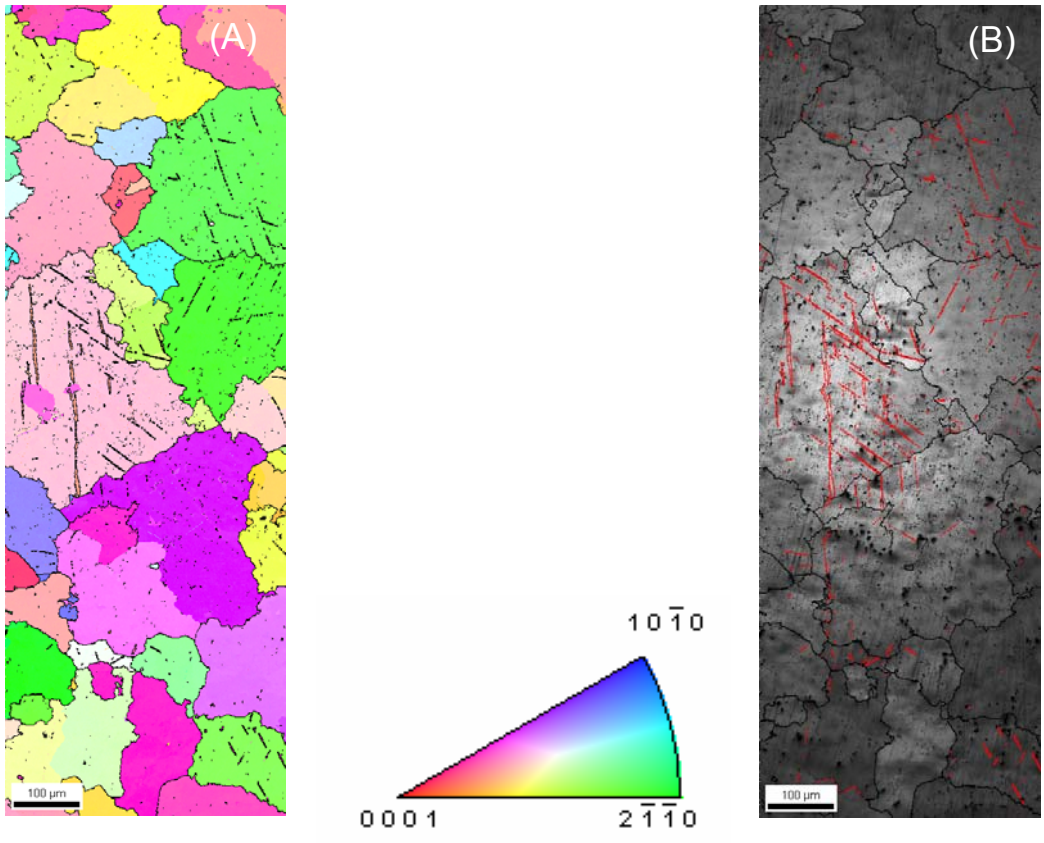

Figure 32 (a) EBSD orientation map, and (b) EBSD image quality map of as cast AS41

6.2 Porosity

Since the AS41 Mg-alloy investigated in this work is not high pressure die cast but permanent mould samples, the influence of porosity is expected to be minimal. The average density of 5 specimens shown in Table 4 is (1.77± 0.0031 g/cm^3) while the bulk porosity of the specimen is (<0.6%). Figure 33 also shows microstructure with porosity on permanent mould AS41 alloy.

Table 4: Density and porosity of permanent mould AS41 Mg-alloy

Samples	Weight in air (g)	Weight in ethanol (g)	Density of sample (g/cm^3)	Percentage (%) porosity
1	16.377	9.069	1.764	0.815
2	16.422	9.130	1.772	0.365
3	16.438	9.139	1.773	0.309
4	16.445	9.143	1.772	0.365
5	16.421	9.131	1.777	0.084

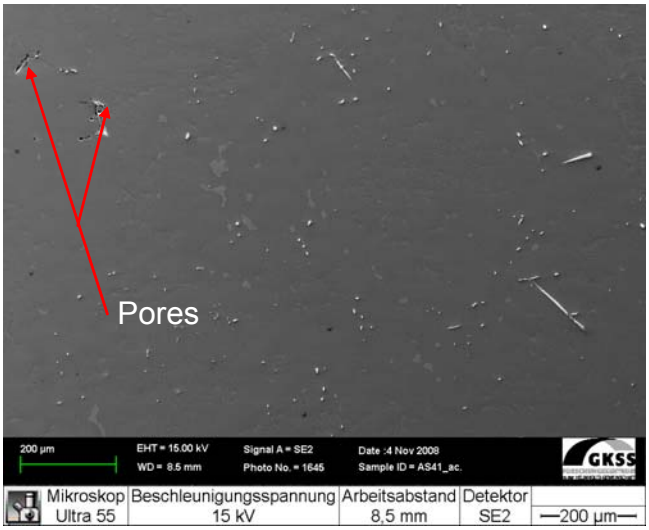

Figure 33: SEM micrograph of as cast AS41 showing the presence of porosity

6.3 Compressive creep result of AS41 Mg-alloy

Figure 34 shows typical compressive creep result of AS41 alloy representing a plot of creep deformation against time at 150 °C. The experiments were allowed to run for at least 200 hours at the temperature of interest. At low stress and temperature values of 40 MPa/ 100 °C, the experiment was terminated after 400 hours. Those of 70 MPa and 90 MPa were allowed to run until minimum creep rate was attained. For the purpose of comparison among stresses and temperature levels, the computation of total plastic deformation was restricted to 200 hours after creep inception. The minimum creep rates were computed by taking the minimum of the first derivative of the strain-time curve at the respective test conditions. The total plastic deformation and the minimum creep rate as determined in this work are shown in Table 5.

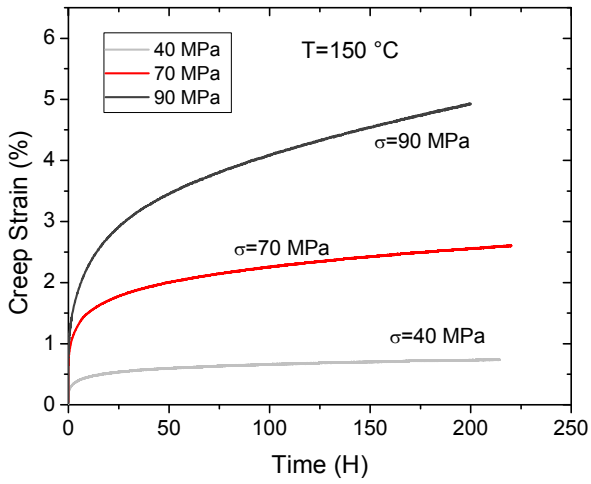

Figure 34: Creep deformation at different stress levels for 150 °C

It could be observed from Table 5 that the minimum creep rate increases with increasing stress and temperature condition. The same is also true for the plastic deformation calculated after 200 hours. The minimum creep rates of permanent mould AS41 alloy at 100 °C were averagely an order of magnitude lower than those at 125 °C and 150 °C.

The total plastic deformation as shown in Table 5 at 100 °C increases from 0.12 % at 40 MPa to 1.30 % at 90 MPa. At 175 °C, a plastic deformation of 0.87 % was measured at 40 MPa and 10.54 % at 90 MPa. That is over 9 % difference between 100 °C and 175 °C at 90 MPa stress level. At 200 °C and 70 MPa, the

total plastic deformation reaches 14.28 %. Figure 35 shows the bar chart comparative representation of creep deformation at 70 MPa for all temperature condition investigated. Figure 36 and Figure 37 show the plots of creep rates with respect to time for 150 °C and 175 °C conditions respectively.

Table 5: Creep results of permanent mould AS41

Test condition	Minimum creep rate ($\dot{\varepsilon}_s$)	Strain at 200 hrs (%)
100 °C/40 MPa	1.85E-10	0.12
100 °C/55 MPa	3.31E-10	0.52
100 °C/70 MPa	5.71E-10	1.28
100 °C/90 MPa	1.83E-09	1.30
125 °C/40 MPa	1.31E-09	1.22
125 °C/55 MPa	2.11E-09	1.41
125 °C/70 MPa	2.75E-09	1.65
125 °C/90 MPa	9.80E-09	2.17
150 °C/40 MPa	2.35E-09	0.75
150 °C/55 MPa	3.53E-09	1.00
150 °C/70 MPa	9.38E-09	2.60
150 °C/90 MPa	2.53E-08	4.90
175 °C/40 MPa	2.36E-09	0.87
175 °C/55 MPa	5.52E-09	1.50
175 °C/70 MPa	2.82E-08	4.95
175 °C/90 MPa	1.17E-07	10.54
200 °C/40 MPa	4.54E-09	1.48
200 °C/70 MPa	1.94E-07	14.28

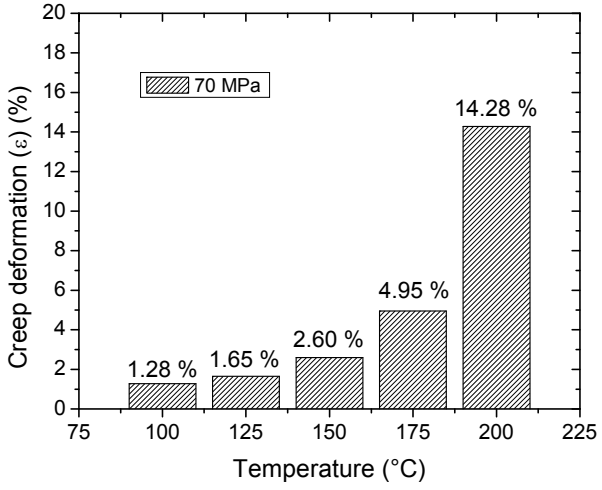

Figure 35: Total plastic deformation measured after 200 hrs at 70 MPa

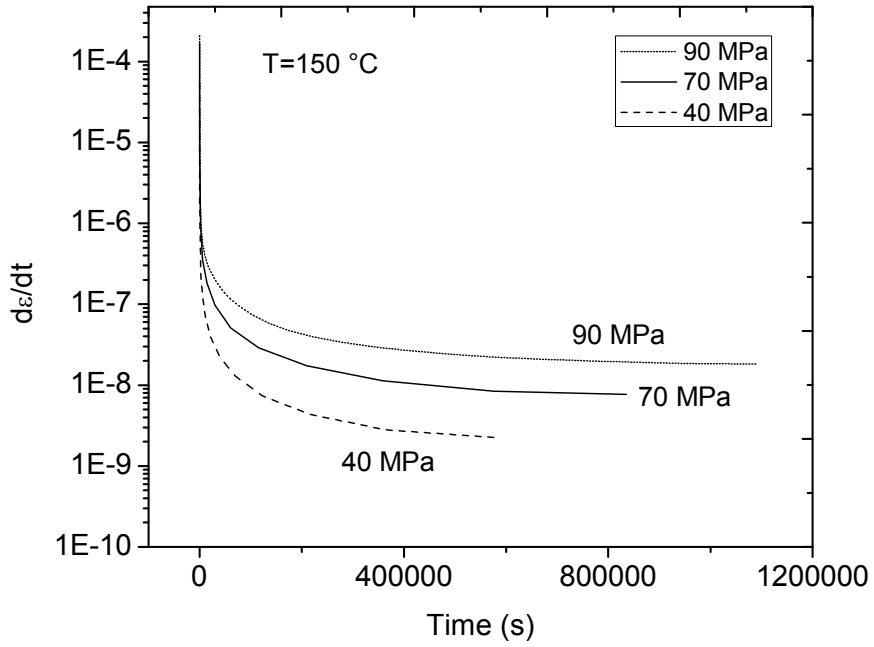

Figure 36: Creep rate with respect to time for permanent mould AS41 at 150 °C

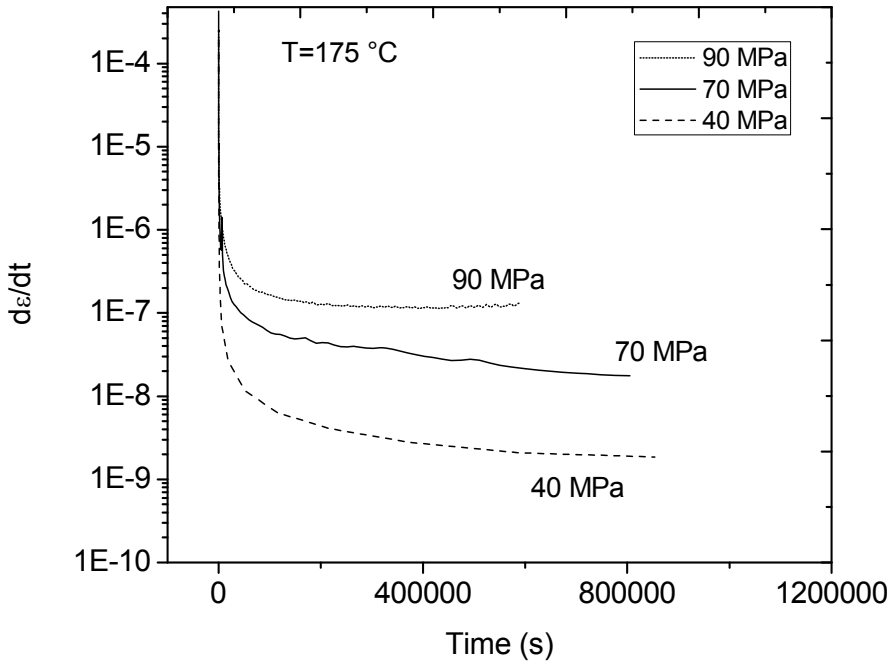

Figure 37: Creep rate with respect to time for permanent mould AS41 at 175 °C

6.3.1 Calculation of stress exponents for permanent mould AS41

The stress dependence of minimum creep rate as expressed by Norton's equation 8 was used in the evaluation of the stress exponents. A plot of the natural logarithm of ($\dot{\varepsilon}_s$) against that of (σ) gives a straight line whose slope is *n* at the same temperature. The stress exponent *n* as seen in Figure 38 ranges from 1.3 at low stress levels to 6 at high stress of 70 and 90 MPa. Information of the creep mechanism associated with these numbers is discussed in section 7.2.

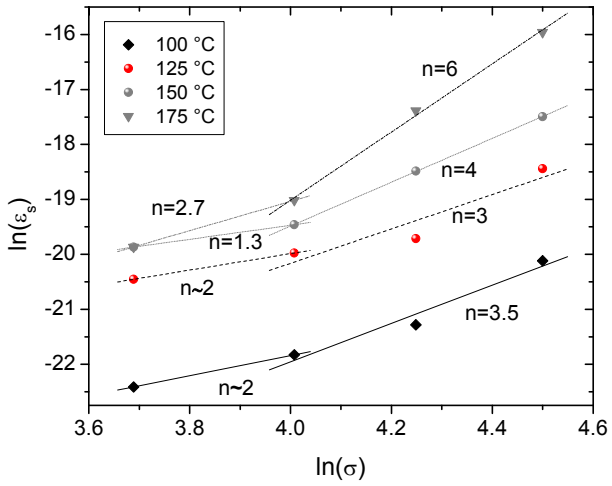

Figure 38: Stress exponents (n) at the investigated temperature

6.3.2 Calculation of activation energy for creep of AS41

The activation energy for creep (Q_c), which gives information about the temperature dependence of the minimum creep rate was also computed using equation 8. A plot of the natural logarithm of the different minimum creep rates ($\dot{\varepsilon}_s$) as shown in Table 5 against the inverse of temperature (*1/T*) yields a straight line whose gradient is equal to ($-Q_c/R$). Figure 39 show the (Q_c) values at different stress conditions. At 55 MPa, (Q_c) value was 50 kJ/mol. 100 kJ/mol and 72 kJ/mol were calculated between temperatures of 200 °C and 100 °C at 70 MPa. The activation energy for creep computed at 90 MPa was 74 kJ/mol. It could be seen from Figure 39 that the activation energy for creep that are calculated for the permanent mould AS41 within the condition investigated in this work are well below that of activation energy for self diffusion of

magnesium. The relationship between creep mechanism and the activation energy of creep with respect to AS41 are further discussed in section 7.2.

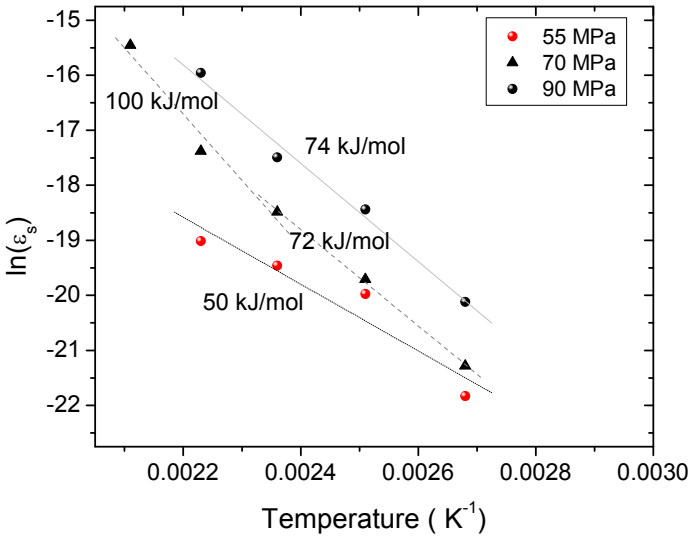

Figure 39: Temperature dependence of the minimum creep rate

6.3.3 Microstructure evolution of AS41 after creep test

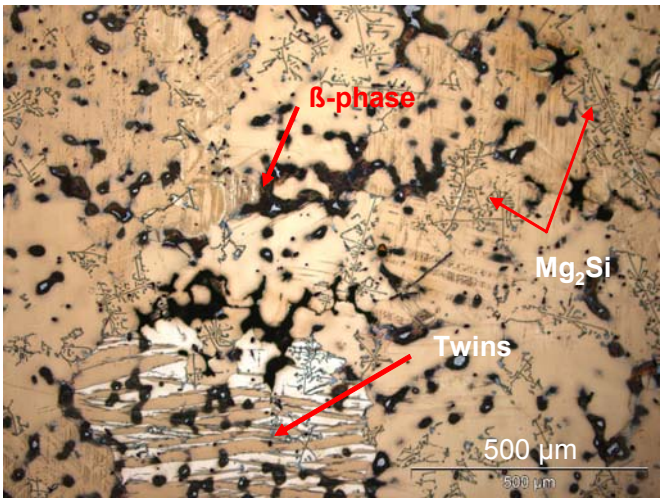

Figure 40: AS41 after creep test at 150 °C/ 70 MPa

Figure 40 shows the optical micrograph of permanent mould AS41 after creep test at stress of 70 MPa and temperature of 150 °C. The presence of twins is clearly seen on most of the grains. Patches of dark regions consist of coarse

incoherent β-phase within the grains and close to the grain boundary. SEM micrograph in Figure 41 shows the presence of pores in the supersaturated eutectic α-Mg matrix. See also Appendix E and Appendix F. Precipitated and coarsened β-phases are observed in the SEM micrograph. There is no detectable change on the Mg_2Si precipitate as can be seen from Figure 41.

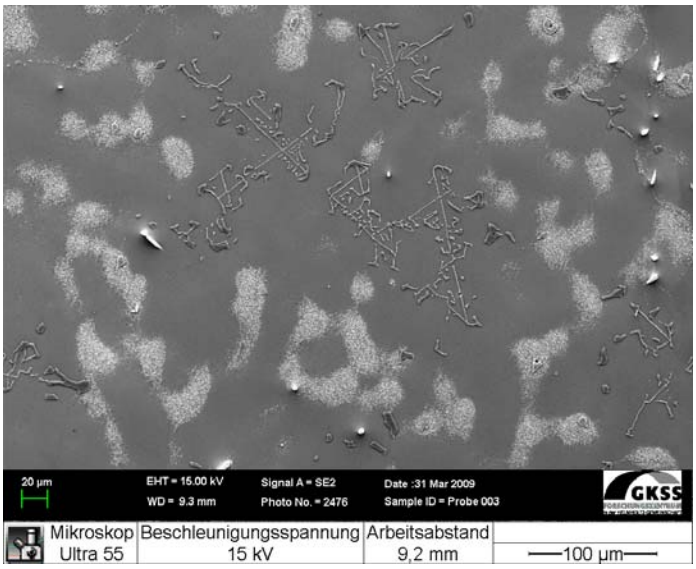

Figure 41: SEM micrograph of AS41 after creep test at 175 °C/ 70 MPa

The TEM micrograph in Figure 42 show formation of subgrains designated as (A) and dislocation walls as (B). The presence of mangled dislocation (C) is also observed. It could be seen that dislocation density increases with temperature when compared 125 °C/70 MPa and 175 °C/ 70 MPa micrograph in Figure 42.

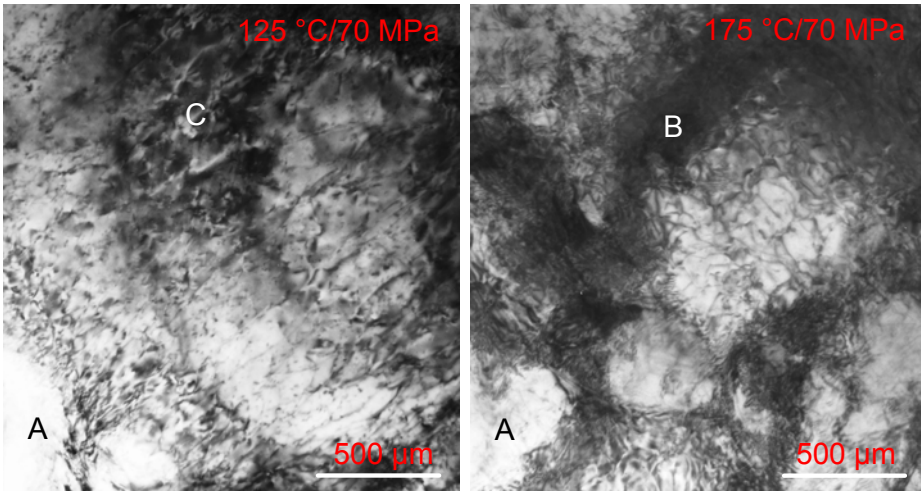

Figure 42: TEM micrograph of AS41 after creep at 125 °C and 175 °C with 70 MPa stress

6.4 BLR experimental results

The result of the bolt load retention test carried out in this work using continuous load cell measuring technique as described in section 4.7 are shown here. Figure 43 shows the BLR behaviour of permanent mould AS41 magnesium alloy investigated. This covers stresses of between 20 MPa and 70 MPa at 100 °C and 125 °C. Sample dimension used is equal to 15 mm thickness and 20 mm external diameter as shown in Figure 23(b).

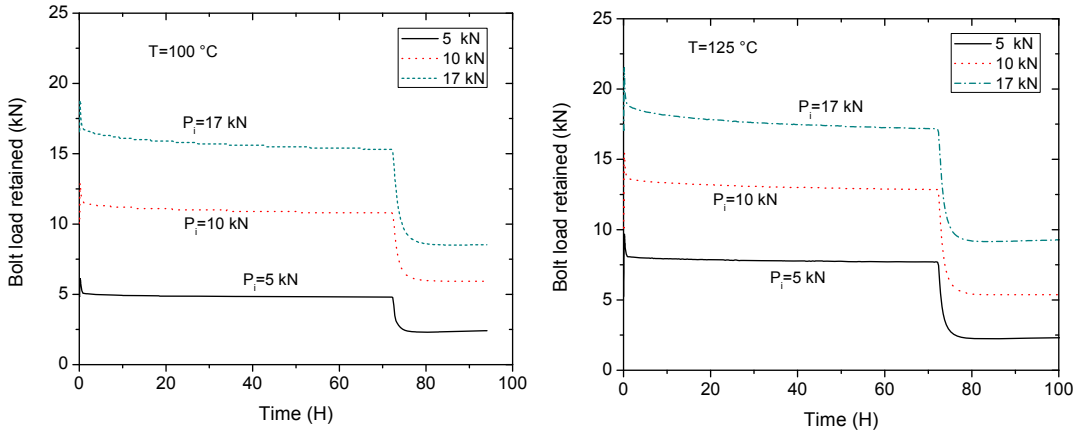

Figure 43: BLR Result of permanent mould AS41 Mg-alloy at 100 °C and 125 °C

Figure 43 show retained bolt load of 90 % for 5 kN load and 94 % for both 10 kN and 17 kN initial preload at 100 °C after 72 hours. From the result as shown in Figure 43, it is also observed that at 125 °C and restricted time frame of 72 hours, permanent mould AS41 magnesium alloy loss approximately 20 % of its fastener clamp load. When the bolted couple was cooled down to room temperature, approximately 50 % of the initial load was lost. For loads of 5 kN, 10 kN and 17 kN, AS41 retained 79 %, 83 % and 80 % respectively at 125 °C. The ratio of P_f/P_i retained for AS41 alloy at 5 kN, 10 kN and 17 kN was 0.43, 0.53 and 0.54 respectively at 125 °C.

The same trend of bolt load loss is also seen in Figure 44 at 175 °C. After 72 hours of BLR test, 9.9 kN load was retained for 10 kN preload and 11.8 kN was retained for 17 kN preload. The BLR of permanent mould AS41 at 125 °C and 175 °C are also expressed as stress (MPa) with respect to time (H). These are shown in Appendix K and Appendix L.

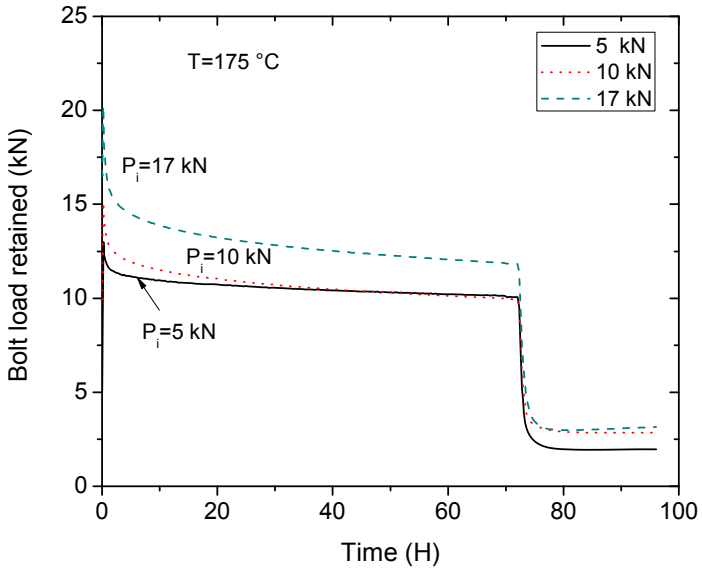

Figure 44: BLR Result of permanent mould AS41 Mg-alloy at 175 °C

6.5 Microstructure of AS41 after BLR test

Optical micrographs of AS41 alloy after BLR test are shown in Figure 45 and Figure 46. The micrographs were taken parallel to the loading direction. It could be seen that twins predominated most part of the microstructure of the BLR samples. Some grains within the microstructures were obviously untwined.

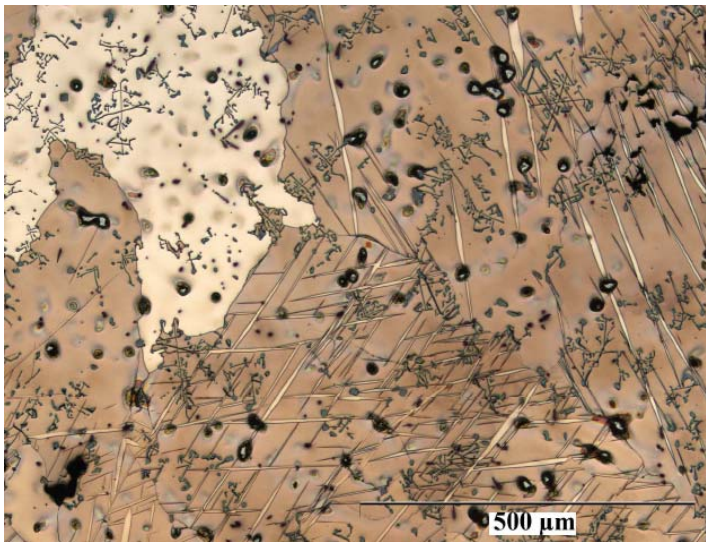

Figure 45: Sample after BLR test at 17 kN/ 125 °C

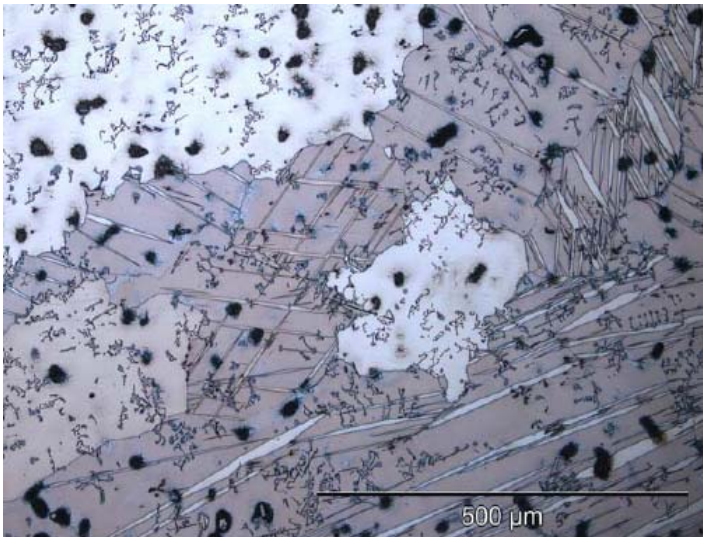

Figure 46: Sample after BLR test at 17 kN/ 175 °C

SEM micrographs were subsequently taken on the samples perpendicular to the loading direction. The SEM micrograph is shown in Figure 47. This also

reveals the presence of twins within the microstructures. Further observations was made using TEM on the samples and these show dislocation networks, and twins within the α-Mg matrix and at the grain boundaries. Figure 48 shows bright field TEM image of AS41 after BLR test at 17 kN/ 125 °C.

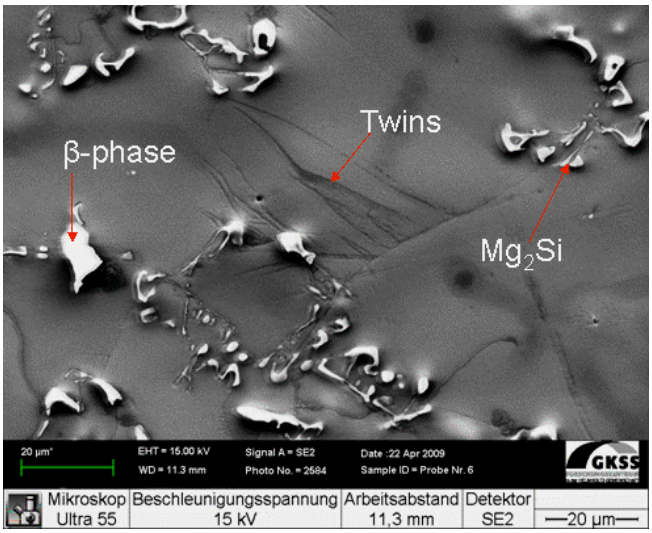

Figure 47: SEM micrograph of AS41 after BLR test at 17 kN/ 150 °C

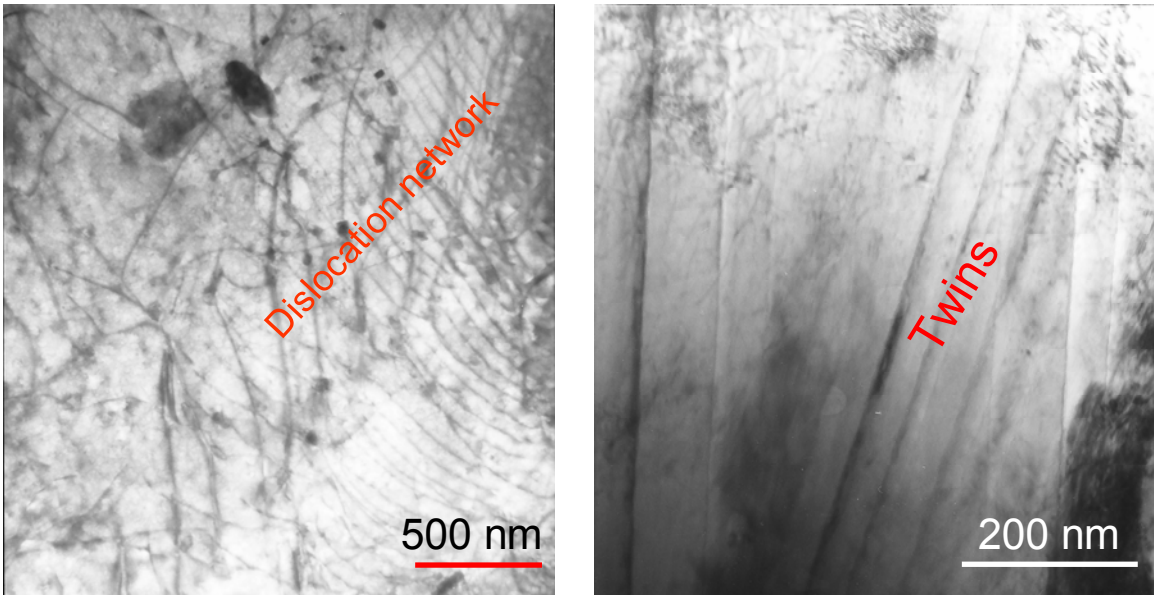

Figure 48: TEM micrograph of AS41 after BLR test at 17 kN/ 125 °C

In Figure 49, the presence of subgrains labelled (1) and dislocation walls (2) were clearly observed within the microstructure of AS41 at higher temperature

of 175 °C and load of 17 kN. Dislocation tangles (3) were also present as seen in Figure 49. Figure 50 shows TEM image of β-phase after BLR at 17 kN/ 175 °C which are normally observed near the dendrite or grain boundaries. They have preferential growth orientation making them have morphology of lamellar.

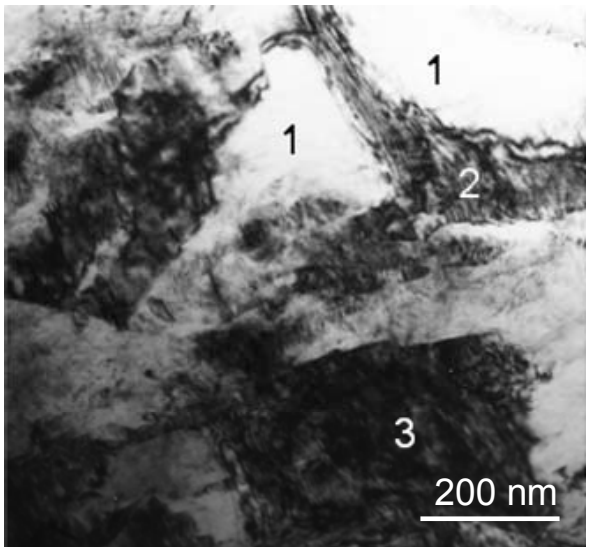

Figure 49: TEM micrograph of AS41 after BLR at 17 kN/ 175 °C

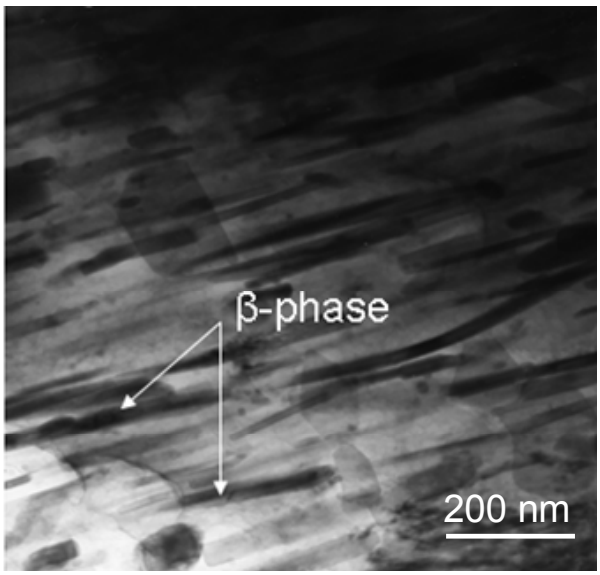

Figure 50: TEM image of β-phase after BLR at 17 kN/ 175 °C

6.6 Factors influencing BLR

6.6.1 Effect of initial load and temperature

The initial load and the operational temperature during bolt load retention test play very important role in determining the degree of clamp load relaxation at bolted joints. The higher the load, the more the stress acting on the specimen and this invariably leads to more deformation on the sample. The result is loss of fastener clamp load at such a joint. Figure 51 shows the influence of initial load (P_i) and temperature on the bolt load retention response of AS41. The symbol C_o represents the ratio of P_R to that of P_K expressed in percentage. This indicates the degree of load retained at test temperature. It could be seen from Figure 51 that the higher the temperature, the more the relaxation experienced by the Mg-alloy. From Figure 51, it is observed that at low stress level and moderate temperature, up to 80 % of the load was retained at test temperatures. Loss of approximately 30 % was experienced for loads of 10 kN and 17 kN which corresponds to 40 MPa and 70 MPa at 150 °C. The load loss increased to 36 % and 42 % at 175 °C for 10 kN and 17 kN load respectively.

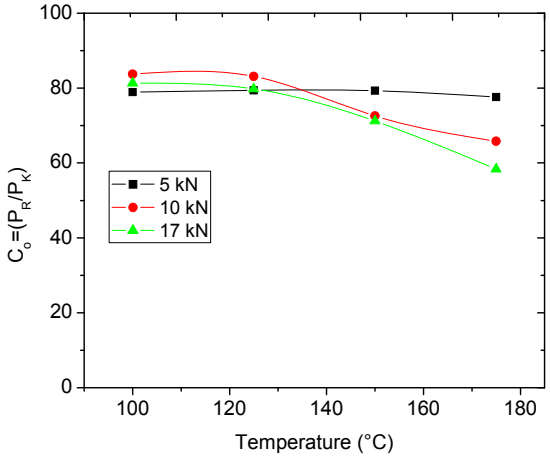

Figure 51: Effect of initial load and temperature on BLR of AS41 Mg-alloy

The same is also true when C_T as shown in Figure 52 is plotted against temperature for respective initial loading conditions. C_T is the sum of the total bolt load retained on the bolted couple throughout the whole process. This is computed by taking the ratio of the final load P_F to that of P_I. This gives an overview of the load behaviour between P_I and P_F after the sample has suffered creep between P_K and P_R. Figure 52 shows a plot of C_T against temperature.

The temperatures here represent the test temperature before cooling the bolted couple back to P_F at room temperature.

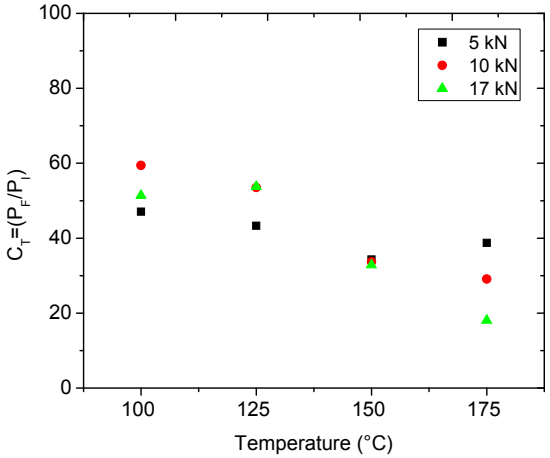

Figure 52: Effect of initial and final load on BLR of AS41 Mg-alloy

From Figure 52, one observes more than 50 % load loss when specimens were cooled down to room temperature. This is for 150 °C and 175 °C in all initial load conditions investigated. At 125 °C, more than 50 % of the initial load was retained for stresses of 40 MPa and 70 MPa on the AS41 Mg-alloy. Generally speaking, the effect of deformation suffered by the AS41 sample during the isothermal phase of P_K and P_R were reflected on the overall BLR results of AS41. In this investigation, the higher the temperature and load, the more the bolt load loss for permanent mould AS41 alloy.

6.6.2 Influence of effective length

In order to investigate the influence of effective length on BLR response of AS41 Mg-alloy, the thickness of the sample was doubled. This means that the effective length of the steel bolt was increased by 15 mm. This increase in length brought the effective length of the bolt to 52 mm. The effective length of the bolt is defined here as the sum of the engagement length plus 0.5 of the head bolt and nut. The term H in Figure 53 and Figure 54 stands for the height of the AS41 sample used in this investigation. From the experimental results in Figure 53, it is observed that the couple with longer effective length show higher bolt load value as compared to that of shorter effective length. An increase of 31 % in bolt load is witnessed at P_k with respect to the initial preload of 17 kN for

the longer effective length couple. In the case of shorter effective length couple, an increase of 20.4 % was recorded at P_k for the same initial preload.

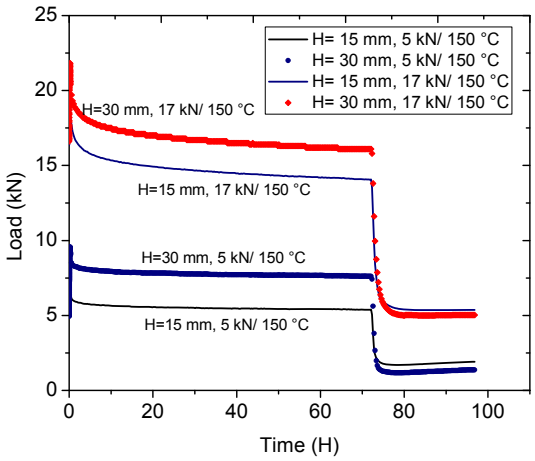

Figure 53: Plot of effective lengths at 150 °C for loads of 5 kN and 17 kN

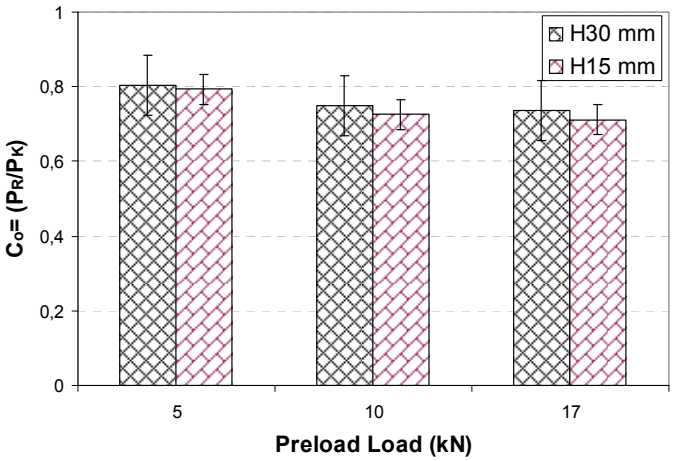

Figure 54: Plot of retained load at 150 °C for longer and shorter engagement length

From Figure 53, an average difference of 2 kN exists between longer and shorter engagement length with respect to the measured bolt load at test temperature as can be seen from the experiment. The percentage bolt load retained for both longer and shorter lengths after 72 hours at 150 °C were close to each other at different preload. At 17 kN preload, a P_r/P_k ratio of 74 % is measured for the longer length as compared to 71 % for the shorter length. For the preload of 10 kN, 75 % load was retained for the longer length while 73 % was recorded for the shorter length. At 5 kN preload, 80 % of the load was

retained as against 78 % for the longer and shorter effective length respectively. Figure 54 shows a comparative plot of the retained load at 150 °C for AS41 alloy. It could be said that the longer effective length retained slightly higher bolt load than that of the shorter.

6.6.3 Effect of bolt stiffness

The stiffness of a joint is determined mainly by the effective elastic moduli of the joint members. In this investigation, high Young's modulus of either bolt or nut results in higher fastener clamp load retention at test temperature. The result of a 30 mm height and 20 mm diameter AS41 tested with steel bolt/ steel nut couple were compared to that of aluminium bolt/ aluminium nut joint. The BLR profile measured for this test is shown in Figure 55 and Figure 56.

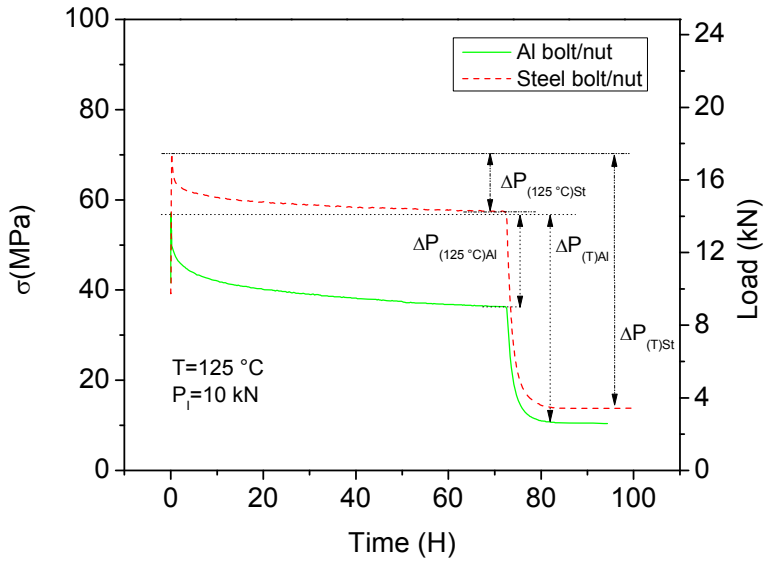

Figure 55: Steel bolt-Aluminium bolt joint tested at 10 kN 125 °C

It could be seen from the plot that the stiffer steel joint retained more load than the less stiff aluminium joint at test temperature. A ratio of P_r/P_k shows clamp load retention of 69 % and 82 % for steel joint at 17 kN and 10 kN initial load respectively. That of aluminium shows 58 % and 64 % for the same condition of initial loads of 17 kN and 10 kN respectively. That is 11 % difference in retained bolt load for the 17 kN preload condition and 18 % difference for the 10 kN preload. The load retained for the 10 kN preload is however larger than that of

17 kN initial load in both the stiffer steel bolted joint and in aluminium bolted joint.

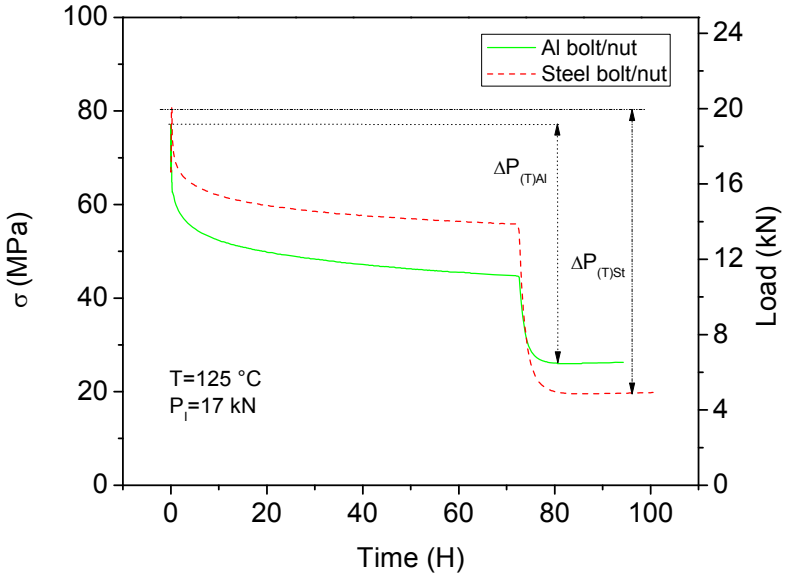

Figure 56: Steel bolt-Aluminium bolt joint tested at 17 kN 125 °C

The total load change $\Delta P_{(T)}$ which is the difference in bolt load from the highest load reached at test temperature (P_k) and the final load (P_F) at room temperature increased for steel bolted couple. At 17 kN preload and temperature of 125 °C, $\Delta P_{(T)Al}$ was 65.9 % while $\Delta P_{(T)Steel}$ was 75.6 %. For the 10 kN preload at 125 °C, $\Delta P_{(T)Al}$ and $\Delta P_{(T)Steel}$ were 81.7 % and 80.4 % respectively.

6.7 Baseline test

Baseline test were conducted in this work to determine the degree of bolt load retention on the testing equipment itself. These were carried out using steel samples of the same equivalent geometrical shape and dimension as that of the AS41 component. Figure 57 show the result of typical baseline test which was done at 125 °C for loads of 5 kN, 10 kN, 12 kN and 17 kN which corresponds to 20 MPa, 40 MPa, 50 MPa and 70 MPa respectively.

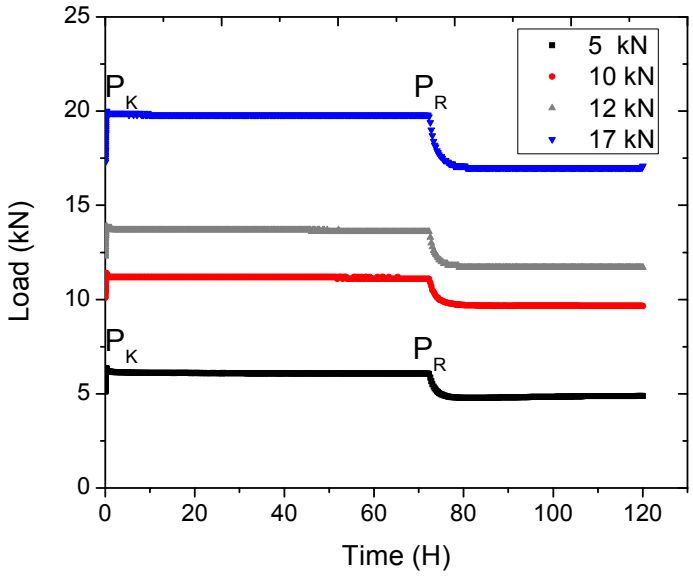

Figure 57: Base line test with steel specimen at 125 °C

The carrying out of baseline test to determine the “baseline profile” of the testing machine is strongly recommended. This is to insure proper evaluation of the overall BLR behaviour of the magnesium component at the interested temperature and stress condition. The baseline test should be restricted to the exact duration and load condition of the proposed BLR test.

Table 6 show important elevated temperature baseline tests between 100 °C and 175 °C computed as the ratio of P_R to P_K. The averages of baseline results of the investigated condition were grouped according to temperature. From the results, it is observed that the degree of bolt load loss on the test equipment increases with temperature.

Table 6: Base line results at different temperature for 15 mm height sample

Temp. (°C)	Load (kN)	P_R/P_K	Average	Standard deviation
100	5	0.9873	0.9912	± 0.0061
	10	0.9889		
	12	0.9891		
	17	0.9995		
125	5	0.9574	0.976	± 0.0138
	10	0.9798		
	12	0.9778		
	17	0.9905		
150	5	0.9376	0.947	± 0.0108
	10	0.9547		
	12	0.9372		
	17	0.9574		
175	5	0.9275	0.942	± 0.0166
	10	0.9289		
	12	0.9487		
	17	0.9620		

6.8 Constant and interrupted BLR tests

In order to simulate the thermo-cyclic loading condition that is often associated with automotive power train components, interrupted BLR test was conducted. Alternating temperature of 125 °C or 150 °C and room temperature was used. For 10 kN/ 125 °C and 17 kN/ 125 °C restricted at 225 hours, constant temperature of 5 hours and interrupted time of 3 hours were maintained. The same condition is also used for that of 150 °C restricted at 350 hours. A comparative plot of constant and interrupted temperature is shown in Figure 58.

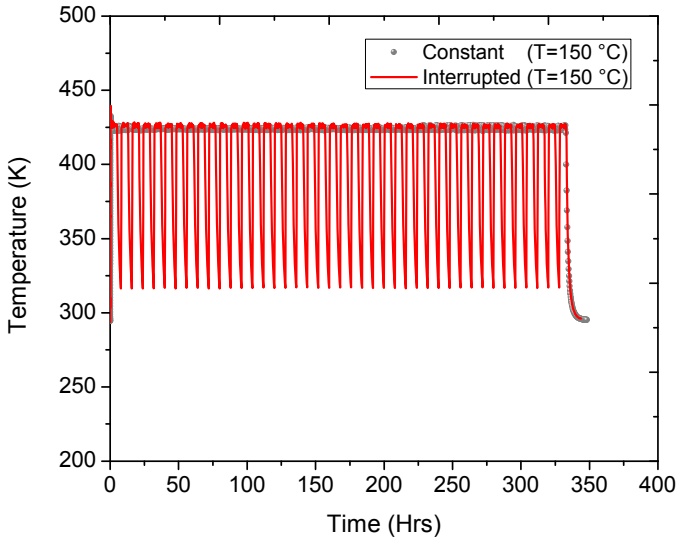

Figure 58: Constant and interrupted temperature profile of a BLR test at 150 °C

The interrupted BLR results were compared to that of the constant temperature condition. The results are shown in Figure 59 and Figure 60. From Figure 59(a&b), it is observed that at 125 °C and stresses less than the yield stress of AS41 Mg-alloy, the BLR results for both constant and interrupted condition show approximately the same relaxation behaviour. 10 kN corresponds to 40 MPa while 17 kN is equal to 70 MPa in this investigation. At stresses close to the yield stress of the alloy (Appendix C), the BLR test conducted at interrupted temperature condition shows better bolt load retention than that conducted under constant temperature condition. The improved retained bolt load is 3.5 % at 125 °C and up to 6.5 % at 150 °C for 17 kN initial preload. Figure 60 shows the compared result at 150 °C.

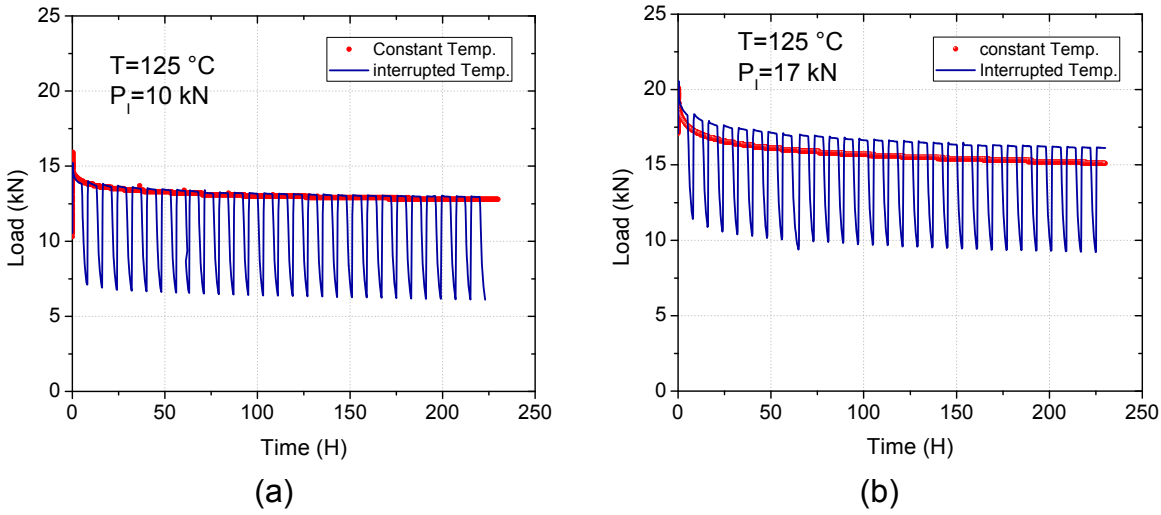

Figure 59: Constant and interrupted BLR test at 10 kN/ 125 °C and 17 kN/ 125 °C

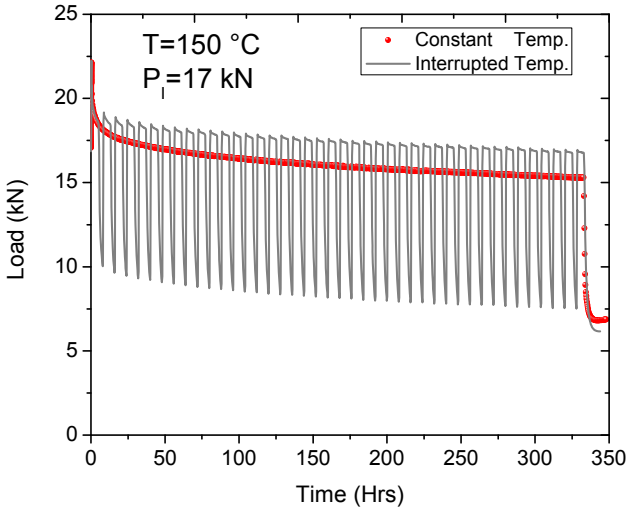

Figure 60: Constant and interrupted BLR test compared for AS41 at 150 °C

6.9 Modelled BLR result

6.9.1 Compliance-creep approach

The values of compliances used for the computation of the equivalent compliance C_{eq} are as follows, C_{mg} = 1.41x10^{-9} m/N, C_{bolt} = 3.16x10^{-9} m/N, C_{washer} = 6.57x10^{-11} m/N and 2.25x10^{-10} m/N for C_{sensor}. Figure 61 show prediction of different loading conditions (5 kN, 10 kN, 12 kN and 17 kN) at various temperatures for AS41 magnesium alloy modelled in this work. The plot represents the highest clamp load reached *P(T)* at different temperatures (100 °C, 125 °C, 150 °C and 175 °C) for specific initial loading condition P_o.

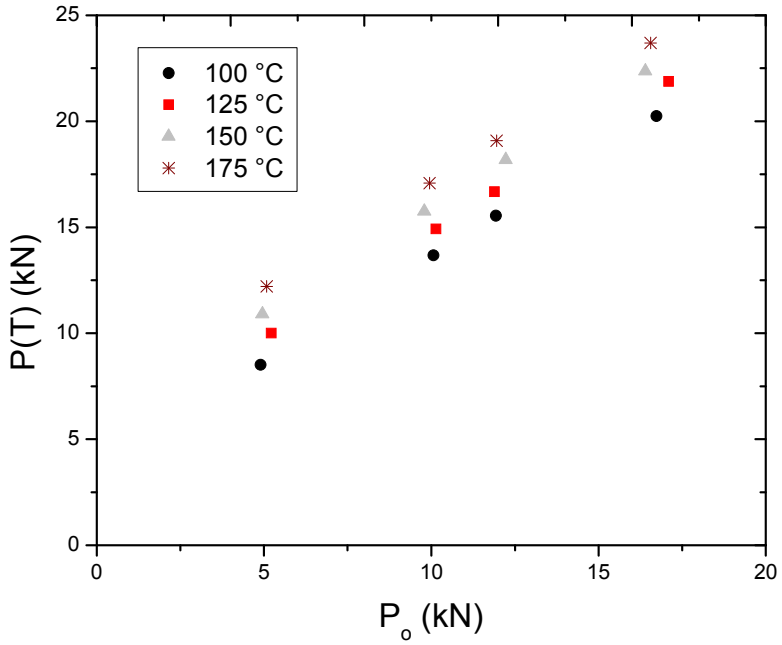

Figure 61: Prediction of the highest load attained according to equation 39

From equation 39 prediction as shown in Figure 61, it is observed that *P(T)* increases with increase in temperature and load. The trend of the result is the same in all the investigated stress and temperature ranges. The results as predicted by equation 39 for the highest load reached at point P_k were compared with the experimental results. This is shown in Figure 62 for temperature conditions between 100 °C and 175 °C. From the plot in Figure 62, it could be seen that the equation makes reasonable prediction within the temperature range studied in this work. The trend is the same for all conditions with equation 39 making slightly higher prediction than the experiments.

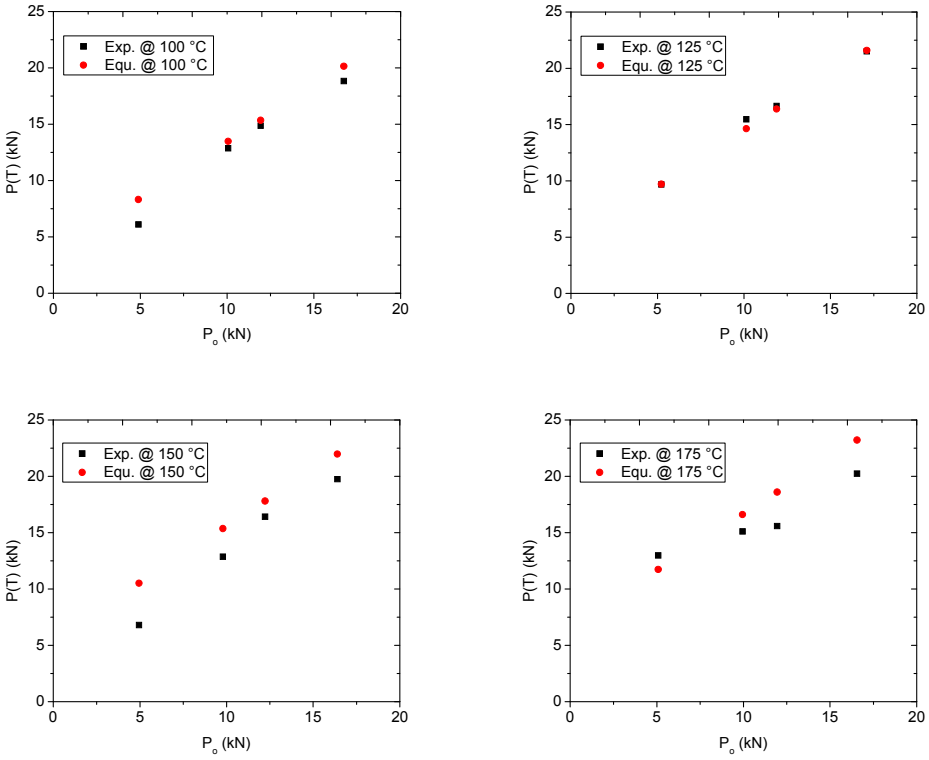

Figure 62: Comparison of equation 39 prediction and experiment

Figure 63 show plot for the evaluation of compressive creep parameter (n_i) according to equation 41. It could be seen that higher n_i values were calculated for higher temperature and stress conditions. Equation 43 was subsequently used to evaluate the time dependent bolt load loss at the AS41 joint.

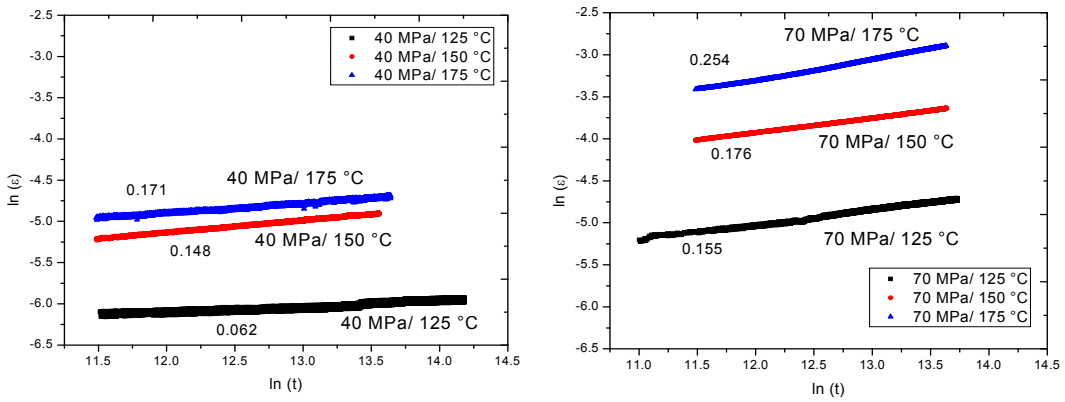

Figure 63: Plot of equation 41 for computation of n_i values

Figure 64 show the time dependent bolt load loss prediction due to creep according to equation 43. The values of K_i used in this work are (0.2143, 0.2132, 0.2126 at 125 °C, 150 °C and 175 °C) respectively. After 72 hours of bolt load, equation 43 made a bolt load prediction of 14.5 kN for permanent mould AS41 loaded at 17 kN initial load. This decreased to 13.7 kN and 11.9 kN at 150 °C and 175 °C for the same initial preload. At 10 kN preload, equation 43 made a BLR prediction of 12.4 kN after 72 hours at 125 °C, this became 11.2 kN at 150 °C and 10.6 kN at 175 °C. Bolt load retention behaviour was also modelled for AS41 for longer duration of up to 350 hours at 10 kN and 17 kN/ 125 °C. The equation predictions are similar to those of Figure 64 restricted at 72 hours.

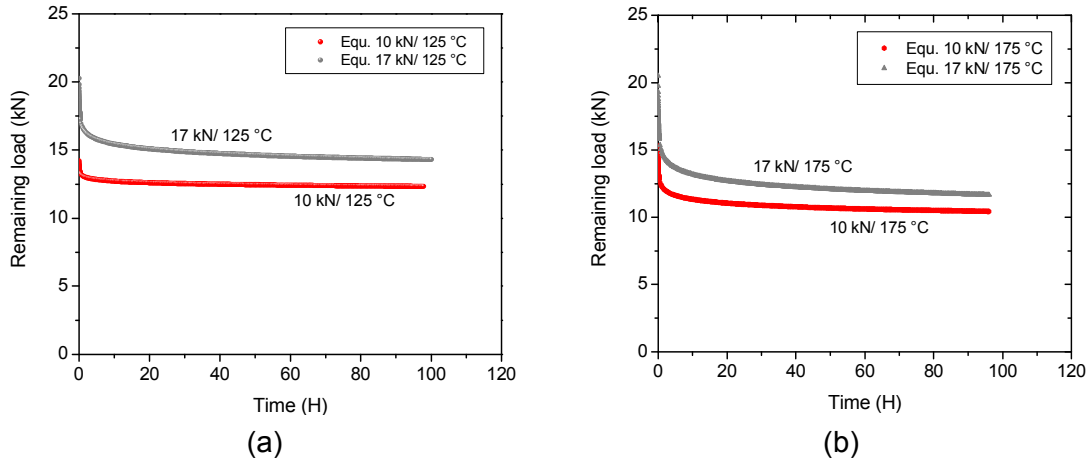

Figure 64: Time dependent bolt load prediction according to equation 43 at (a) 125 °C and (b) 175

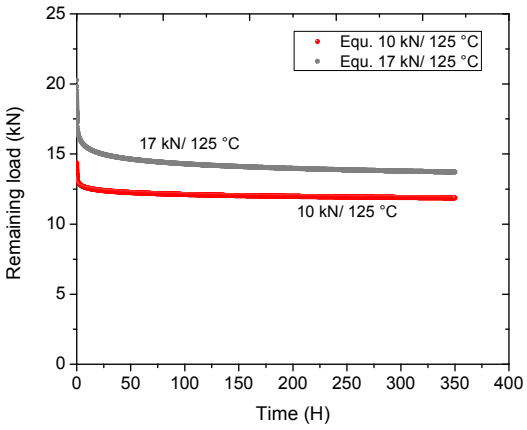

Figure 65: BLR prediction according to equation 43 at 125 °C up to 350 hours

6.9.2 FEA approach

Where as typical experiments for AS41 were carried out in our lab as explained already in the experimental section, information about the steel bolt material properties were sourced from open literature. For clarity, detailed results of the yield strength, ultimate compressive strength and thermal expansion coefficients are shown in Appendix C and Appendix D. This is because the focus of this work is not on compression test or thermal expansion properties of AS41. Effort is made to limit the result in this section on the FEA modelling of bolted AS41 Mg-alloy.

6.9.2.1 Application of FEA on bolted joint

The tightening of the bolted couple was such that during the application of torque on the bolt head, the end part of the M10 steel bolt was assumed to undergo uniform displacement. The bolt itself is strained in tension concurrently during tightening of the bolt. By surface contact, the head of the bolt exerts compressive stress on the AS41 magnesium alloy through the washer and the high precision steel load cell which is between the bolt head and the magnesium alloy.

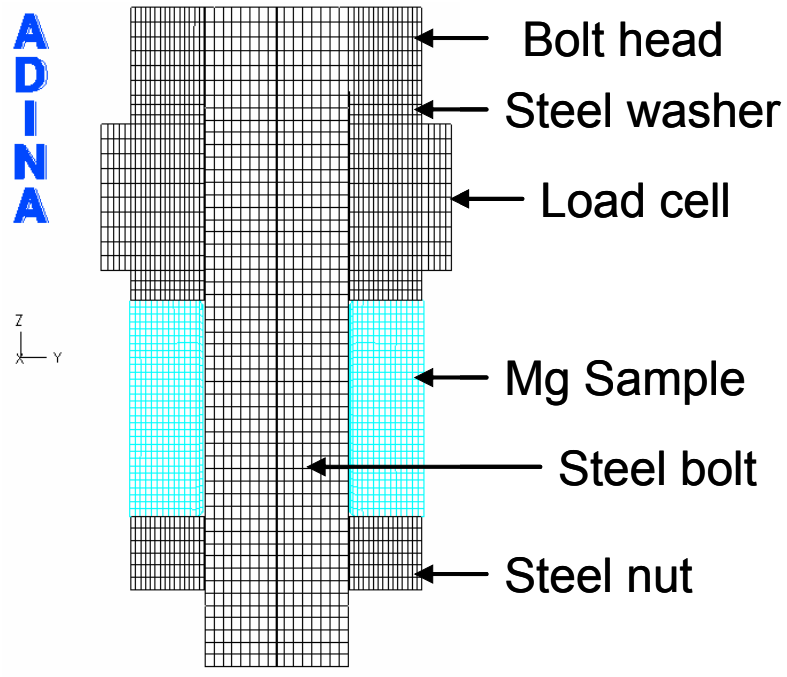

Figure 66: Finite element mesh for the bolted joint

Refer to Figure 26 for the schematic representation of a cylindrical through bolt permanent mould AS41 alloy used. Figure 66 shows the finite element mesh of the bolted joint. The stress distribution in a typical bolt joint with a load cell is shown in Figure 67. From the model, it could be observed that the stresses on the bolted joint are not uniformly distributed within its members.

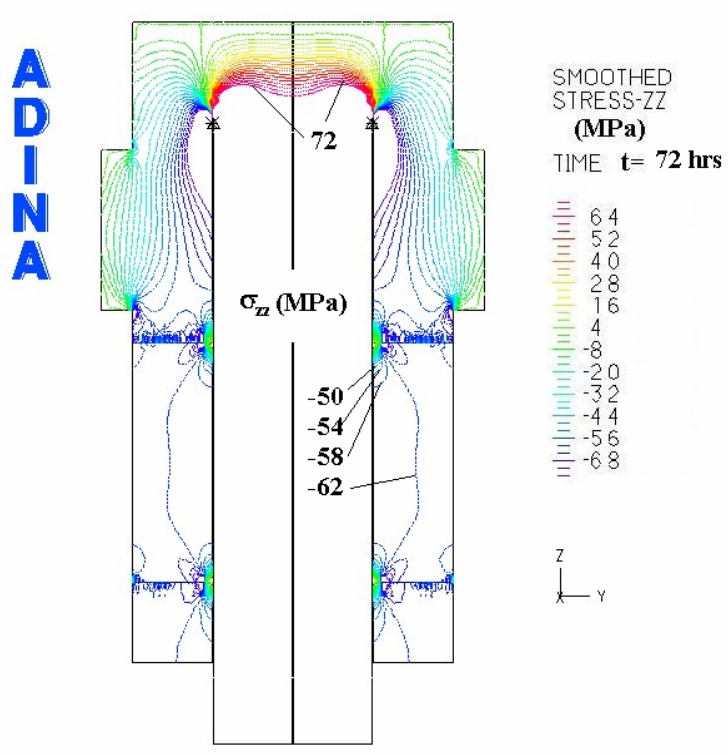

Figure 67: Stress distribution in a bolt joint torqued with a 70 MPa stress

6.9.2.2 Three parameter creep equation and bolt load prediction

Compressive creep test were carried out as mentioned earlier in the experimental section in other to evaluate the three parameters used in this work. Since a through hole cylindrical AS41 magnesium alloy used for BLR was also employed in the creep test, this produced a gauge diameter of 17 mm, height of 15 mm and stressed area of 227 mm^2. The creep deformation with respect to time is shown in Figure 68 at different stress levels for temperatures of 125 °C and 150 °C for the evaluation of parameter *n* with respect to equation 45.

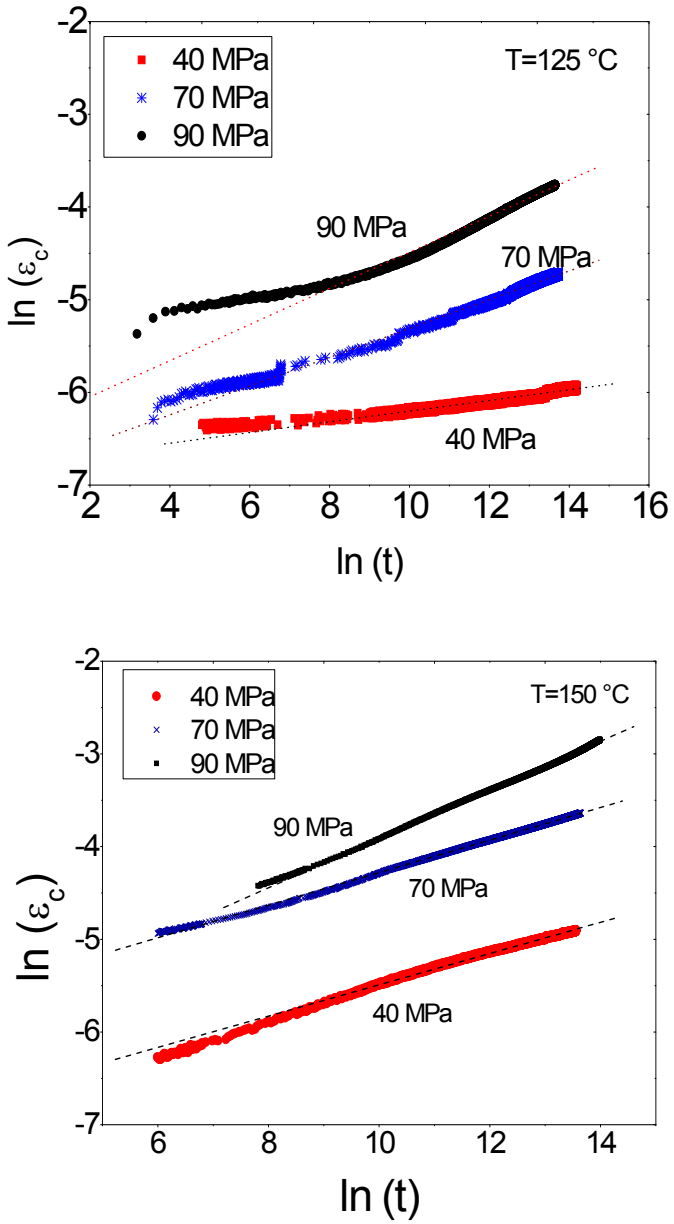

Figure 68: Plot of the natural logarithm of creep strain against time at various stress levels for 125 °C and 150 °C for the evaluation of the parameter *n* according to equation 45

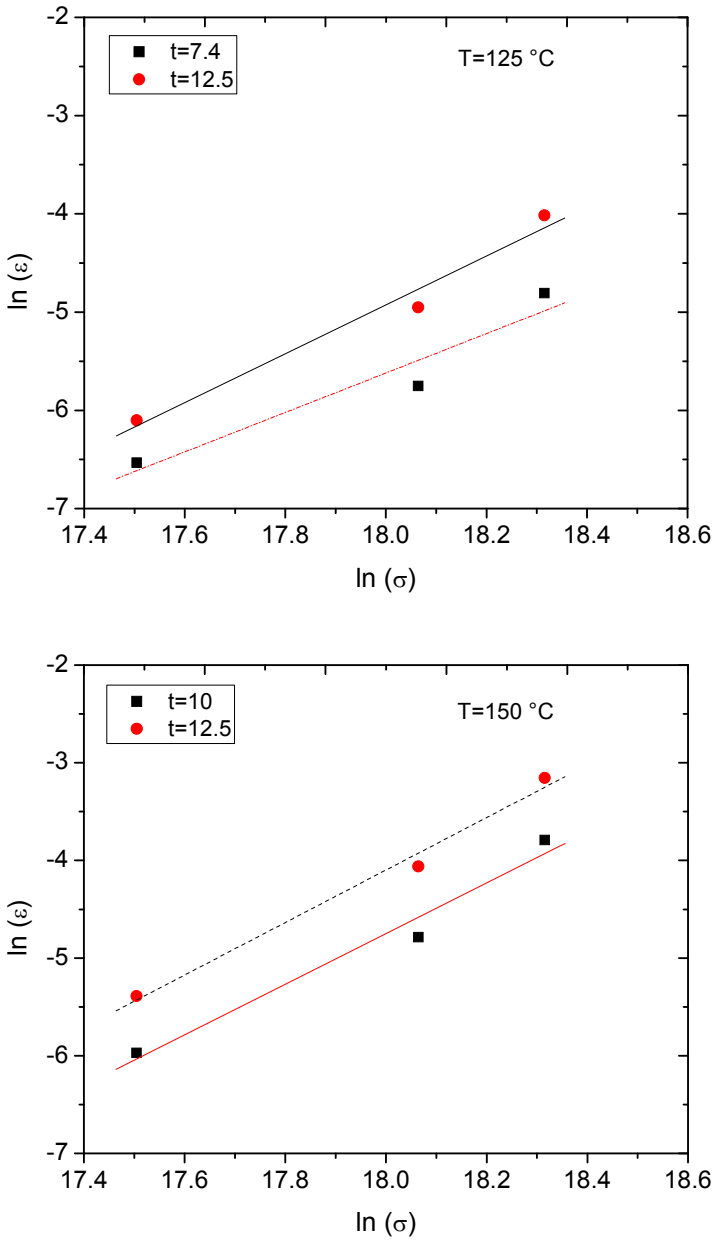

Figure 69: Plot of creep strain against stress at different times for the evaluation of the parameter *m* at 125 °C and 150 °C according to equation 45

At constant time ln(t) = 7.4 and ln(t) = 12.5, Figure 69 show the plot of creep strain against stress (σ) at 125 °C and that of 150 °C at constant time of ln(t) = 10 and ln(t) = 12.5. The stresses were in Pascal and times in seconds. The fitted lines in Figure 69 at various determined time scale are approximately parallel to each other indicating the creep strain dependence on the m^{th} power of the applied stress (σ). The creep material properties used for permanent mould AS41 magnesium alloy in FEA for 125 °C were: C = 4.38078 x 10^{-22},

m = 2.20 and n = 0.1956. At 150 °C, the values were 5.0276 x 10^{-18} for C, 1.8681 for m and 0.1692 for n.

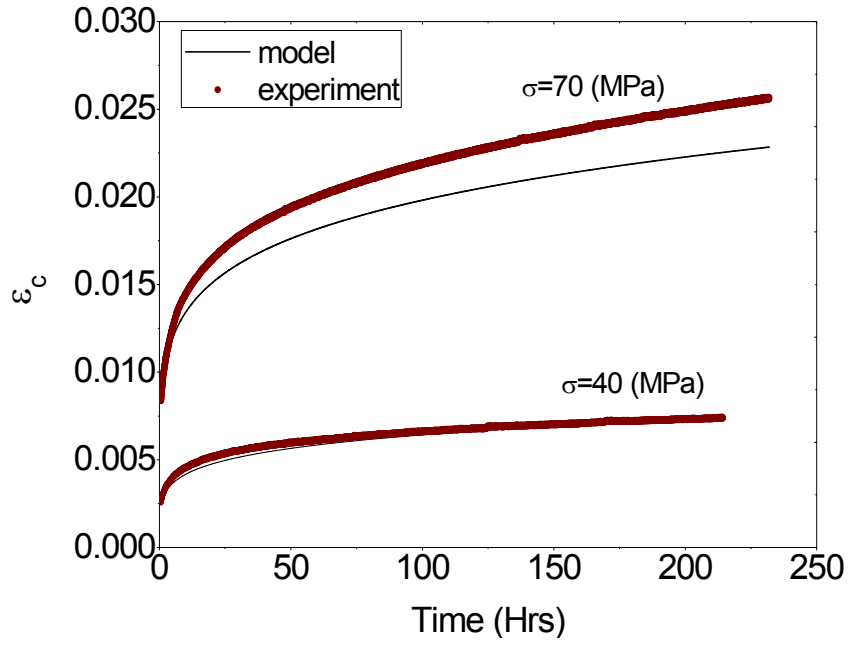

Figure 70: Comparative creep strain of AS41 as a function of time at different stress levels for 150 °C according to equation 44. Solid lines are model predictions while symbols are experimental data

The results of the typical compressive creep experiments are compared with that of the “three-parameter” creep model as represented in equation 44. As could be seen in Figure 70, the experiment and the model show reasonable agreement. The agreement between the “Three parameter” creep equation and the experimental creep result as shown in Figure 70 indicates that this creep model can be used in the material model for bolt load retention simulation. The time dependent retained clamp load predicted by equation 47 for AS41 magnesium alloy at 125 °C and 150 °C are shown in Figure 71.

From Figure 71, the BLR prediction after 72 hours was 13.23 kN at 10 kN/ 125 °C. At 17 kN/ 125 °C, the BLR prediction after 72 hours was 15.06 kN. Similar trend are also observed in that of 150 °C as shown in Figure 71. That of 175 °C is also shown in Figure 72.

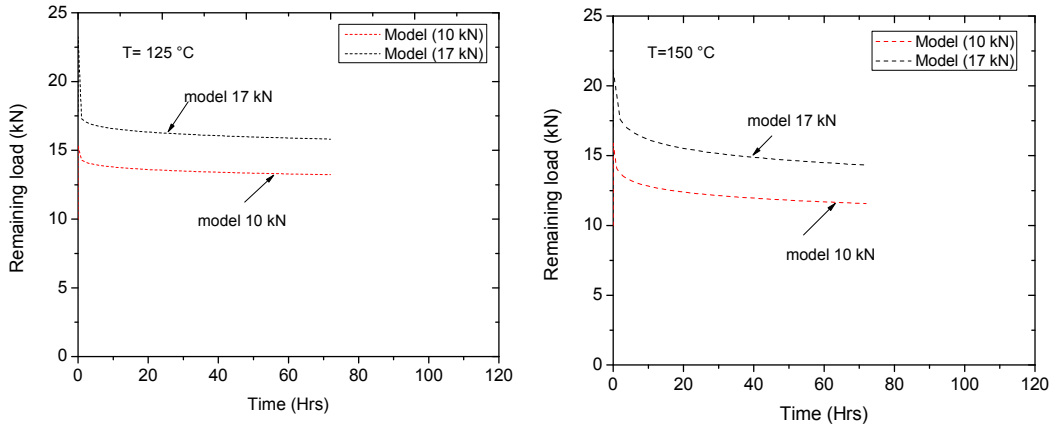

Figure 71: Predicted time dependent clamp load for 10 kN and 17 kN initial preload at 125 °C and 150 °C

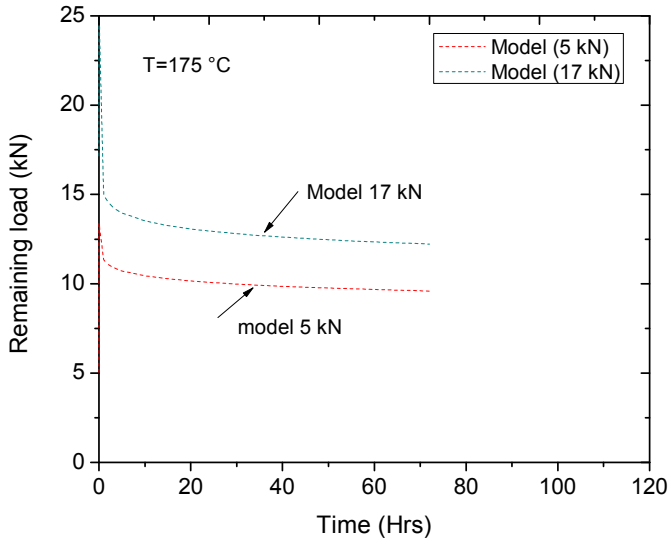

Figure 72: Predicted time dependent clamp load for 5 kN and 17 kN initial preload at 175 °C

6.10 Hardness response of AS41 after BLR and creep test

The hardness of the BLR and creep tested materials were measured parallel to the loading direction. The surface of the stressed area (A_s) was measured to gain insight on the strain hardening as a result of BLR and creep test on the magnesium alloy sample AS41. The tested surface is shown in Figure 73.

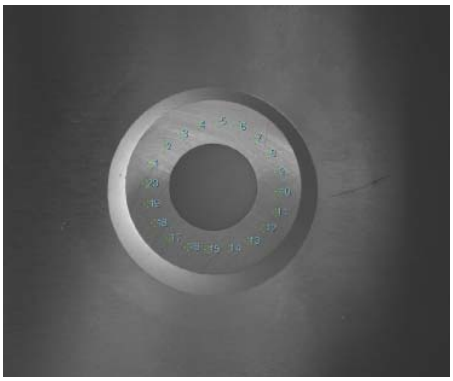

Figure 73: BLR and creep sample tested surface

Table 7: Hardness values of BLR and creep deformed sample

Hardness values with test method HV 5		
Condition	BLR Samples	Creep Samples
As cast	47.9±4.2	47.9±4.2
70 MPa/100 °C	49.8±4.9	50.8±3.2
70 MPa/125 °C	50.3±4.2	54.2±3.4
70 MPa/150 °C	50.0±3.7	55.8±3.8
40 MPa/150 °C	53.0±3.1	55.1±4.7

From the result of the hardness test as shown in Table 7, it is observed that the hardness values of the creep deformed samples are larger than those of BLR test deformed samples. The hardness values of BLR deformed samples with initial stress of 70 MPa were averagely 4.5 % larger than the undeformed AS41. For creep deformed samples at the same initial stress condition, the hardness values were approximately 12 % larger than the as cast undeformed sample. This is about 7 % differences between the BLR deformed samples and the creep deformed samples. At 40 MPa initial stress, the Vickers hardness value of the BLR tested sample was 2.1 HV lower than the creep deformed sample which is 4.4 % difference with respect to the undeformed permanent mould AS41.

7 Discussions

7.1 Evolution of microstructure during solidification process

The solidification process of permanent mould AS41 Mg-alloy is such that the initial phase to solidify from liquid melt is the Mg-rich dendrites. These are mostly the α-Mg matrix. Subsequently the intermetallic phases (Mg_2Si and $Mg_{17}Al_{12}$) were formed as the solidification proceeds. As observed already in Figure 31, alloying elements are seen saturated close to the dendrite and grain boundary regions. Point analysis shows that the volume fraction of Al in solid solution is well below those in the saturated regions (Table 3). It has been observed that during elevated temperature exposure, these saturated regions undergo precipitation to form fine $Mg_{17}Al_{12}$ phase (Figure 41). These precipitates will have a pronounce effect on the creep and bolt load retention response of AS41 Mg-alloy.

The presence of α-Mg matrix, Mg_2Si and $Mg_{17}Al_{12}$ have been confirmed in the microstructure of as cast AS41 (Figure 28, Figure 29 and Figure 30). Due to the slow cooling rate associated with permanent mould cast technique, the Mg_2Si assumed coarse microstructure of the order of several microns in length. Previous investigation on the solidification behaviour of commercial Mg-alloys show that the binary eutectic reaction ($L \rightarrow \alpha$-$Mg+Mg_2Si$) begins when the solid mole fraction of α-Mg was 0.325 at 614 °C [72]. At 432 °C, a ternary eutectic reaction that involves $Mg_{17}Al_{12}$ was also observed. The reaction ($L \rightarrow \alpha$-$Mg+Mg_2Si+Mg_{17}Al_{12}$) started when the solid mole fraction of α-Mg was 0.959. The last phase to solidify was $Mg_{17}Al_{12}$. This is why they are mostly seen pushed to grain boundary areas. At room temperature, $Mg_{17}Al_{12}$ contribute to room temperature mechanical property of Mg-Al alloys. This role is however reversed at elevated temperature. $Mg_{17}Al_{12}$ and Mg_2Si have melting temperature of 437 °C and 1085 °C respectively.

The presence of Al_8Mn_5 was not observed by TEM in this work. However, EDX analysis in Table 3 shows the presence of Al-Mn-Si phases which correspond to P2 and P5 precipitates of the SEM micrograph in Figure 29.

The small volume fractions of Mn in AS41 alloy maybe the reason why Al_8Mn_5 was not observed by TEM. The solidification sequence for permanent mould

AS41 alloy is therefore as follows: Precipitation of α-Mg matrix followed by Mg_2Si phase and subsequently β-$Mg_{17}Al_{12}$.

7.2 Compressive creep behaviour of AS41 alloy

Several works have been carried out on the creep of die cast magnesium alloys in the past [33, 38, 40, 41, 73, 74]. Most of those investigations were carried out on pure magnesium, AZ and AM series. Other works include those of references [39, 75-80]. Few activities have also been observed on AE and AS series [81-84, 43]. A different creep mechanism was suggested by Pekguleryuz [43] for AS41 below 150 °C. Since the creep investigations were carried out by the author of reference [43] only at 150 °C, and with limited samples, this claim could not be experimentally verified. To adequately address this, extensive creep investigation was carried out between temperatures of 100 °C to 200 °C and between stresses of 40 MPa and 90 MPa for the permanent mould cast AS41 alloy. Table 5 shows the creep conditions, minimum creep rate and corresponding creep strain after 200 hours.

From the calculation of stress exponent as seen in Figure 38, the stress exponent *n* as measured in this work were approximately 2 at low stress regions of 40 MPa and 55 MPa with temperatures of 100 °C to 150 °C. The activation energy for creep as shown in Figure 39 for constant stress condition of 55 MPa was 50 kJ/mol. This is well below the activation energy for self diffusion of magnesium which is 135 kJ/mol. Invariably, this means that diffusion will preferentially occur within the grain boundary and dendrite regions rather than the bulk of the matrix. This suggests creep by grain boundary diffusion and subsequent sliding at sufficient creep time within these stress and temperature range. At high stress regions of 70 MPa and 90 MPa for the permanent mould AS41, the stress exponent *n* was averagely between *n*~ 4-6. However, the activation energy for creep (Q_c) within 70 MPa and 90 MPa constant stress condition were between 72 kJ/mol and 100 kJ/ mol. Although the activation energy are relatively high compared to 50 kJ/ mol as observed at low stress conditions, the activation energy for creep (Q_c) was still below that of self diffusion of magnesium. Stress exponent values of between 4-6 suggest creep mechanism dominated by dislocation climb. Previous creep investigations of pure Mg and Mg-alloys show similar results for stress exponents but with

relatively varied activation energy for creep [85-89]. In those previous reports, *n* values close to 3 were believed to be creep controlled by viscous glide. For *n* values between 4 and 7, creep controlled by dislocation climb was proposed. Stress exponents higher than 7 were believed to be particle strengthening controlled creep. However there is still need to correlate the microstructure with these creep mechanisms as the understanding of those are important to elevated temperature creep resistance Mg-alloy development.

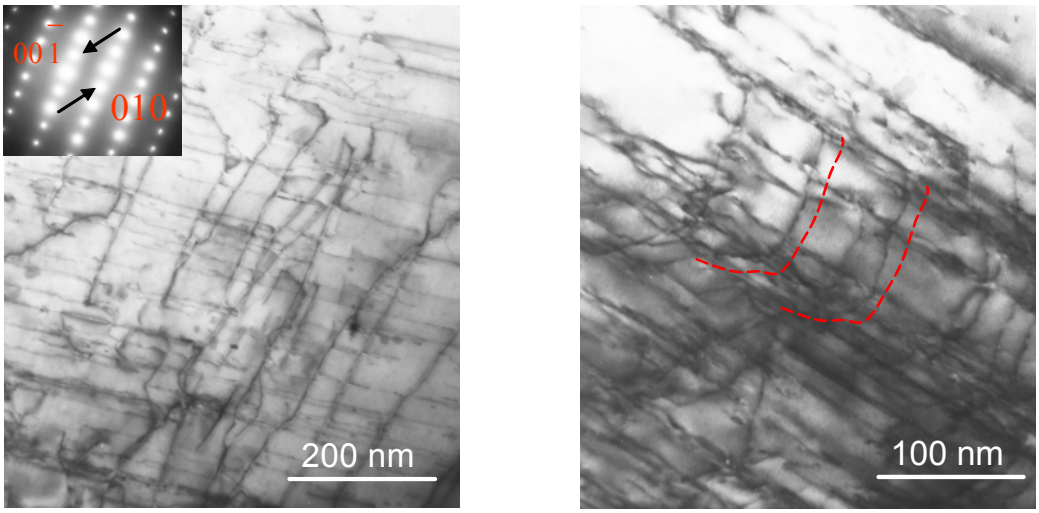

(a) (b)

Figure 74: (a) Dislocation lying in primary α-Mg matrix, zone axis [100], (b) TEM micrograph showing dislocation cross slip

Figure 74(a) represents TEM micrograph showing dislocation lying on the basal plan with zone axis [100]. From the result in this work, the dominant creep mechanisms for permanent mould AS41 Mg-alloy are grain boundary sliding and dislocation climb. Figure 74(b) shows the TEM micrograph of cross slip of dislocation. Al segregation within the eutectic and dendritic regions play significant role in the overall creep behaviour of AS41. Figure 75 shows SEM micrograph of pores development on the Al segregated regions of AS41 alloy deformed at 70 MPa/ 175 °C.

During solidification, the segregation of solute occurs near the grain boundaries and dendritic regions. It has been reported that Al segregation increases the local homologous temperature *(T_H)* of Mg-Al alloys within these regions [72, 73]. The segregation of alloying elements cause these regions to yield first by pore development as shown in Figure 75 followed by cracks and fracture when the

samples are tested in tensile mode. See also Figure 31 for comparison of as-cast and creep deformed AS41. The grain boundary regions are loosely bonded together in comparison to the α-Mg matrix: This leads to high atomic migration and consequently yields easily during creep deformation. The activation energy at the grain boundary regions are lower than that of self diffusion as also found in this work. Any act to reduce primary alloying element segregation or reinforcement of the grain boundary regions will definitely improve the creep properties of Mg-alloys.

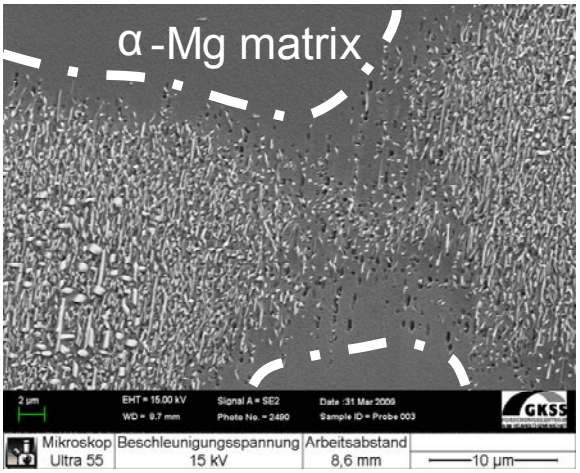

Figure 75: SEM micrograph of pores development on Al-segregated regions

Formation of stable intermetallics, which leads to reduction of grain boundary regions and increasing grain sizes, are some of the practical ways to delaying dislocation movement in Mg-alloys. Others include, reduction of the volume concentration of β-phase by alloying elements and again by solid solution strengthening [55, 89-94]. As reported by Huang et al. [73] and several other authors [93, 94], heat treatment is also a very important tool to improve creep properties of Mg-alloys. Application of T4 heat treatment brings about solute homogenization while T6 encourages precipitation that is beneficial to slowing down dislocation movement at elevated temperature. Another important way of Mg-alloys creep improvement is the addition of hard reinforcements to create Mg-alloy composites [95-97]. These include carbides and oxides such as SiC, B_4C, and Al_2O_3. These processes have been proven to improve the creep performance of Mg-alloys by forming obstacles and consequently create resistance to dislocation motion. The role of borides such as ZrB_2 and TiB_2 in

creep of Mg-alloys is yet to be investigated. In the AS41 alloy studied in this work, the formation of “Chinese script (Mg_2Si) helps to improve the creep response of this alloy. Although the coarse and brittle nature of Mg_2Si is believed to be slightly detrimental to the creep behaviour of this alloy, addition of alloying elements like Ca has been proven to modify this “Chinese script” morphology which improved its creep response [98].

There seems not to be any process suggesting a different creep mechanism below 150 °C for AS41 as suggested in reference [43]. In all the temperature and stress levels studied in this work, the dominant creep mechanisms are the grain boundary sliding at low stress regions of 40 – 55 MPa with temperature up to 150 °C. At high stress regions of 70 – 90 MPa and temperatures up to 200 °C, dislocation climb becomes the rate controlling creep mechanism. Twinning is also an active mode of deformation during creep of AS41 alloy. The effect of solute segregation is however seen as having great influence on the creep property of AS41 Mg-alloy. The reduced volume fraction of β-$Mg_{17}Al_{12}$ phase and the presence of thermal stable Mg_2Si within the grain and around the grain boundaries are instrumental to improved creep property as seen in AS41.

7.3 Evolution of microstructure during and after BLR test

This section discusses the microstructure of permanent mould AS41 Mg-alloy during and after BLR test. It covers from the as cast condition as shown in Figure 28, to BLR test with stress up to 70 MPa and temperature of 175 °C. Apart from few inherent dislocations that exists in the as cast condition of AS41, what is conspicuously seen is also the presence of tensile twins which are formed during preparation. These twins form high angle boundaries with misorientation > 15 °. The EBSD orientation map in Figure 32(a) shows the orientation relationship of the twins and the matrix. The red lines on the EBSD image quality map in Figure 32(b) are tensile twinning boundaries. High angel boundaries are designated with black lines in both orientation map and image quality maps. These twins which are caused by sample preparation are not the same as the twins that are observed after P_k in stage (II) and (III) of Figure 27.

It is a well known fact that twin is an active mode of deformation in hexagonal closed packed crystals of which magnesium alloys are involved [24, 28, 99]. This is also true for AS41 as is observed in this investigation. The twins are tensile twins although the BLR samples were deformed under compression. This is because during BLR test, only planes that are favourably aligned for these tensile twins were affected with twinning. As can be seen from the EBSD image quality map for the stage (II) condition in Figure 76, not all the grains have twins present in them. The observed tensile twins caused a rotation of approximately 86 ° of the basal plane around the $<11\bar{2}0>$ axis. The rotation is clearly seen in Figure 77.

In Mg-Al alloys, deformation in the c-direction can occur by $\{10\bar{1}2\}<10\bar{1}1>$ twinning or by the <c+a> slip $\{\bar{1}122\}<11\bar{2}3>$. Deformation in the c-axis can however be influenced by twinning as observed by Wonsiewicz and Kelley [28, 100], this could cause twinned region to re-orientate as to enable favourable basal slip condition. In magnesium alloys few researchers have reported observation of <c+a> $\{\bar{1}122\}<11\bar{2}3>$ slip systems [101, 102]. A combination therefore of slip due to dislocation movement and twins during BLR test determines to a great extent the rate of bolt load relaxation. Where as events like dislocation climb annihilates dislocations and makes room for recovery, in the case of twinning the direction of shear is definite and cannot be reversed [107].

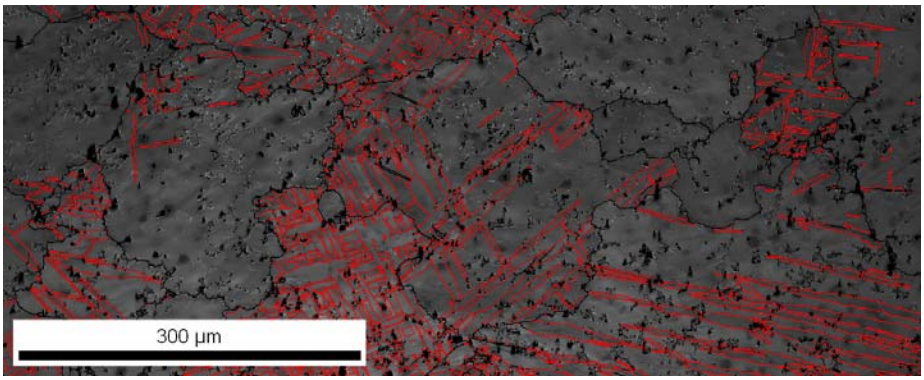

Figure 76: EBSD map fo AS41 showing twinned and untwinned grains in stage (II) of the BLR test at 70 MPa/ 175 °C

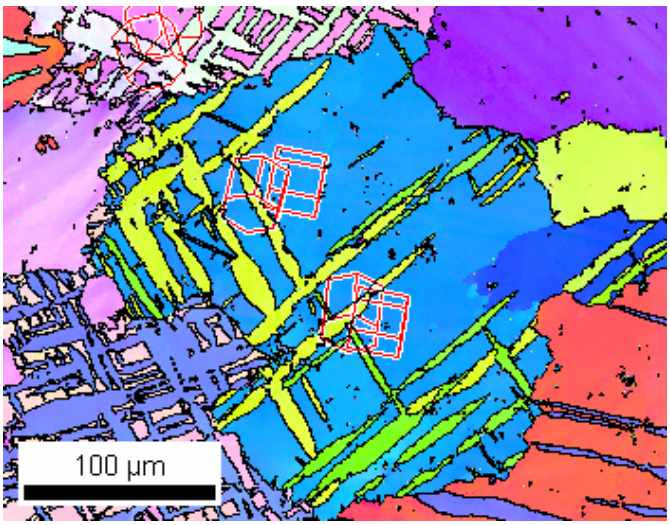

Figure 77: Crystal orientation of matrix and twins

As observed in permanent mould AS41 in this investigation, twins were more predominant at higher stresses than at lower stress condition. This is already shown in Figure 45, Figure 46, Appendix I and Appendix J. The overall BLR response of AS41 is dependent on the initial load, test temperature and the bolting constraints. These important factors determine the nature and density of both dislocation and twins which controls the BLR behaviour of magnesium alloys at microscopic level.

The evolution of subgrains in stage (III) as shown in Figure 49 indicates that dynamic recovery and recrystallization is taking place. This is seen at sufficiently elevated temperature and stress of 175 °C and 70 MPa. Figure 78(a) shows TEM micrograph and diffraction pattern of sample deformed under bolt load of 17 kN and 175 °C with a retained bolt load of 58 % after 72 hours. The

corresponding diffraction ring indexation in Figure 78(b) is consistent with α-Mg matrix.

In general, what is evidently observed in chronicling the deformation process of BLR behaviour of permanent mould AS41 is summarized below. At the inception of bolt load deformation, randomly distributed dislocation at the α-Mg matrix builds up from the (0001) basal plane and in the $<11\bar{2}0>$ most closely packed direction of the plane. Tensile twins with orientation relationship of ~86 ° with respect to the basal plane around the $<11\bar{2}0>$ axis become dominant. Continue deformation into stage (III) of the BLR test leads to recovery and subsequent appearance of cells and subgrain boundaries as seen in Figure 78.

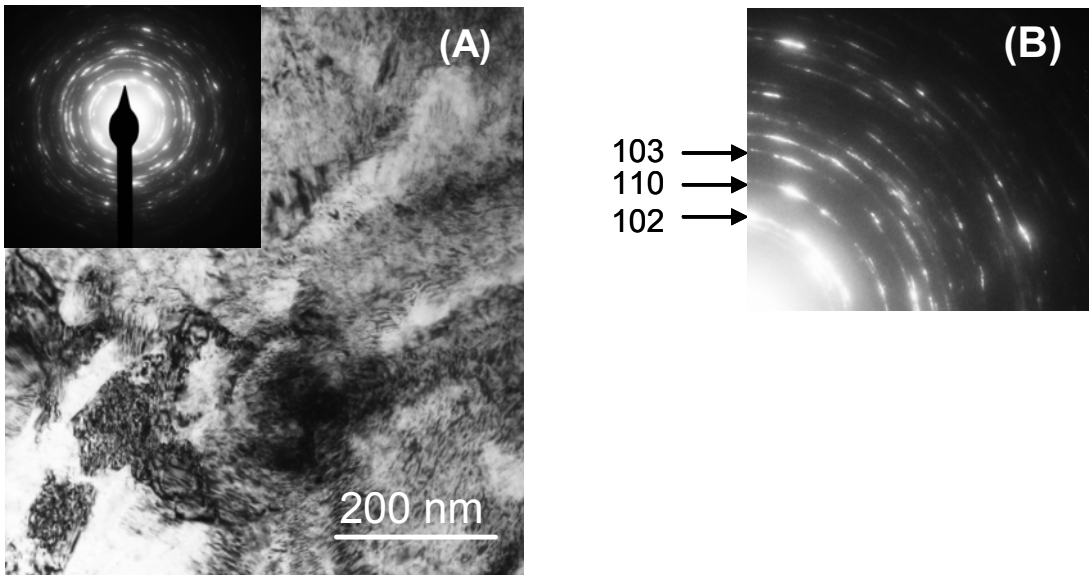

Figure 78: (a) TEM image of dislocation, subgrain and diffraction pattern from AS41 BLR sample tested at 17 kN/ 175 °C. (b) Diffraction pattern indexation is consistent with α-Mg matrix.

Depending on the stress and temperature, the cells and subgrain misorientation develops and widens. The result of mobile dislocation build up and annihilation are formation of new boundaries, reduction of cell size and subgrain regions. Based on the result in this work, at low temperature and stress, twins are dominant. At high temperature and stress twins and dislocations are dominant mechanisms. It will be important to mention here that in-situ bolt load retention test will throw more light on the microstructure evolution of magnesium component at elevated bolt load retention test.

7.4 Factors affecting BLR of AS41

7.4.1 Initial load and temperature

A look at Figure 13 which is the graph of bolt load retention of Mg-alloys at room temperature shows that bolt load loss is almost negligible at room temperature. That is true for all the materials measured at this temperature without exceeding the materials yield strength. However this is different with homologous temperature (T_H) approaching 0.4 as shown in Figure 14 and Figure 27. The major reason is that from this (T_H) range, Mg based materials are susceptible to creep. The tendency for atomic migration increases with increase in temperature. Dislocation movement through the microstructure of AS41 at this temperature range is also influenced. For Mg-alloys, $0.4(T_H)$ is approximately 96 °C. This is low for powertrain application, but relatively high for Mg-alloys. Since bolt load retention response of AS41 is a function of its creep behaviour, and creep is a thermally activated process, an increase in temperature will increase deformation due to creep. Invariably, this will affect the fastener clamp load retained after BLR test. Higher initial preload also means higher stress on the AS41 specimen during BLR test. This means more dislocations are generated and propelled as the initial preload and test temperature increases. The consequence is loss of bolt load with increase in initial preload and test temperature.

For AS41 as observed in this work, the increase in temperature weakens the saturated α-Mg + β-$Mg_{17}Al_{12}$ phase region of the microstructure and this increases the strain on the sample. Again, the increase in load due to thermal expansion mismatch induces additional stress on the AS41 sample at the beginning of the BLR test. This becomes higher with higher initial preload and increases the chances of permanent bolt load loss. On the other hand, the presence of Mg_2Si which is a thermal stable phase assisted in providing reasonable bolt load retention on AS41 alloy upto 150 °C as shown in this work.

As already seen from Figure 51 and Figure 52, increase in the initial load and temperature, decreases the amount of bolt load retained on AS41 Mg-alloy joint. Temperature and load influence were clearly seen as from 150 °C as can be observed in Figure 51. At moderate stress of 40 MPa, 83 % of the initial preload was retained at 100 °C and 125 °C. This decreased to 73 % and 66 %

at 150 °C and 175 °C for the same stress level. The trend is also the same at 70 MPa. It is observed that 81 % of the preload was retained at 100 °C and subsequently deceased to 71 and 58 % at 150 °C and 175 °C respectively. It must be however mentioned that the absolute load retained at a bolted joint increases with increase in initial preload. A similar trend was reported by Sohn et al. [108] for an AE42 and AZ91 die cast (alloy-flange/ alloy-case) assembly. Some influences such as coupon thickness are readily made manifest as the temperature increases [2]. A comparison of Figure 1 of the work of reference [108] for die cast AZ91 shows that at 150 °C and 175 °C, the degree of bolt load retention for this alloy was independent of the initial preload. This is because excessive creep deformation caused complete loss of the initial preload. The dynamics of heating of typical powertrain components are a little different than total temperature circulation as used in this work. This means that a reasonable safety margin could be achieved using bolt load retention testing procedure for automotive application with respect to load and temperature.

7.4.2 Effective length

In most cases, not the full length of the bolt is engaged in coupling a joint. This is especially true for through joint conditions such as the one used in this investigation. This leads to the introduction of the term effective length. It is the actual bolt length engaged in maintaining the joint. Doubling the coupon height as shown in result of section 6.6.2 will increase the effective length of the joint. Effective bolt length influences the stiffness of the joint and this has overall effect on the load drop in the whole bolted couple. At room temperature, longer effective length means slightly lower load at the joint than for a shorter effective length. The load drop is then directly proportional to the stress area and inversely proportional to the effective length. As such, AS41 Mg-alloy loaded at room temperature with a shorter bolt will experience slightly more stress than that loaded with a longer bolt.

At elevated temperature, a different loading profile is observed as seen in Figure 53. Although both samples were loaded at the same condition of either 5 kN or 17 kN at 150 °C, the one with longer effective length shows higher load increase. This is averagely 2 kN which translates to approximately 10 % difference in load between longer and shorter length for both 5 kN and 17 kN preload respectively. The increase in load at the inception of BLR test for the

longer effective length is partly connected to the thermal expansion response of the bolted couple since thermal expansion behaviour are length dependent. More materials were available to respond to thermal load on the longer specimen than in the shorter coupon. For stiffer joints, the dynamics of load increase are a little different depending on the preload and temperature of interest [2]. The knowledge and application of effective length at bolted joint of magnesium components could be use in solving thermal differential problems [1].

From equation 49 in section 7.6.2, it is observed that the joint stiffness K_J is proportional to the Young's modulus E and the stressed area A_S. K_J is also inversely proportional to the effective length L_J. This means that increase in either Young's modulus of the joint components or the stressed area will increase the stiffness of the joint, but the reverse is true for the effective length. This explains the reason why the couple with longer effective length retained more load at test temperature as shown in Figure 53 and also in Figure 79.

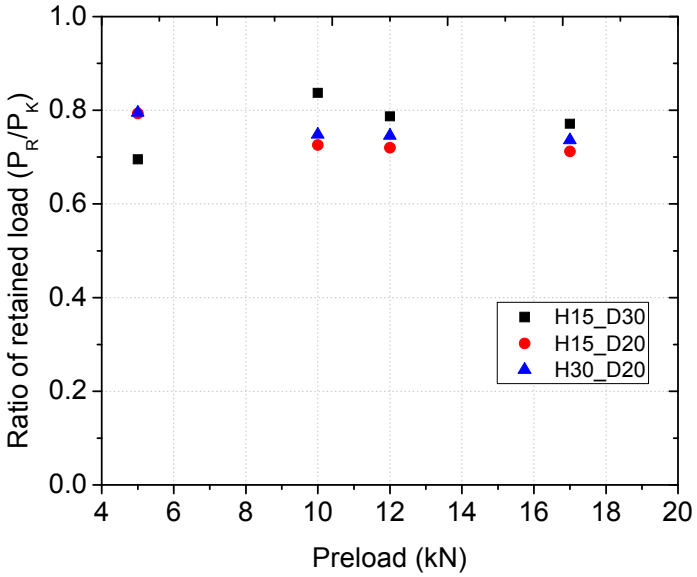

Figure 79: A comparative plot of coupon geometry on retained bolt load at 150 °C

The increase in stress area as can be seen in Figure 79 improved the retained bolt load of AS41. The letters H and D in Figure 79 stands for coupon height and diameter in (mm) respectively. The coupon with 30 mm diameter retained more bolt load than those with 20 mm diameter. This shows that the application of larger washer (more surface area) in magnesium bolted joint will help in

reduction of excessive bolt load loss at elevated temperature. However care should be taken as excessive use of washer will also increase the effective length thereby reducing the stiffness of the joint.

The relationship between joint stiffness and bolt load could be complicated as observed by [109, 110] especially at very high plastic deformation. This is because the rate of deformation is higher at elevated temperature for less stiff joints such as magnesium alloys under high stress conditions. Strain hardening, recovery and recrystallization events on the magnesium sample will further complicate the dependency of stiffness on bolt load. However, within the temperature and load range that is investigated in this work, the stiffness dependency on bolt load makes reasonable estimation.

When the bolted couples were cooled back to room temperature, the coupon with the doubled height however shows slightly lower retained clamp load. This is of course in comparison to the shorter coupon. For the couple tested at 150 °C and cooled down to room temperature, the P_F/P_I ratio was 24 % at 5 kN. Others were 32 % and 30 % for 10 kN and 17 kN load respectively. The results are for the 30 mm thickness coupon. In the case of 15 mm thickness coupon, approximately 34 % of the load was retained for 5 kN, 10 kN and 17 kN preloads respectively.

The slightly loss in bolt load at room temperature for the longer effective length as observed is as a result of the plastic deformation suffered by the coupon during the stage (i) of the BLR test. The 31 % increase in load for the coupon loaded at 17 kN as a result of the thermal load translates to a total clamp stress of approximately 93 MPa. This is already over the yield strength of permanent mould AS41 at 150 °C. The result is a permanent deformation that could be observed when the thermal load is removed.

7.4.3 Stiffness influence

The degree of opposition of an elastic structure to deformation under an applied force is termed stiffness. This quantity is an extensive material property and is geometry dependent. This means that the structure of the material, contact surface area or volume fraction of the material involved, play roles in determining the final stiffness of a joint. As shown in Figure 55 and Figure 56 of the result section, steel bolt/nut which provides a higher joint stiffness retained

more clamp load at test temperature than Al bolts/nut. The steel bolt joint retained 11 % load higher than Al bolt joint at 17 kN. For 10 kN initial preload, it was 18 % higher as shown in Figure 55. The reason for this is connected to the stiffness of the bolted couple. Lower Young's modulus means lower stiffness as a result the equivalent compliance (C_{eq}) increases according to equation 36, 37 and 38. This correspondingly reduces the ΔP according to equation 35. The BLR property of the alloy under consideration is a function of the respective elastic moduli of the materials composing the joint and also the time dependent creep behaviour of the AS41 alloy. Since the creep behaviour of the AS41 is similar under the same temperature condition, it follows therefore that the BLR result as shown in Figure 55 and Figure 56 originates from the difference in bolting materials. Figure 80 shows the inception of the (BLR) test of steel and Al bolts at 10 kN/ 125 °C and 17kN/ 125 °C.

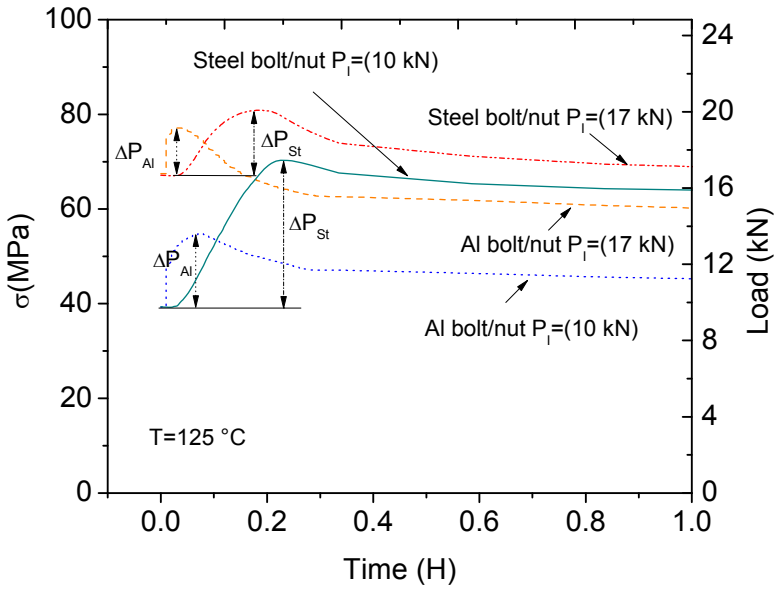

Figure 80. Inception stage of (BLR) test showing peak value (P_k) of steel and Al bolt loaded at 10 kN and 17 kN/ 125 °C

The increase in ΔP as observed in Figure 55 and Figure 56 of the result section are shown again in Figure 80. This represents the highest bolt load reached (P_k) at test temperature for steel and Al bolts. As can be seen, this is higher for steel than Al 7075 bolt. This also means that the local surface pressure on the AS41 component in contact with the bolt head is higher for the steel bolted component than in Al bolted component. At low initial preload level, this additional load (ΔP)

occasioned by the thermal stress is not detrimental to the AS41 bolted component since (ΔP) and the initial preload are still within the elastic regime of the AS41 sample. However, for higher initial preload, this thermal stress could become detrimental as deformation becomes irreversible due to very high local surface pressure on the AS41 component. The consequence is that, the total deformation observed for the steel bolted joint becomes more than the one observed in Al bolted component as seen in Figure 56. This will subsequently lead to more loss of fastener clamp load in steel bolted AS41 joint than in Al bolted AS41 joint.

Similar investigation [61] using self-tapping Al (7075, 6056) bolts on Mg-alloy samples show Mg-alloy retaining higher load on Al bolted components than steel bolted components. The difference that exists between this work and those of reference [61] stems from the nature of bolting. This investigation uses a through sample with Al (7075) bolt and Al nut and washers while those of reference [61] screwed in the Al bolt into the Mg-alloy sample. Other works include those of references [103-106] where the use of Al bolts have been shown as having improved fastener clamp load over those of steel bolts. Generally speaking, the required length of thread engagement increases with increasing bolt strength and decreasing nut strength. This implys that in design, space and weight saving with Al bolts and Mg alloy components is possible using Al bolts.

When the stiffness of the coupon was made stiffer than magnesium component while maintaining steel bolt, the result is also improved bolt load. As reported in reference [108], when an Al sample 380 Al was compared with AZ91D and AE42, the 380 Al coupon shows better fastener clamp load retention than the magnesium components at 125 °C and 175 °C. In the same work, when either a steel case or 380 Al case was bolted together with AE42 alloy flange, the bolt load retained was better than when AE42 case and flange was used. The trend is also true as reported in similar investigations [4, 5] for steel and Al components. Improving the stiffness of a magnesium component joint will improve its overall bolt load retention behaviour at elevated temperature. Application of Al alloy bolts with better Young's modulus will improve the fastener clamp load retention property of magnesium joints with through sample geometry.

7.5 Factors affecting BLR testing procedures

7.5.1 Uniform preload and waiting time before BLR test

It is observed that the waiting time after torquing the bolted couple before the BLR experiment begins is very important. There is need to maintain constant preload and waiting time for all the experiments before starting BLR test. Uniform intervals between actual loading and BLR test are crucial to having repetitive result. This is because, the Mg-alloy bolted joint begins to lose fastener clamp load immediately the torque wrench is removed from the bolt head after torquing. Longer waiting time results to loss in clamp load at room temperature. Figure 81 shows the percentage load loss after torquing an AS41 Mg-alloy joint with load of 17 kN at room temperature up to 150 hrs.

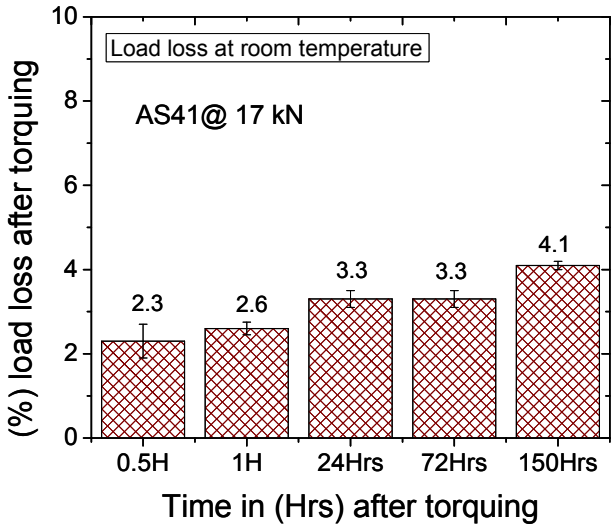

Figure 81: Load loss after torquing a permanent mould AS41 Mg-alloy joint with a 17 kN load at room temperature

Load loss of ~2.3 % was witnessed after 30 minutes of removing the torque wrench from the head bolt. This load loss increased to 2.6 % after 1 hour, which is an increase of 0.3 % in another 30 minutes. After 24 hours, another 0.7 % loss was observed totalling 3.3 %. This was approximately same up to 72 hours. After 150 hours, another 0.8 % was recorded bringing the whole load loss at room temperature to 4.1 % after removing the torque wrench from the head bolt.

This observed phenomenon differs from material to material. The type of test fixture used, amount of initial preload and tightening techniques will influence the degree of room temperature load loss. As can be inferred from Figure 81, 2.6 % of the whole room temperature load loss occurred between 0-1hr. It is recommended that during tightening, the desired preload be passed by up to 3 % and wait for at least 1 hour before BLR test begins. The over tightening will make up for the room temperature relaxation that occurs after torquing the head bolt. This will insure that BLR test begins with uniform initial preload and consequently improves repeatability of results.

Figure 82 show three different BLR measurements done on an AS41 alloy joint at 17 kN/ 150 °C. Measurements were restricted to 48, 72 and 92 hours at 150 °C. All samples were over torqued by 3 % of the desired preload, waited for 1 hour before BLR measurements. This minimises deviation and improve BLR experimental results.

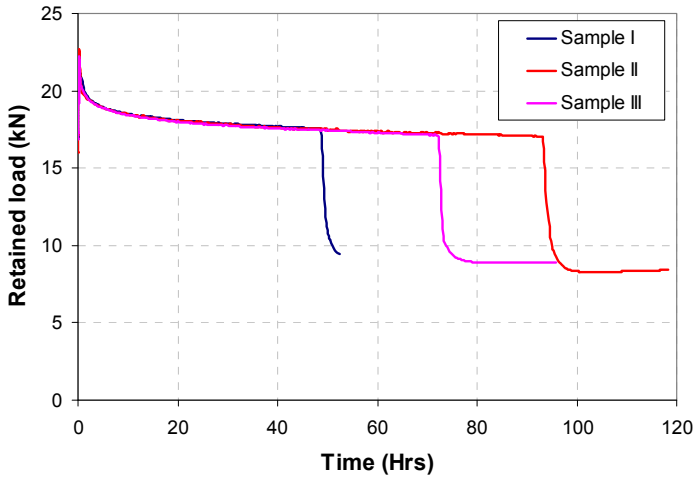

Figure 82: Bolt load retention result for AS41 alloy at 17 kN/ 150 °C. Sample height = 15 mm, diameter = 30 mm

7.5.2 Load measurement techniques

A continuous load measurement technique is recommended for chronicling the BLR result during BLR test. Some of the previous works simply measured the initial preload and then the final load at test temperature [2, 54]. Others made use of torquing angle counting like in the case of Noranda [56]. The major drawback of these kinds of load measurement and recording methods is that, there is no information about the bolt load relaxation rate. The possibility of

thermal cycle BLR measurement becomes increasingly tedious with the above mentioned techniques. In continuous load measurement approach, the total thermal and load history of the BLR process are recorded [4, 79, 108, 111]. This makes more information available for further data analysis.

Two often used continuous load measuring techniques are the instrumented bolt and the load-cell techniques [3, 5, 90, 109, 112, 113]. Since the steel bolt is an integral part of the joint, the instrumentation of the steel bolt for embedment of strain gauges may influence the strength of the steel bolt and therefore its stiffness. This will invariably influence the degree of fastener clamp load retention in Mg-alloy joint. Another potential influence that may arise in using instrumented bolt technique is the problem of “hysterisis”. This is with respect to the embedded strain gauges and the steel bolt at elevated temperature. It is likely that this could influence the bolt load retention values especially during heating up to test temperature at the inception of the BLR test and during cooling down to room temperature. The authors of reference [110] suggested possible ways of solving these problems, however this needs more investigations.

It is recommended that continuous load measurement should cover the whole four stages of the BLR test as shown in Figure 14 and Figure 27. Where as the most important part of the BLR test are stages (ii-iii) at test temperature, stage (iv) is also of interest. This gives information of the state of retained load after the Mg-alloy bolted joint has undergone thermal and load cycle from stages (i-iv). It has been found that the (P_f) values can drop as much as 52 % in permanent mould AS41 Mg-alloy joint with respect to its (P_r) value. As found in this investigation, the load drop increases with increase in temperature. At 100 °C, a load drop of 30 % was recorded for 17 kN initial load. The percentage load drop increased to 47.9 % and 51.9 % for the same initial load of 17 kN at 150 °C and 175 °C respectively. This is relatively high in comparison to the work of reference [110] but comparable to the works of [3, 5, 114]. The differences in the intrinsic BLR test apparatus may account for these discrepancies. Refer to baseline test diagram in Figure 57. The final load (P_f) at room temperature after BLR test is observed to be recovered back to the (P_r) values on reheating to the test temperature. This is already shown in Figure 59 and Figure 60 of the interrupted BLR test. The ratio of (P_f/P_i) as shown in Figure 52 is a measure of

the lowest load retained at bolted joint for AS41 Mg component between stages (i-iv). This information can only be obtained from a complete continuous load measurement approach.

Other load measurement techniques include those proposed by Osgood [115], and those outlined by Bickford [1] including ultrasonic methods. According to Osgood, techniques like usage of micrometer to measure bolt elongation or application of deformable elongation indicator is a viable way for load measurement. Others include using of break-off portions of threaded nuts which are configured so that the driving torque induces the desired preload. Some of these methods still need to be optimized for higher accuracy. The ultrasonic load measuring method makes use of a sensor or transducer mounted on the head bolt. This gives a two-way conversion of electronic signal and mechanical vibration [1, 116]. The generated echo runs through the bolt and is reflected by the bolt's end which is again converted to electronic signal. The transit time required for the echo to make its round trip is recorded. The major advantage of the ultrasonic technique over load cells and strain gauges is its ability to determine the clamp load without any impact on the joint compliance. Its disadvantage however with respect to load cell measuring technique, is its indirect measurement technique itself. The indirect measurement method is influenced by the temperature, plastic elongation and stress in the bolt [116]. Temperature above 200 °C is considered critical to ultrasonic measuring technique [1]. Availability of modern electronic devices over the last years has improved the degree of accuracy of the ultrasonic measuring method. This method will be especially suitable for real time load measurement for power train application when they are perfected.

7.5.3 Need for baseline test in BLR experiments

The BLR test apparatus is a combination of sensor, steel bolt, steel nut and washers in the case of this study. For instrumented BLR test assembly [3, 5], the strain gauges are normally embedded in the steel bolts. This therefore means that the basic elements of the BLR test couple which include bolts, nuts and washers are also present. These members of the BLR test apparatus reveal an inherent bolt load loss at elevated temperature. The bolt load loss were evidenced when torqued to a specific stress condition, heated to a desired temperature and allowed for a period of time as shown in Figure 57. The

amount of bolt load loss on the equipment as measured along (P_K-P_R) reaches an average of 6 % for the investigated load conditions at 175 °C after 72 hours. At 125 °C and 150 °C, the equipment bolt load losses measured were 2 and 5 % respectively after 72 hours. The scatters observed in Table 6 are within experimental margin that arises from different initial load conditions. What is obviously observed is a trend in the retained bolt load loss on the equipment as the temperature increases.

The choice of hardened steel component was suggested based on the fact that, the temperature of interest in this work is about 0.1 of the homologous temperature for steel. No serious plastic deformation on the test couple was expected within the investigated temperature and stress range. Figure 83 show the BLR experiments on permanent mould AS41 with baseline and without baseline computation.

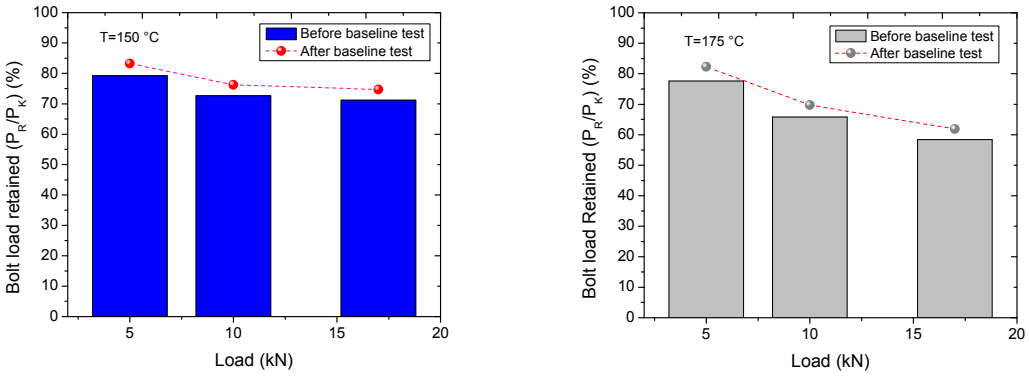

Figure 83: Load retained before and after baseline value computation at 150 °C and 175 °C

Appropriate interpretation of the bolt load retention behaviour of magnesium alloy demands the recognition and inclusion of the baseline test. This should be part of the final determination of the BLR value of the component under investigation. Excluding this will under estimate the BLR property of the magnesium component by the very same quantity of load loss exhibited by the test equipment itself. Before bolt load retention test are carried out on magnesium components, it is recommended that baseline test be also done for steel sample of the same specification. Different sample geometry and sizes may influence the baseline test. In the case of specific application with complex shapes, effort should be made to replicate such test samples using steel

samples which will consequently be used for baseline analysis. The true BLR result of the Mg-alloy component measured after a specific time can then be evaluated. This is equal to the BLR values plus the baseline test at the same load, temperature and restricted time condition.

7.6 Modelling BLR of Mg-alloys

7.6.1 Compliance – Creep relationship

7.6.1.1 Stage (I) of BLR test

The Battles' and Arimonds' models [54, 60], did not make provision for the initial stage of the BLR test response of the investigated alloys. This is already introduced in section 2.6.3 in the literature review of this work. The consequence is that equations 27 and 29 can not be used for stage (i) prediction. As seen from Figure 27 on the bolt load retention test curve, it is observed that stage (i) is an integral part of the BLR curve of Mg-alloys. The knowledge of this stage is however critical to the (BLR) behaviour of Mg-alloys. In this study as shown in section 6.9, equations (35 and 39) were used to predict this initial stage. The change in load ΔP that is observed at the beginning of the experiment is a very important part of BLR test. This is observed when either the torqued couple is inserted into the oil bath at test temperature or when the couple is heated to test temperature. Adequate prediction of this load designated as P_k in the BLR diagram (Figure 14) could be a useful tool during design in determining allowable load a joint can sustain at temperature without exceeding its load bearing limit from cold start of an engine to its service temperature.

Steel and magnesium have different thermal expansion properties. The thermal expansion coefficient of Mg is more than that of steel (α_{mg} = 26 x 10^{-6} m/m.k, α_{steel} = 12 x 10^{-6} m/m.k). This means that the expanded Mg samples are compressed by the steel bolt and washers. Sometimes, depending on the amount of the preload and the type of magnesium alloy, it is possible to exceed the yield strength of this alloy. Appendix C shows the yield properties of permanent mould AS41 at different temperature conditions. Considering the service temperature investigated in this study, it is assumed that no plastic deformation occurred on the steel components. The steel part only expanded within the elastic regime. The clamp load as a result of thermal expansion mismatch of the couple in relationship to temperature is usually described using equation 30 [3, 51].

The issue with equation 30 is that it makes very high prediction of the change in load. A comparison of equation 30 according to Pettersen et al. [3, 51] is plotted

against equation 35 of this work and compared with experimental result for a preload of 12 kN at different temperatures. This is shown in Figure 84. From the plot, it could be seen that equation 30 made prediction of several orders of magnitude higher than equation 35 in relationship with the measured value.

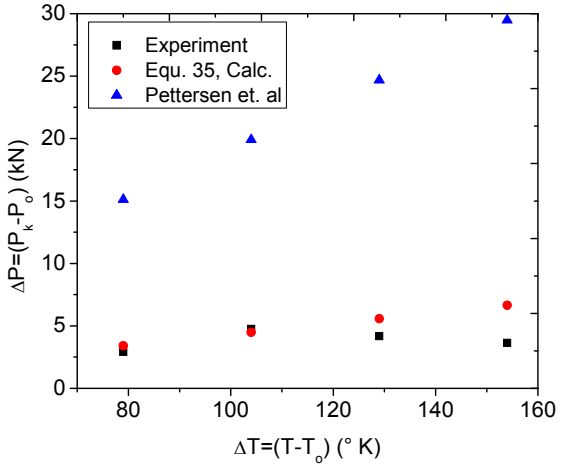

Figure 84: Comparison of experiment and equations 30 and 35 [3, 51]

In modelling the change in load *(∆P)* as a result of the thermal load with equation 35, a couple of assumptions were made. It was assumed that the steel washers which were compressed with the magnesium alloys have the same thermal expansion coefficient as the steel bolt. This means that they do not contribute to *(∆P)* by increasing the length. ∆*P* as a result of thermal loading should include the equivalent compliance of members of the joint *(C_{eq}),* the change in temperature *(∆T),* the length of the magnesium alloy *(l_{mg})* and the difference in the thermal expansion coefficients of magnesium alloy and steel bolt *(α_{mg} - α_{steel})*. This is already shown in equation 35.

In comparing the model and the experiment, it is observed that the model and the experiment are in good agreement as shown in Figure 62. At temperatures of 100 °C and 125 °C, the model made almost an identical prediction of the behaviour of AS41 at P_k. As the service temperature was increased to 150 °C and 175 °C, the model prediction was slightly higher than the experimental result especially with increase in load at 175 °C. This is because of the instantaneous deformation under thermal loading at higher temperature. The AS41 was already yielding at this temperature with the load on it and some of the deformation becomes irreversible in nature. The deformation on the

magnesium sample caused the loss of fastener clamp load witnessed on the experiment and as such the model prediction was higher than the experiment.

7.6.1.2 Stages (II) and (III) of the BLR test

The second and third stages as shown in Figure 27 represent the total relaxation behaviour of a particular bolted joint at test temperature. As mentioned earlier in section 5, stages (ii) and (iii) obeys the same law with the difference being the relaxation rate at different stages. The bolt load relaxation rate is higher at the (ii) stage than at the (iii) stage. Generally, 10-40% of the total bolt load loss in Mg-alloy joint occurs in the first 5 hours after inception of (BLR) test. The remaining bolt load loss occurs in the third stage. The thermal load just after the couple was inserted into the oil bath exerted more stress on the AS41 component. This increase in load generates more dislocations within the microstructure of the AS41 component. Quenching the AS41 alloy at this point in oil at 20 °C as was carried out in this investigation and observed under TEM show presence of dislocations. Figure 85 shows the TEM microstructure of stage (ii) for an AS41 component loaded at 70 MPa/ 125 °C.

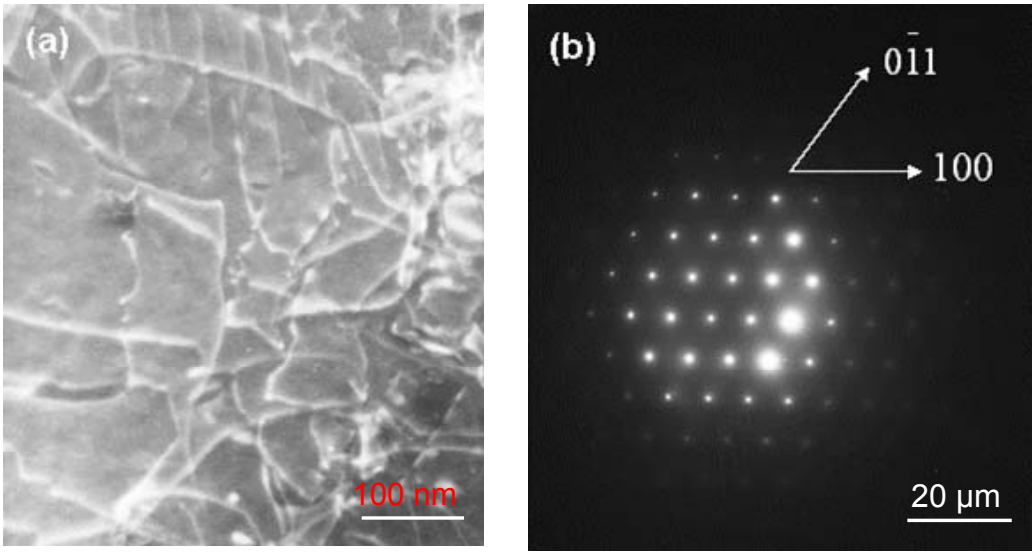

Figure 85: Showing (a). Two-beam condition with $\vec{g} = 100$, (b). Diffraction pattern of the TEM micrograph with zone axis $[011]$

Strings of dislocation build ups running through the microstructure of AS41 could be clearly observed in Figure 85(a). The stress induced on the specimen as a result of the thermal load reaches a threshold load at *(P_k)* depending on the temperature and loading variables. This is subsequently followed by a “neo

recovery" process. It is suggested that the rate of annihilation of dislocation at the beginning of stage (ii) is high and that means higher recovery rate and by extension higher joint relaxation rate. An in-situ BLR test is expected to give more information on the state of the sample and of the joint under specific testing condition. Figure 86 however shows the total relaxation in stage (II). That is the first 5 hours of (BLR) test and compares it with stage (III), the last 67 hours in a 72 hours restricted BLR experiment.

It is seen from Figure 86 that stage (II) made up more than half of the total bolt relaxation at elevated temperature. Stage (II) as seen in Figure 86 is sensitive to temperature. An increase in temperature from 125 °C to 175 °C shows an increase in load relaxation of approximately 10 % for a preload of 12 kN and 14 % for that of 17 kN. It could also be inferred that higher preload creates higher stress on the AS41 Mg component as a result higher relaxation is witnessed on the bolted joint with higher preload. Establishing the amount of load/stress a Mg-alloy component will sustain in a bolted joint without failure is therefore critical at stage (II). Tolerance should be given to account for the thermal load increase and stage (II) relaxation when bolting Mg-components for engineering applications.

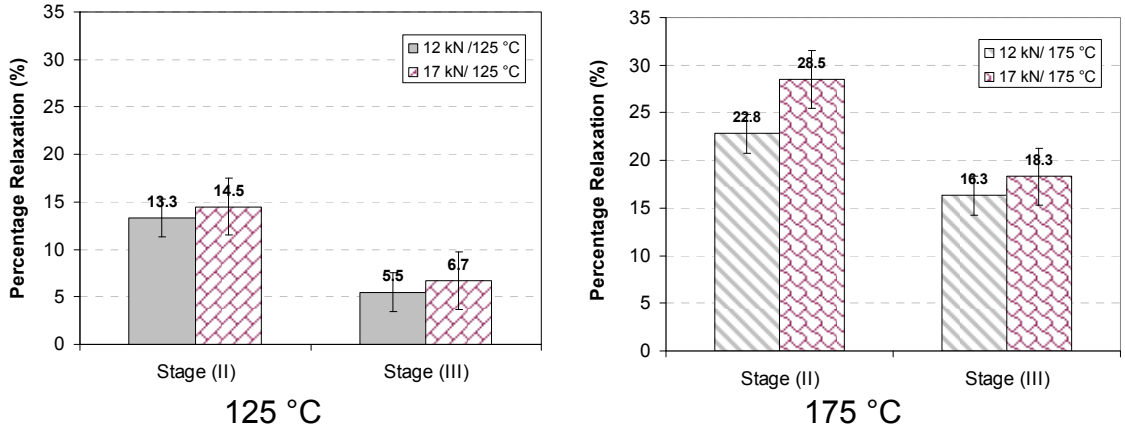

Figure 86: Total relaxation in stage (II) and (III) for AS41 alloy loaded at 12 kN and 17 kN at 125 °C and 175 °C respectively

7.6.1.3 Predicting stages (II) and (III) in an AS41 joint

The relaxation observed at these stages is generally believed to be as a result of creep of the Mg-alloy component [3, 51, 60]. Another major factor influencing the degree of bolt load retention is also the stiffness of the whole bolted couple [51, 110]. These include the bolt, nut, washers and the Mg component itself. As

shown in Figure 67, the stress in a joint is distributed within the jointed couple [1]. That means, the load is shared between the bolting components and the Mg-alloy joint. It is important to mention here that models attempting to predict bolt load retention behaviour at elevated temperature are expected to include these important elements (creep behaviour of the component and stiffness response of the joint). Compliance is the inverse of stiffness.

Since most powertrain components are loaded in compressive mode [48], it becomes more appropriate to employ compressive creep response of the joint component in modelling BLR behaviour. As can be seen from Figure 87, equation 43 made very reasonable prediction of stages (II) and (III).

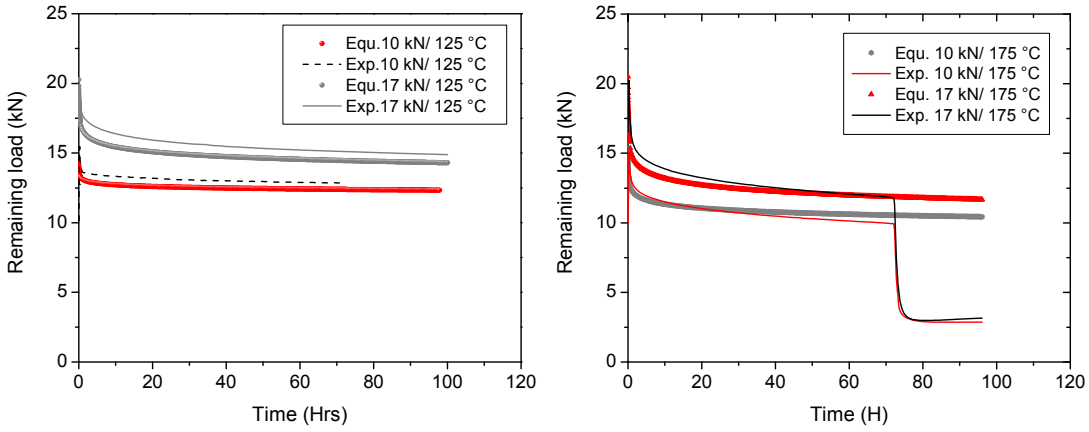

Figure 87: Bolt load retention prediction according to equation 43 compared to measured (BLR) result for preloads of 10 kN/ 17 kN and temperatures of 125 °C/ 175 °C

At 125 °C, while the equation prediction at preload of 17 kN after 72 hours was 14.5 kN, the measured value was 15.09 kN. This is a difference of 4.4% between the model prediction and experiment with respect to (P_k). At 150 °C and 175 °C, the model prediction differs with the measured (BLR) with 3.1 % and 0.65 % respectively for a preload of 17 kN. That of 17 kN/100 °C shows a model prediction of 15.01 kN and a measured value of 15.31 kN. The plotted comparison is shown in Figure 88.

What can also be seen from Figure 88 in both the equation predicted and the measured value is that the amount of bolt load retained decreases with increase in test temperature. Elastic modulus is a measure of the binding forces within the atomic structure of a material, temperature increase will lower the elastic modulus of the AS41. This accounts for the decreasing values of K_i with

increasing temperature as seen in section 6.9 of this work. This is reasonable as K_i is elastic modulus dependent. The result is that the total deformation with time will be higher at higher temperature as dislocation movement encounters lesser opposition.

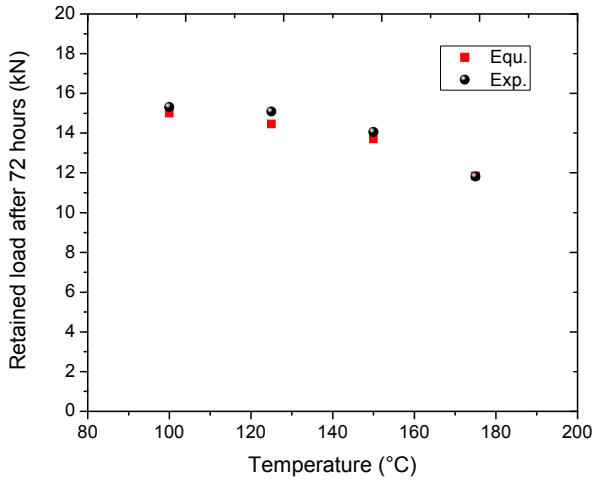

Figure 88: Retained load after 72 hours at 17 kN (equation 43 and experiment compared)

In general, the compliance-creep approach of BLR modelling made reasonable prediction of the BLR response for AS41 Mg-alloy. The prediction of the major BLR stages, that is (i-iii) were in good agreement with the experimental results. Influences of things like porosity, volume fraction of second phases directly in contact with the bolted joint and sample surface could affect the BLR result.

7.6.2 FEA modelling approach

The laboratory simulation of magnesium alloy behaviour at bolted joint using FEA tries to reflect real service situation as closely as possible. Previous work [117] used an approach similar to point loading situation to model the stress state with time at bolted joint. This investigation however uses a contact loading approach. For the washer-joint contact model used in this work, the effective stressed area depends mainly on the geometry of the specimen. Important is also the washer that makes the contact to the bolt. The stressed area does not depend directly on the surface of the bolt itself or the nut but on the washers. The FEA computation of effective stressed area (A_s) was done by first calculating the stiffness of the joint K_J using equation 48. (F) is the average load and (ΔL) is equal to the net displacement on the contact surface of the joint. The

stressed area was then substituted from equation 49 since the elastic modulus is known.

$$K_J = \frac{F}{\Delta L} \qquad \text{Equation 48}$$

$$K_J = \frac{EA_s}{L_J} \qquad \text{Equation 49}$$

The authors of reference [118] reported an average of 30 % difference between the FEA computed stressed area and that of equation 25. The supposedly underestimation of the stressed area by equation 25 is expected to lower the joint stiffness.

The FEA model applied in this investigation using ADINA [71] assumes that the total deformation (ε_t) at the AS41 bolted joint is a combination of the elastic strain (ε_e), plastic strain (ε_p) and creep strain (ε_c) as shown in equation 46. From equation 47, it is observed that both the elastic and plastic part is temperature dependent. The plastic strain part of equation 47 can further be expressed as equation 50 [119].

$$\varepsilon_p = \frac{\sigma_{YS}}{E(T)}\left(\frac{\sigma}{\sigma_{YS}}\right)^N \qquad \text{Equation 50}$$

$$\frac{\sigma_{YS}}{\sigma_{UCS}} = \left[a\left(0.002 - \frac{\sigma_{YS}}{E(T)}\right)\right]^{1/N} \qquad \text{Equation 51}$$

N is the strain hardening exponent. For power law materials, when σ_{ys} and σ_{ucs} are known, the value *N* can be estimated. The term (*a*) in equation 51 is approximately equal to 1 at 0.2 % offset yield stress.

It is assumed that the M10 steel bolt and washers used in this work expanded within the elastic regime only, considering the applied temperature. This is approximately 0.1 of the melting temperature of steel bolt. The plastically deformed magnesium alloy due to creep at the exposed temperature causes loss of fastener clamp load on the bolted joint. The degree of loss of clamp load depends among other things, on the operating temperature, stress involved and the compressive creep behaviour of the magnesium alloy.

In order to take into account the metal temperature change with respect to time, transient thermal analysis was conducted for the simulation. Structural analysis was subsequently performed to evaluate the time dependent bolt load loss as a result of variation in temperature gradient during FE simulation. In the case of AS41 magnesium alloy at 125 °C, the material model to simulate the period of tightening the bolt and putting it into the oil bath was changed from thermal plastic to thermal elastic. This is based on the fact that not all the thermal plastic properties of AS41 alloy were available at the temperatures from 20 °C to 125 °C. Hence a bi-linear relationship was used in the thermal-plastic-creep material model for simulation of the creep regime.

Table 8 compares the FEA prediction in this work with the measured (BLR) after 72 hours for different stress and temperature conditions. The difference between FEA prediction and measured values varies across the load and temperature ranges.

Table 8: FEA prediction and measured (BLR) after 72 hours at test temperature

T (°C)	Pre-stress (MPa)	FEA (kN)	Measured (kN)
125	40	13.23	12.85 ± 1.00
	70	15.06	17.16 ± 2.57
150	40	11.57	9.34 ± 1.13
	70	14.33	14.06 ± 1.92
175	40	11.68	9.94 ± 1.67
	70	12.21	11.82 ± 0.93

The retained load with respect to P_k at 125 °C shows that the model prediction was higher than the experiment by 3.3 % for stress of 40 MPa. In the case of 70 MPa stress, a retained load of 15.06 kN which is equal to bolt load loss of 31.9 % was predicted against 20.2 % measured value. For 150 °C and 175 °C, the model makes higher prediction than the measured value as can be seen from Table 8.

Similar work [118] on HPDC AM50 shows an FEA prediction higher than the measured (BLR) values for an instrumented bolt technique. From equation 47, it is observed that the elastic modulus to a great extent influences the deformation at the bolted joint at elevated temperature. As can be seen from Table 8, the FEA prediction reflects the effect of increasing test temperature on the bolt load retained at P_r after 72 hours. P_r being equal to the bolt load retained at test

temperature as shown in Figure 14. The trend of the FEA prediction is similar to that of measured values as the test temperature increases from 125 °C to 175 °C. See also Figure 89.

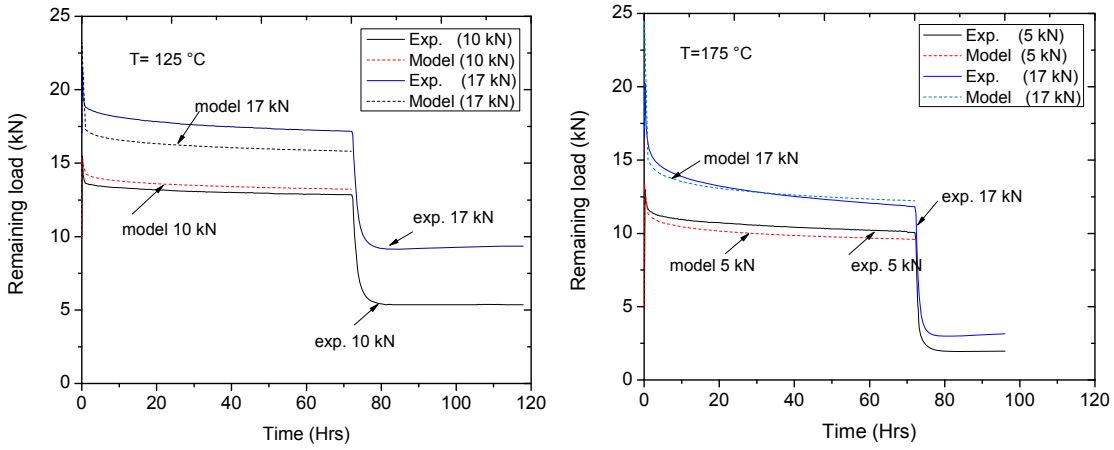

Figure 89: Comparative plot of time dependent retained clamp load at bolted joint for 125 °C and 175 °C. Broken lines are model predictions while solid lines are measured values

Possible sources of error may emanate from elevated temperature compression and creep data used in FEA modelling. The influence of porosity on the test samples, amount of second phases clamped by the bolt may also influence the experimental results. In general what can be observed between the FEA prediction and experimental result is the retained bolt load sensitivity to temperature.

From Figure 89, it is observed that different phases of the BLR experiments were reasonably predicted. This includes load increase as a result of thermal expansion difference of the couple during BLR measurements at the inception of the test. The first phase of the slopes which were characterized by prominent bolt load loss was also evident by the model which was consequently followed by asymptotic decrease in retained clamp load. It could be seen that considering the large scatter of the creep and BLR response of permanent mould AS41 magnesium alloy, experiment and model show good agreement.

7.7 Comparing creep and (BLR) of AS41

Comparing the creep tested and BLR tested permanent mould AS41 coupons show some similarities and differences. The hardness response of creep deformed samples and BLR deformed samples show that the hardness of creep deformed specimens was higher than those of BLR deformed specimens. A closer look at the TEM micrographs in Figure 42 shows that more dislocations in creep deformed samples manifested itself in form of dislocation walls, dislocation networks and dislocation tangles. They act as obstacles during hardness test and increase the hardness of the creep deformed AS41 samples. The presence of subgrains and or subboundaries increases the hardness of creep deformed samples.

The differences in those samples, although loaded with the same initial stress originates from the clamping constraints. See Figure 25, Figure 22 and Figure 67. In the case of BLR test sample, the initial load was shared between the AS41 specimen and the bolting materials. For creep samples, the specimen is directly compressed by the steel blocks so that the clamped sample experiences the entire initial load. As creep test are run at constant engineering stress condition, the true stress on the sample may have been higher in creep test than in BLR test. This could result in more strain hardening on the magnesium sample. The 7 % and 4.4 % differences that were recorded between the hardness values of creep and BLR samples loaded at 70 MPa and 40 MPa initial stresses may have been as a result of these influences.

It may be important to mention at this point that where as BLR response of Mg-alloys are partly a consequence of creep behaviour of the component, creep response of Mg-alloys are not consequence of their BLR behaviour. A seemingly appropriate way to model BLR behaviour of Mg-alloy is to use creep information of the material rather than predicting creep behaviour of the material using BLR data.

8 Conclusions

- From creep investigation in this work, it was found that at low stress regions of 40-55 MPa with temperature up to 150 °C, grain boundary sliding is the dominant creep mechanism. At high stress region of 70-90 MPa and temperature up to 200 °C, dislocation climb becomes the rate controlling mechanism. Pore development around solute segregated regions is found to influence creep deformation. The reduced volume fraction of β-Mg phase and the presence of thermal stable Mg_2Si within and around the grain boundaries assist to improve creep behaviour of AS41 Mg-alloy.
- It was identified that the inception of BLR deformation is characterized by randomly distributed dislocation at the α-Mg matrix on the (0001) basal plane and in the $<11\bar{2}0>$ most closely packed direction. Tensile twins with orientation relationship of ~86 ° with the basal plane around $<11\bar{2}0>$ axis were dominant. Continued deformation into stage (iii) of the BLR test leads to recovery and appearance of cells and subgrain boundaries within the microstructure. These observations are with respect to the loads (5 kN-17 kN) and temperatures (100 °C-175 °C) investigated.
- Effect of temperature, load (initial and final), effective length and stiffness on the BLR of permanent mould AS41 were identified. It was observed that at temperature ~23 °C, loss of AS41 fastener clamp load was less than 5 % in all the load levels (5 kN-17 kN) investigated up to 150 Hrs. At homologous temperature approaching 0.4 and above, bolt load retained at AS41 joint was between 58 % and 83 % depending on the initial load and test temperature. Increase in initial load and temperature, decreases the amount of bolt load retained on an AS41 Mg-alloy joint. Increasing the effective length by 40 % will increase the absolute load on an AS41 bolted joint by ~10 %. Stiffer joints retained more load at test temperature whereas more loss of fastener clamp load are witness by stiffer joints on cooling back to room temperature.
- A simple and realistic bolt load retention testing equipment using continuous load cell measuring technique was established. It was found

that uniform waiting time and uniform initial load before starting BLR test is important to having a repetitive result. A 3 % extra load on the desired preload and an average waiting time of 1 hour is recommended before starting BLR test. The importance of running a baseline test before the actual BLR test was also established. It was found that neglecting baseline test can underestimate the BLR result by up to 6 % for permanent mould AS41 Mg-alloy over the load range, temperature and duration of test investigated. Isothermal BLR test was also found to give a conservative result than interrupted BLR test for AS41 Mg-alloy.

- The bolt load retention response of AS41 Mg-alloy was successfully modeled using compliance-creep and FEA approaches. This is with respect to applied load and temperature. In both compliance-creep and FEA approaches, the model and the experiment show reasonable agreement. For the compliance-creep method, the model differs with the experiment by between 0.65 % and 4.4 % in all the conditions investigated. FEA approach however gives more information on the stress distribution at the bolted joint which compliace-creep approach do not provide.

9 Outlook

- Future works in bolt load retention of magnesium alloys should involve conducting an in-situ BLR test on magnesium samples. This could be done using neutron diffraction or electron synchrotron techniques in order to gain more insight on the microstructure evolution during BLR test.
- Investigation on the influence of alloying elements, grain size and heat treatment on bolt load retention response of magnesium alloys are recommended. This will guide the way to optimizing Mg-alloys for elevated temperature BLR application. Important also is exploring further, the possibility of applying stiffer Al-alloy bolts for joining Mg-alloy components.
- In the future, it is expected that typical powertrain replica will be cast from a heat resistant Mg-alloy. For specific automotive powertrain application, BLR testing should be tailored to that particular design parameter. This means that the expected design parts should be produced with the exact bolting/joint configuration and expected operating temperature. The bolt load retention behaviour of this Mg-alloy component will be evaluated using instrumented bolt measuring technique.
- Future work should include BLR test on die cast samples since most automobile applications are die cast parts. This will allow for testing higher load values that are of importance to automotive industries. It is also recommended that BLR test be carried also in corrosive environment. It is of more practical importance and may show different relaxation behaviour.

10 Reference

[1] J. H. Bickford, “An Introduction to the Design and Behavior of Bolted Joints”, (New York, Mercel Dekker Inc.), (1995).

[2] E. G. Sieracki, J. J. Velazquez, K. Kabiri, “Compressive stress retention characteristics of high pressure die casting magnesium alloys”, SAE Technical Paper Series 960421, (1996).

[3] K. Pettersen, S. Fairchild, “Stress relaxation in bolted joints of die cast magnesium components”, SAE Technical Paper Series 970326, (1997).

[4] A. P. Druschitz, E. R. Showalter, “Bolt load compressive stress retention testing of magnesium alloys”, SAE Technical Paper Series 2003-01-0187, (2003).

[5] F. C. Chen, J. W. Jones, T. A. McGinn, J. E. Kearns, A. J. Nielsen, J. E. Allison, “Bolt load retention and creep of die-cast magnesium alloys”, SAE Technical Paper Series 970325, (1997).

[6] S. Xu, G. Williams, R. Bouchard, J. P. Thomson, M. Sahoo, “Bolt load retention testing of magnesium alloys for automotive engine cradle applications”, Light Metals Technology, LKR Austria, (2005) 283-288.

[7] D. M. Magers, “A global review of magnesium parts in automobiles”, Design and Production Considerations for Magnesium Automobile Parts Seminar, Tokyo, Japan, (1996).

[8] S. Schumann, “Future use of magnesium in cars-potentials and prerequisite”, 12th Magnesium Automotive and User Seminar, Aalen, Germany, (2004) 13-14.

[9] E. N. D. Andrade, “The distribution of slide in a right six-face subject to pure shear”. Proceedings of the Royal Society of London series A 85, 580 (1911) 448-461.

[10] A. H. Cottrel, B. A. Bilby, “Dislocation theory of yielding and strain ageing of iron”, Proceedings of the Physical Society of London 62 (1949) 49-62.

[11] F. Garofalo, “Fundamentals of Creep and Creep-rupture in Metals”, (New York, McMillian), (1965).

[12] O. D. Sherby, P. M. Burke, “Mechanical behaviour of crystalline solids at elevated temperature”, Progress in Materials Science 13 (7) (1967) 325-390.

[13] F. Garofalo “An empirical relation defining stress dependence of minimum creep rate in metals”, Transactions of the Metallurgical Society of AIME 227 (1963) 351.

[14] H. Hübner, “Physics of High-Temperature Strength, Guide to Accompany the Graduate Course”, (Technische Universität Hamburg-Harburg, Germany) (2002).

[15] F. C. Monkman, N. J. Grant, "An empirical relationship between rupture life and minimum creep rate in creep-rupture tests”, Proc. ASTM 56 (1956) 593-605.

[16] F. R. N. Nabarro, “Deformation of crystals by motion of single ions”, The physical Society (1948) 75-90.

[17] C. Herring, “Diffusional viscosity of a polycrystalline solid”, Journals of Applied Physics 21 (1950) 437.

[18] R. L. Coble, “A model for the boundary diffusion controlled creep in polycrystalline materials”, Journals of Applied Physics 34 (1963) 1679.

[19] J. Weertman, “Theory of steady-state creep based on dislocation climb”, Journal of Applied Physics 26 (1955) 1213-1217.

[20] C. R. Barret, W. D. Nix, “A model for steady state creep based on the motion of jogged screw dislocations” Acta Metallurgica. 13 (1965) 1247-1258.

[21] F. R. N. Nabarro, “Steady-state diffusional creep”, Philosophical Magazine 16 (1967) 231.

[22] J. Harper, J. E. Dorn, “Viscous creep of aluminum near its melting temperature”, Acta Metallurgica 5 (1957) 654-665.

[23] H. E. Friedrich, B. L. Mordike, “Magnesium Technology“, (Berlin Heidelberg, Springer Verlag), (2006).

[24] P. G. Partridge, “The crystallography and deformation modes of hexagonal closed packed metals”, Metallurgical Reviews (1967) 169-194.

[25] P. B. Hirsch, J. S. Lally, “Deformation of magnesium single crystals”, Philosophy Magazine 12 (1965) 595.

[26] E. F Emley, “Principles of Magnesium Technology”, (Oxford, Pergamon Press), (1966).

[27] P. W. Bakarian and C. H. Matthewson, “Slip and twinning in magnesium single crystals at elevated temperature”, Transactions of the Metallurgical Society of AIME 152 (1943) 226-254.

[28] B. C. Wonsiewicz, W. A. Backofen, “Plasticity of magnesium crystals”, Transactions of the Metallurgical Society of AIME 239 (1967) 1422-1431.

[29] R. E. Reed-Hill and W. D. Robertson, “Deformation of magnesium single crystals by non-basal slip”, Transactions of the Metallurgical Society of AIME 209 (1957) 496-502.

[30] U. F. Kock and D. G. Westlake, “The importance of twinning for the ductility of CPH polycrystals”, Transactions of the Metallurgical Society of AIME 239 (1967) 1107-1109.

[31] C. S. Roberts, “Magnesium and its Alloys”, (New York, Wiley) 1960.

[32] T. A. Trozera, J. Mote, J. E. Dorn, “Activation energies for basal slip in Magnesium single crystals”, Transactions of the ASM 53 (1961) 123-135.

[33] G. V. Raynor, “The Physical Metallurgy of Magnesium and its Alloys”, (London, Pergamon Press), (1959).

[34] C.S. Roberts, “Creep behaviour of extruded electrolytic magnesium”, Transactions of the Metallurgical Society of AIME 5 (1953) 1121-1126.

[35] A. R. Chaudhuri, H. C. Chang, N. J. Grant, “Creep deformation of magnesium at elevated temperatures by nonbasal slip”,Transactions of the Metallurgical Society of AIME 203 (1955) 682.-688.

[36] H. J. Frost and M. F. Ashby, “Deformation-mechanism maps”, (Oxford, Pergamon Press), 1982.

[37] K. Lövold, “Transient creep in pressure die-cast magnesium alloys”, Z. Metallkde., 67 (1976) 514-517.

[38] W. K. Miller, “Creep of die cast AZ91 magnesium at room temperature and low stress”, Metallurgical Transactions A 22A (1991) 873-877.

[39] H. Gjestland, G. Nussbaum, G. Regazzoni, O. Lohne, O. Bauger, “Stress-relaxation and creep behaviour of some rapidly solidified magnesium alloys”, Material Science and Engineering 134 (1991) 1197-1200.

[40] M. S. Dargusch, G. L. Dunlop, “Elevated temperature creep and microstructure of die-cast Mg-Al alloys”, Magnesium Alloys and their Applications, eds:. B. L. Mordike, K. U. Kainer, (Frankfurt, Germany, Werkstoff-Informationsgesellschaft mbH) (1998) 277-282.

[41] Q. Y. Han, B. K. Kad, S. Viswanathan, “Design perspectives for creep-resistant magnesium die-casting alloys ”Philosophical Magazine 84 (2004) 3843-3860.

[42] F. Hollrigl-Rosta, E. Just, J. Kohler, H. J. Melzer, “Magnesium in Volkswagen“, Light Metal Age 8, (1980) 22-29.

[43] M. O. Pekguleryuz, “Development of creep resistant magnesium die casting alloys” Material Science Forum 350-351 (2000) 131-140.

[44] I. Gupta, J. C. M. Li, “Stress relaxation, internal stress, and work hardening in some bcc metals and alloys” Metallurgical Transactions 1 (1970) 2323.

[45] ASTM Standard E 328-86. Standard test methods for stress relaxation for materials and structures, Vol. 03.01 (2000).

[46] B. Watzinger, P. Weidinger, F. Breutinger, W. Blum, I. Erlangen, R. Rösch, H. Lipowsky, H. G. Haldenwanger, “Creep and stress relaxation of commercial cast magnesium-aluminum based alloys, Magnesium Alloys and their Applications, eds:. B. L. Mordike, K. U. Kainer, (Frankfurt, Germany, Werkstoff-informationsgesellschaft mbH) (1998) 259-264.

[47] T. K. Aune, T. J. Ruden, “High temperature properties of magnesium die casting alloys”, SAE Technical Paper Series 920070, (1992).

[48] T. K. Aune, D. Albright, “Stress relaxation behaviour of magnesium die casting alloys”, SAE Technical Paper Series 910412, (1991).

[49] W. Riehemann, “Detection of internal stresses in metal matrix composites by stress relaxation measurements”, Materials Science Forum 210-213 (1996) 511-518.

[50] J. Kiehn, W. Riehemann, K. U. Kainer, “Stress relaxation of short fiber reinforced Mg metal matrix composites after thermal cycling”, Material Science Forum 210-213 (1996) 503-510.

[51] S. Xu, J. P. Thomson, M. Sahoo, “A review on stress relaxation and bolt load retention of magnesium alloys for automotive application”, Canadian Metallurgical Quarterly 43 (2004) 489-506.

[52] VDI 2230, Systematische Berechnung hochbeanspruchter Schraubenverbindungen; Zylindrische Einschraubverbindungen, Verein Deutscher Ingenieure, (Düsseldorf, Germany), (2003).

[53] G. Meyer, D. Strelow, “Simple diagram aid in analysing forces in bolted joints”, Assembly Engineering 28 (1972) 28-33.

[54] C. J. Bettles, M. S. Dargusch, “Creep and bolt load retention of sand cast electron MEZ”, Magnesium Alloys and their Applications, ed:. K. U Kainer, (Wiley-VCH Verlag GmbH, Germany), (2000) 705-710.

[55] C. J. Bettles, L. Zheng, K. Venkatesan, M. Qian, “The effect of grain size on the bolt load retention behaviour of AMC-SC1”, Magnesium Alloys and their Applications, ed:. K. U Kainer, (Wiley-VCH Verlag GmbH, Germany), (2004) 128-133.

[56] P. Labelle, “Heat resistant magnesium alloys for power-train applications”, SAE Technical Paper Series 2001-01-0424, (2001).

[57] P. Labelle, M. O. Pekguleryuz, M. Lefebvre, R. Bouchard, “New aspects of temperature behaviour of AJ52X, creep resistance magnesium alloys”, SAE Technical Paper Series 2002-01-0079, (2002).

[58] E. A. Nyberg, R. H. Jones, S. G. Pitman, R. D. Carnahan, R. F. Decker, “High temperature-creep resistant magnesium alloys: Advances in thixomolding automotive components”, SAE Technical Paper Series 2000-01-1126, (2000).

[59] E. A. Nyberg, D. J. Edwards, R. H. Jones, “Microstructure and microchemistry of creep resistant magnesium alloys”, Magnesium Technology 2000, ed:. J. N. Hryn, TMS, (2000) 169-173.

[60] J. Arimond, “Bolt load retention modeling from creep performance data”, SAE Technical Paper Series 950485, (1995).

[61] G. Gerstmayr, W. Eichlseder, “Creep and relaxation behaviour of self-tapping Al-bolts in Mg die cast alloys for power train components”, Magnesium Alloys and their Applications, ed:. K. U Kainer, (Wiley-VCH Verlag GmbH, Germany), (2009) 1097-1106.

[62] S. J. P. Longworth, “The bolting of magnesium components in car engines”, A dissertation submitted for the degree of masters in philosophy, University of Cambridge. 2001.

[63] D. J. C. Mackay, “Probable networks and plausible predictions-A review of practical Bayesian methods for supervised neural networks”, Network-Computation in Neural System 6, 3(1995) 469-505.

[64] D. J. C. Mackay, “Bayesian non-linear modelling for the prediction competition”, Fundamental theories of physics, 62 (1996) 221-234.

[65] J. Tenner, D. A. Linkens, P. F. Morris, T. J. Bailey, “Prediction of mechanical properties in steel heat treatment process using neural networks”, Ironmaking and Steelmaking 28, 1 (2001) 15-22.

[66] S. S. Lee, N. Kim, “Relaxation analysis of bolt load in single bolted joints fastening thermosetting polymer”, Key Engineering Materials 324-325 (2006) 1245-1248.

[67] T. Jaglinski, A. Nimityongskul, R. Schmitz, R. S. Lakes, “Study of bolt load loss in bolted aluminum joints“, Journal of Engineering Materials and Technology 129 (2007) 48-54.

[68] V. Kree, J. Bohlen, D. Letzig, K. U. Kainer, “The metallographical examination of magnesium alloys”, Praktische Metallographie-Practical Metallography 41 (2004) 233-246.

[69] ASTM Standard E 9-89a. Standard test methods of compression testing of metallic materials at room temperature vol. 03.01 (2004).

[70] ALTHEN Meß-und Sensortechnik Manual, (2004).

[71] ADINA, Theory and Modeling Guide, vol. 1, (ADINA Research and Development Inc, Watertown, USA), (2001).

[72] Q. Y. Han, E. A. Kenik, S. R. Agnew, S. viswanathan, “Solidification behaviour of commercial magnesium alloys”, Magnesium Technology, ed:. J. N. Hyrn, TMS, (2001) 81-86.

[73] Y. D. Huang, H. Dieringa, N. Hort, T. Abu Leil, K. U. Kainer, Y. L. Liu, “Effects of segregation of primary alloying elements on the creep response in magnesium alloys” Scripta Materialia 58 (2008) 894-897.

[74] S. R. Agnew, K. C. Liu, E. A. Kenik, S. Viswanathan, “Tensile and compressive creep behaviour of magnesium die cast alloy AM60B”, Magnesium Technology 2000, eds:. H. I. Kaplan, J. N. Hryn, B. Clow, TMS, (2000), 285-290.

[75] M. O. Pekguleryuz, J. Renaud, “Creep resistance in Mg-Al-Ca casting alloys”, Magnesium Technology, eds:. H. I Kaplan, J. Hryn, B. Clow, TMS, (2000) 279-284.

[76] A. A. Luo, T. Shinoda, “Development of a creep resistant magnesium alloys for die casting applications”, Magnesium Alloys and their Applications, eds:. B. L. Mordike, K. U. Kainer, (Frankfurt, Germany, Werkstoff-Informationsgesellschaft mbH) (1998) 151-156.

[77] M. O. Pekguleryuz, P. Labelle, D. Argo, E. Baril, “Magnesium die casting alloy AJ62X with superior creep resistance, ductility and die

castability", Magnesium Technology, ed:. H. I. Kaplan, TMS, (2003) 201-206.

[78] A. Aghion, B. Bronfin, F. Von Buch, S. Schumann, H. Friedrich, "Dead sea magnesium alloys newly developed for high temperature application", Magnesium Technology, ed:. H. I. Kaplan, TMS, (2003) 177-182.

[79] K. Y. Sohn, J. W. Jones, J. J. Berkmortel, H. Hu, J. E. Allison, "Creep and bolt load retention behavior of die-cast magnesium alloys for high temperature applications: Part 2 of 2", SAE Technical Paper Series 2000-01-1120, (2000).

[80] T. Abu Leil, Y. Huang, H. Dieringa, N. Hort, K. U. Kainer, J. Bursik, Y. Jiraskova, K. P. Rao, "Effect of heat treatment on the microstructure and creep behavior of Mg-Sn-Ca alloys", Materials Science Forum 546-549 (2007) 69-72.

[81] H. Dieringa, "Vergleichende Untersuchungen zum Zug- und Druckkriechverhalten der verstärken Magnesiumlegierung AE42", PhD Thesis, Hamburg University of Technology, Hamburg, Germany, (2006).

[82] P. Zhang, "Creep behaviour of the die-cast Mg-Al alloy AS21", Scripta Materialia 52 (2004) 277-282.

[83] I. P. Moreno, T. K. Nandy, J. W. Jones, J. E. Allison, T. M. Pollock, "Microstructural stability and creep of rare-earth containing magnesium alloy", Scripta Materialia 48 (2003) 1029-1034.

[84] S. M. Zhu, M. A. Gibson, J. F. Nie, M. A. Easton, T. B. Abbott, "Microstructural analysis of the creep resistance of die-cast Mg-4Al-2RE alloy", Scripta Materialia 58 (2008) 477-480.

[85] H. Dieringa, Y. Huang, P. Maier, N. Hort, K. U. Kainer, "Tensile and compressive creep behaviour of Al_2O_3 (Saffil (R)) short fiber reinforced magnesium alloy AE42", Material Science and Engineering A 410 (2005) 85-88.

[86] B. Jing, S. Yangshan, X. Shan, X. Feng, Z. Tianbai, "Microstructure and tensile creep behaviour of Mg-4Al based magnesium alloys with alkaline-earth elements Sr and Ca additions", Materials Science and Engineering A 419 (2006) 181-188.

[87] H. Liu, Y. Chen, Y. Tang, S. Wei, G. Niu, “Tensile and indentation creep behaviour of Mg-5% Sn and Mg-5% Sn-2% Di alloys”, Materials Science and Engineering A 464 (2007) 124-128.

[88] C. J. Boehlert, K. Knittel, “The microstructure, tensile properties, and creep behaviour of Mg-Zn alloys containing 0-4.4 wt.% Zn”, Materials Science and Engineering A 417 (2006) 315-321.

[89] S. M. Zhu, B. L. Mordike, J. F. Nie, “Creep properties of a Mg-Al-Ca alloy produced by different casting technologies”, Material Science and Engineering A 483 (2008) 583-586.

[90] O. Anopuo, Y. Huang, H. Dieringa, N. Hort, K. U. Kainer, A. K. Khan, “Mechanical properties and corrosion performance of AZ-Mg alloys modified with Ca and Sr”, SAE Int. Journals of Material Manufacturing 1 (2008) 103.

[91] C. J. Bettles, M. A. Gibson, “Microstructural design for enhanced elevated temperature properties in sand-castable magnesium alloys”, Advance Engineering Materials 5 (2003) 859-865.

[92] N. Hort, Y. D. Huang, T. Abu Leil, P. Maier, K. U. Kainer, “Microstructural investigations of the Mg-Sn-xCa system” Advanced Engineering Materials 8 (2006) 359-364.

[93] H. Ferkel, B. L. Mordike, “Magnesium strengthened by SiC nanoparticles”, Materials Science and Engineering A 298 (2001) 193-199.

[94] M. Regev, E. Aghion, A. Rosen, M. Bamberger, “Creep studies of coarse-grained AZ91D magnesium castings”, Materials Science and Engineering A 252 (1998) 6-16.

[95] S. K. Thakur, B. K. Dhindaw, N. Hort, K. U. Kainer, “Some studies on the thermal-expansion behavior of C-fiber, SiC_p, and in-situ Mg_2Si-reinforced AZ31 Mg alloy-based hybrid composites”, Metallurgical and Materials Transactions A 35 (2004) 1167-1176.

[96] H. Dieringa, K. U. Kainer, “Particles, fibers and short fibers for the reinforcement of metal materials”, Metal Matrix Composites, ed:. K. U. Kainer (Wiley-VCH Verlag GmbH, Germany), (2003) 55-76.

[97] H. Z. Ye, X. Y. Liu, “Review of recent studies in magnesium matrix composites”, Journal of Materials Science 39 (2004) 6153-6171.

[98] O. Anopuo, Y. Huang, N. Hort, H. Dieringa, K. U. Kainer, “Bolt load retention and creep of AS41 alloyed with 0.15 % Ca”, SAE Technical Paper Series 10M-0074 (2010).

[99] M. H. Yoo, “Slip, twining, and fracture in hexagonal closed packed metals”, Metallurgical Transactions A 12 (1981) 409-418.

[100] E. W. Kelley, W. J. Hosford, “Plane-strain compression of magnesium and magnesium alloy crystals”, Transactions of the Metallurgical Society of AIME 242 (1968) 5-13.

[101] J. F. Stohr, J. P. Poirier, “Electron microscope study of pyramidal slip {11-22}<11-23> in magesium”, Philosophical Magazine 25 (1972) 1313-1329.

[102] H. Tonda, S. Ando, “Effect of temperature and shear direction on yield stress by {1122}<1123> slip in hcp metals”, Metallurgical Transactions A 33 (2002) 831-836.

[103] H. Leitner, I, Godor, W. Eichlseder, C. Hinteregger, “Relaxation der Vorspannkraft von Magnesium-Schraubverbindungen unter betriebsähnlichen Bedingungen”, Giesserei 92 (07) (2005) 36-43.

[104] C. Haberling, G. Haldenwangr, “Leichtbaupotenzial mit Aluminiumschrauben”, Der Zuliefermarkt fuer konstrukteure und technische Einkaeufer 4 (2001) 48-51.

[105] U. Arz, C. Berger, B. Kaiser, U. Kremer, “Relaxationsverhalten von Schrauben aus Aluminiumlegierungen bei 150 °C”, Konstruktion 4 (2003) 70-74.

[106] C. Friedrich, “Fastening of light weight components with elements made of aluminium”, SAE Technical Paper Series 2000-01-1118, (2000).

[107] M. A. Meyers, O. Voehringer, V. A. Lubarda, “The onset of twinning in metals: a constitutive description”, Acta Materialia 49 (2001) 4025-4039.

[108] K. Y. Sohn, J. A. Yurko, J. W. Jones, J. E. Kearns, J. E. Allison, “Bolt-load retention behavior of die-cast AZ91D and AE42 magnesium” SAE Technical Paper Series 980090, (1998).

[109] K. Pettersen, J. I. Skar, “Bolted Joints in magnesium components”, Magnesium Alloys and their Applications, eds:. B. L. Mordike, K. U. Kainer, (Frankfurt, Germany, Werkstoff-informationsgesellschaft mbH) (1998) 607-612.

[110] S. Xu, G. Williams, G. Shen, R. Bouchard, M. Sahoo, R. Osborne, “Bolt-load retention testing of magnesium alloys for automotive applications”, SAE Technical Paper Series 2006-01-0072, (2006).

[111] E. Baril, P. Labelle, A. Fischersworring-Bunk, “AJ (Mg-Al-Sr) alloy system used for new engine block”, SAE Technical Paper Series 2004-01-0659, (2004).

[112] O. Anopuo, G. Shen, S. Xu, N. Hort, K. U. Kainer, “Elevated temperature and varied load response of AS41 at bolted joint”, Magnesium Technology 2009, eds:. E. A. Nyberg, S. R. Agnew, M. R. Neelameggham, M. O. Pekguleryuz, TMS, (2009) 509-514.

[113] T. B. Cameron, “Use of threaded fasteners in die cast magnesium”, SAE Technical Paper Series 860289, (1986).

[114] C. J. Bettles, C. T. Forwood, D. S. Jones, J. R. Griffiths, M. T. Frost, D. H. St.John, M. Quian, G.-L. Song, J. F. Nie, “AMC-SC1: A new magnesium alloy suitable for powertrain applications”, SAE Technical Paper Series 2003-01-1365, (2003).

[115] C. C. Osgood, “How plasticity influences bolted-joint design-preload and fatigue concepts, Machine Design, (1972) 104-107.

[116] G. Hartmann, “Potentials and limitations of ultrasonic clamp load testing”, SAE Technical Paper Series 2007-01-1668, (2007).

[117] G. Fritsche, “Grundlagen einer genaueren Berechnung statisch und dynamisch beanspruchter Schraubenverbindungen”, PhD Thesis, Technische Universität Berlin, Germany, (1962).

[118] G. Shen, S. Xu, “Finite element simulation of bolted joints and magnesium bolt-load retention behaviour”, SAE Technical Paper Series 2007-01-1032, (2007).

[119] M. T. Kirk, R. H. Dodds, “J and CTOD estimation equations for shallow cracks in single edge notch bend specimens”, Journals of Testing and Evaluation 21 (1993) 228-238.

11 Appendix

11.1 Symboles

A	Material constant
A_C , A_{NH}	Constants
A_{Sec}	Stressed area
α_{Mg} , α_{Steel}	Thermal expansion coefficient of Mg, steel washers and bolt
b	Burgers vector
β	Material constant
C	Temperature and stress dependent constant
C_{ij}	Compliance matrix
C^f	Bolt compliance
C_o^b	Initial boss compliance
$C_{(t)}^b$	Time dependent boss compliance
c_o	Equilibrium concentration of vacancies in crystal lattice
D	Nominal bolt diameter
D_b	Joint hole diameter
D_H	Washer diameter
D_j	Joint diameter
D_v	Vacancy diffusion coefficient
d	Average grain diameter
d'	Average distance travelled by vacancy
δ	Deflection
δ/d	Area of grain boundary region
ΔF	Increase in load
ΔF_B	Change in bolt load
ΔF_J	Change in joint load
ΔH	Joint deflection
$\Delta H'$	Compression of joint after application of external load
ΔT	Increase in temperature
ΔL_C	Change in length of bolt

$\Delta L'$	Bolt elongation after application of external load
E	Young´s modulus
ε	Creep strain
ε_o	Instantaneous strain
ε_p	Primary strain
ε_s	Secondary strain
ε_t	Tertiary strain
$\varepsilon_{(t)}$	Total strain
$\varepsilon_{(T)}$	Transient strain
ε_f	Fracture strain
ε_T	Overall steady state creep
ε_{diff}	Diffusion flow creep
ε_{disl}	Dislocation creep
ε_{gb}	Grain boundary sliding controlled creep
$\dot{\varepsilon}$	Creep rate
$\dot{\varepsilon}_s$	Secondary creep rate
F	Force
F_o	Initial load
$F_{(t)}$	Bolt load
F_p	Axial force
G	Shear modulus
J_v	Flux density
K	Spring constant
k	Boltzmann´s constant
K_B	Bolt stiffness
K_T	Total stiffness
K_N	Nut stiffness
K_W	Washer stiffness
K_J	Joint stiffness
L	Nominal length
L_B	Length of unthreaded bolt
L_C	Combined length of bolt

L_G	Grip length
L_t	Threaded length
L_j	Joint length
L_X	External tension load
$l_{mg}, l_{washer}, l_{bolt}, l_{sensor}$	Lengths of Mg sample, steel washers, steel bolt and sensor
λ	Wavelength
m	Constant
n	Stress exponent
P_i	Initial load applied at room temperature
P_f	Final load retained after test at room temperature
P_k	Highest load attained during heating to test temperature
P_r	Load attained at constant temperature
$\rho_{ethanol}$	Density of ethanol
Q_c	Activation energy of creep
Q_{sd}	Activation energy of self diffusion
R	Gas constant
S_{ij}	Stiffness matrix
SF_6	Sulfur hexaflouride
σ	Stress
T	Temperature
t	Time
t_f	Time to fracture
Φ_k	Load factor
Ω	Volume of vacancy produced

Appendix A: EDX mapping of the microstructure of as cast AS41

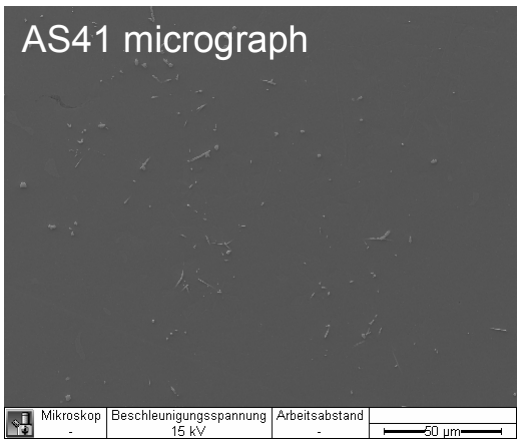

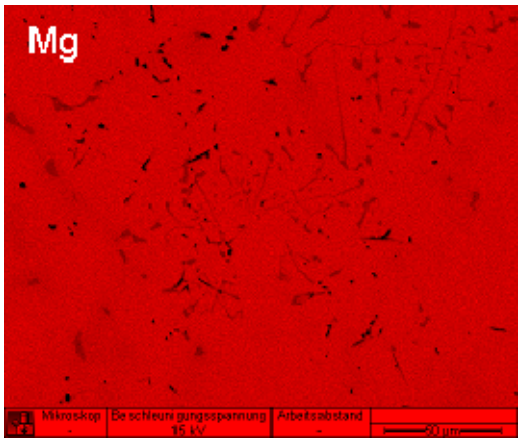

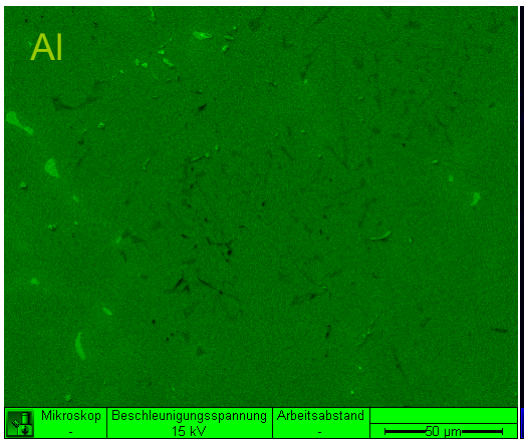

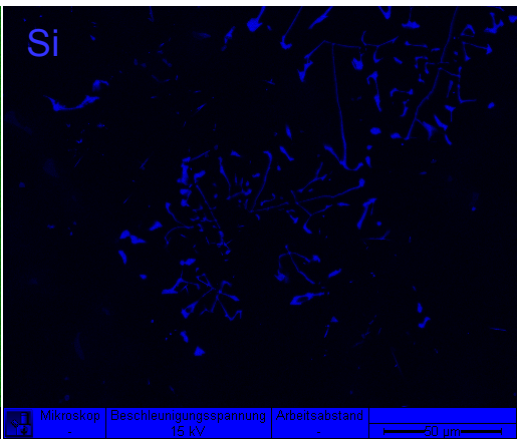

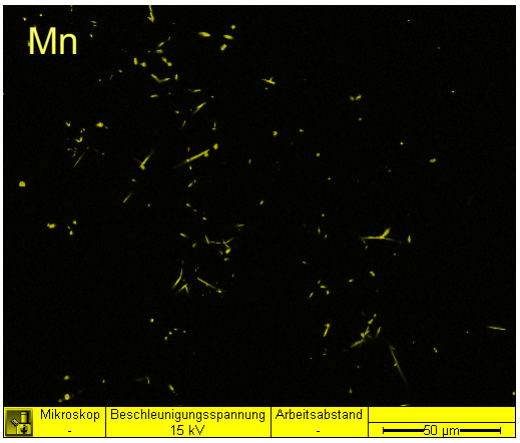

Appendix B: Diffraction spectra from point analysis with respect to Table 3

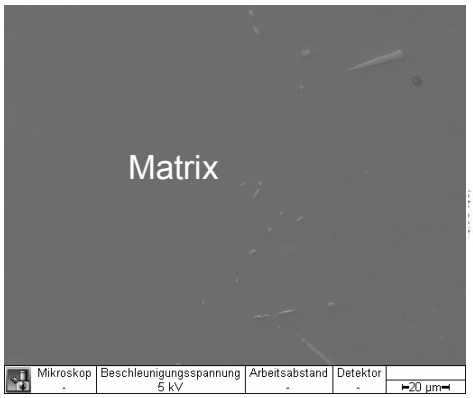

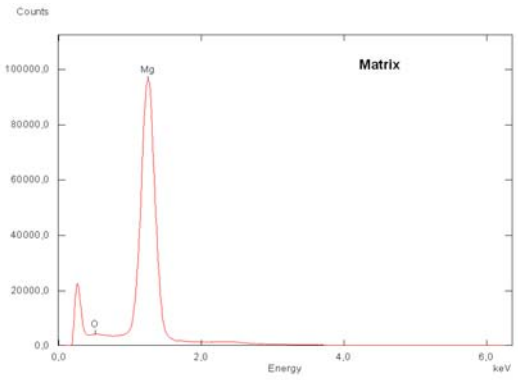

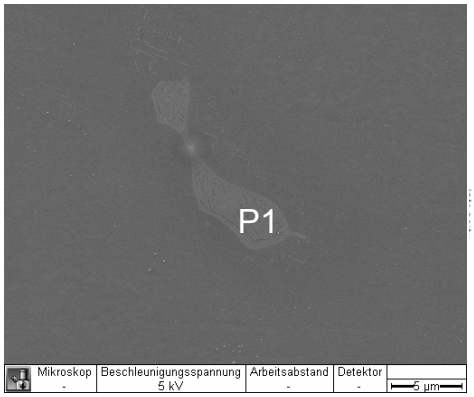

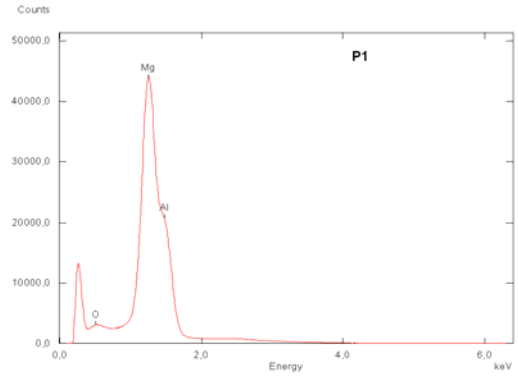

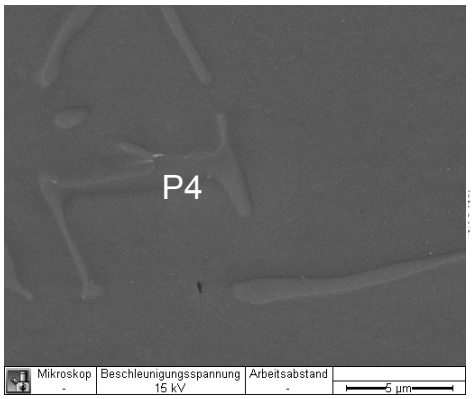

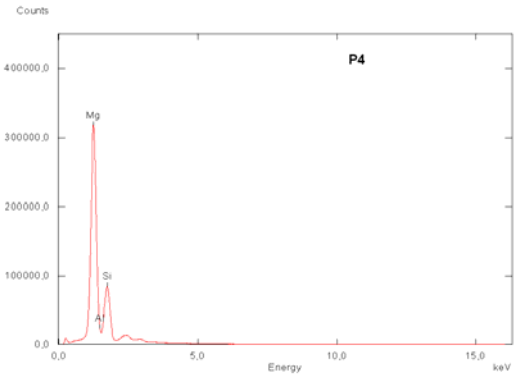

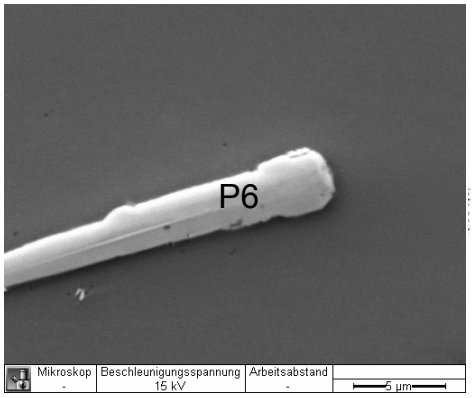

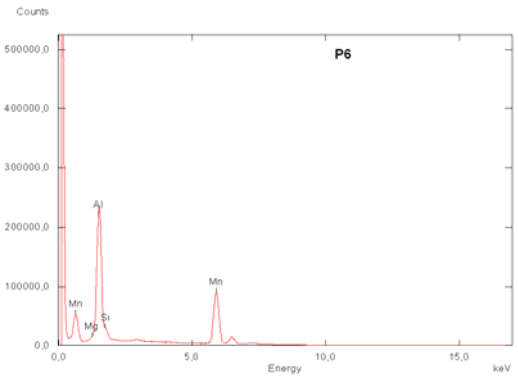

Appendix C: Yield strength and compressive strength of AS41 at the investigated temperatures

Alloy Condition	Yield Strength	Ultimate Compressive Strength
AS41 @ Room Temp	70 ± 2.00	275.74 ± 1.68
AS41 @ 100 °C	69.69 ± 6.90	261.45 ± 8.17
AS41 @ 125 °C	67.53 ± 2.40	251.01 ± 5.11
AS41 @ 150 °C	64.25 ± 4.60	232.84 ± 10.76
AS41 @ 175 °C	65.57 ± 1.58	217.16 ± 6.81

Appendix D: Thermal expansion coefficient of AS41 alloy at different temperature ranges

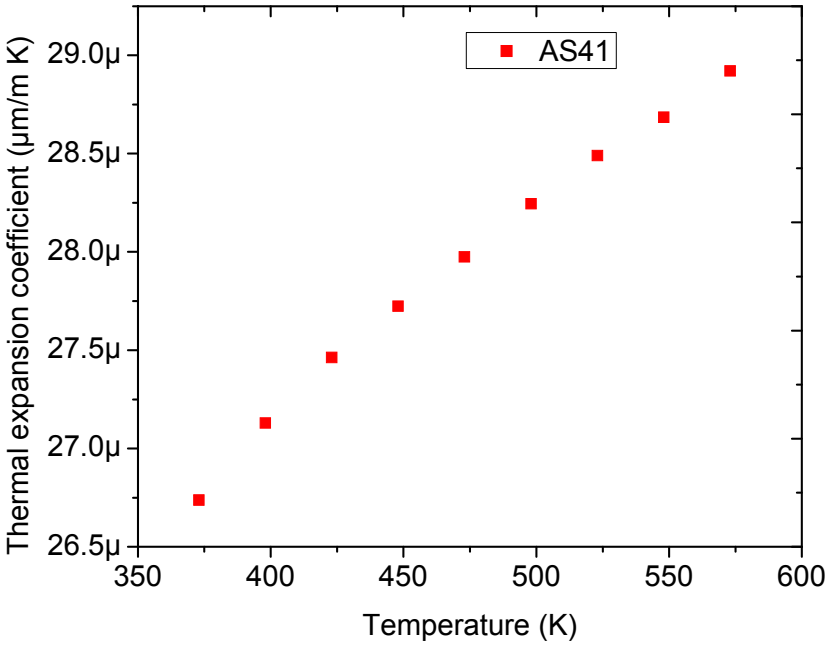

Appendix E: SEM micrograph of creep deformed (70 MPa/ 150 °C) sample showing pores in the supersaturated eutectic α-Mg matrix

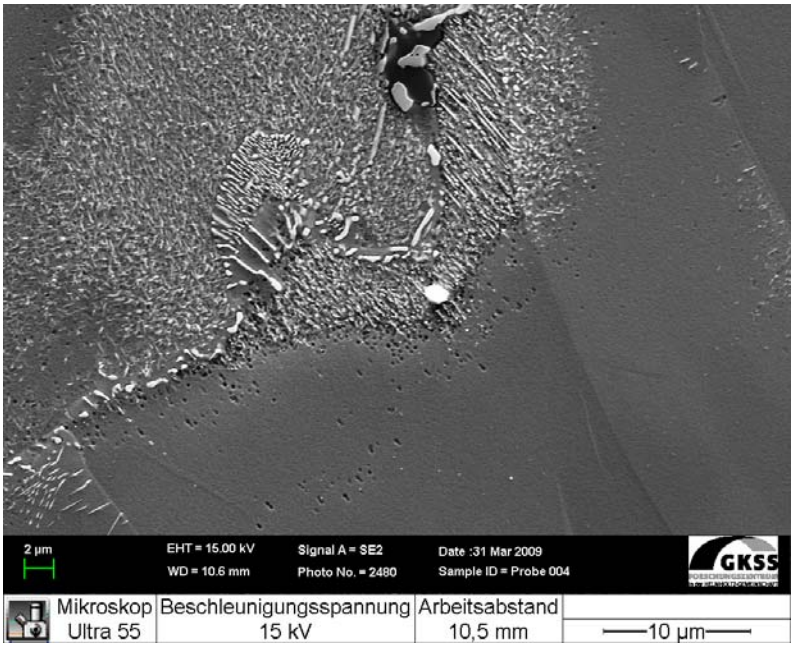

Appendix F: SEM micrograph of creep deformed (70 MPa/ 175 °C) sample showing pores in the supersaturated eutectic α-Mg matrix

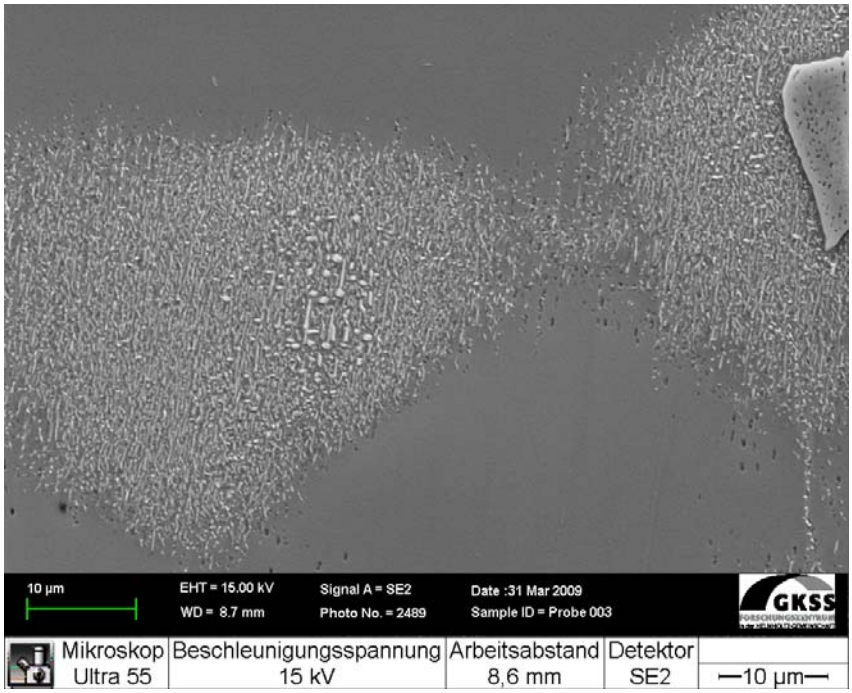

Appendix G: SEM micrograph of creep deformed AS41 (70 MPa/ 175 °C) showing precipitation of fine $Mg_{17}Al_{12}$ within dendritic and grain boundary regions

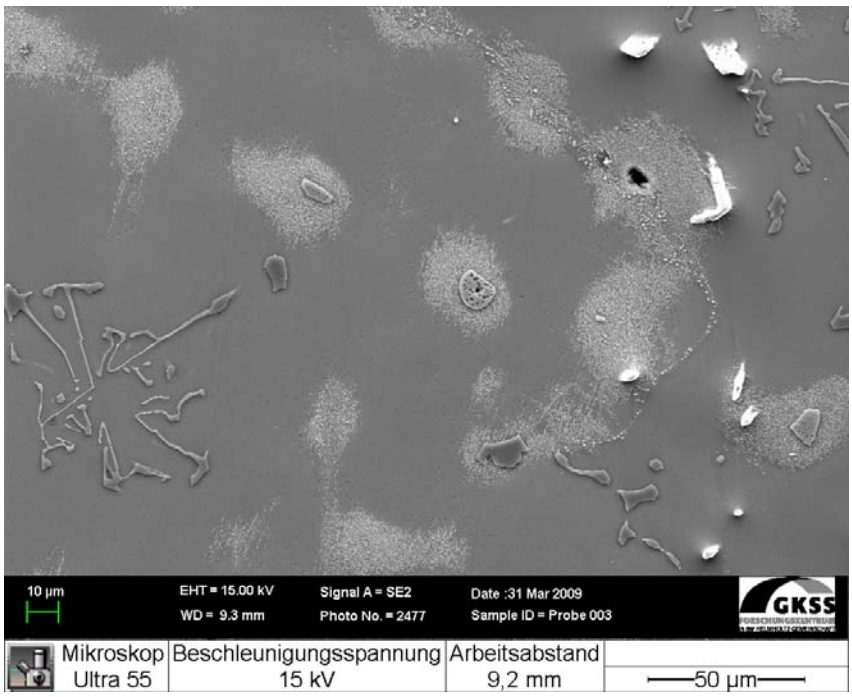

Appendix H: TEM micrograph of $Mg_{17}Al_{12}$ precipitate after creep at 70 MPa/ 175 °C

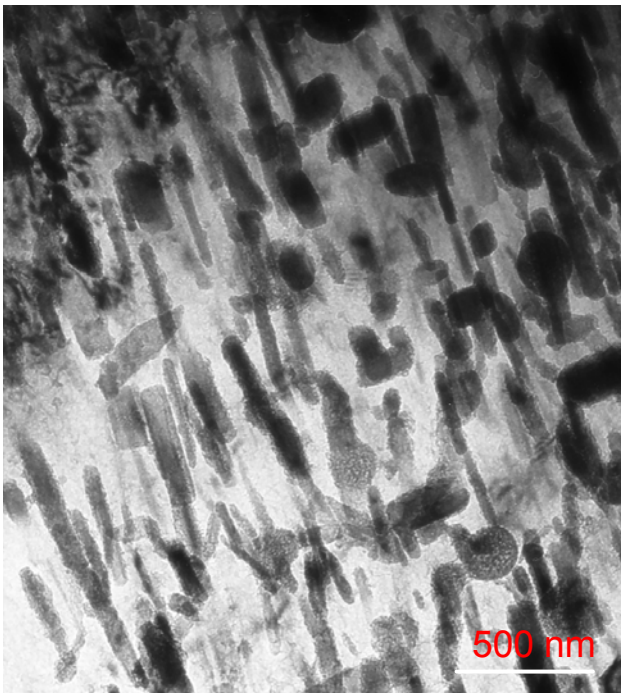

Appendix I: Sample after BLR test at 10 kN/ 125 °C showing twins

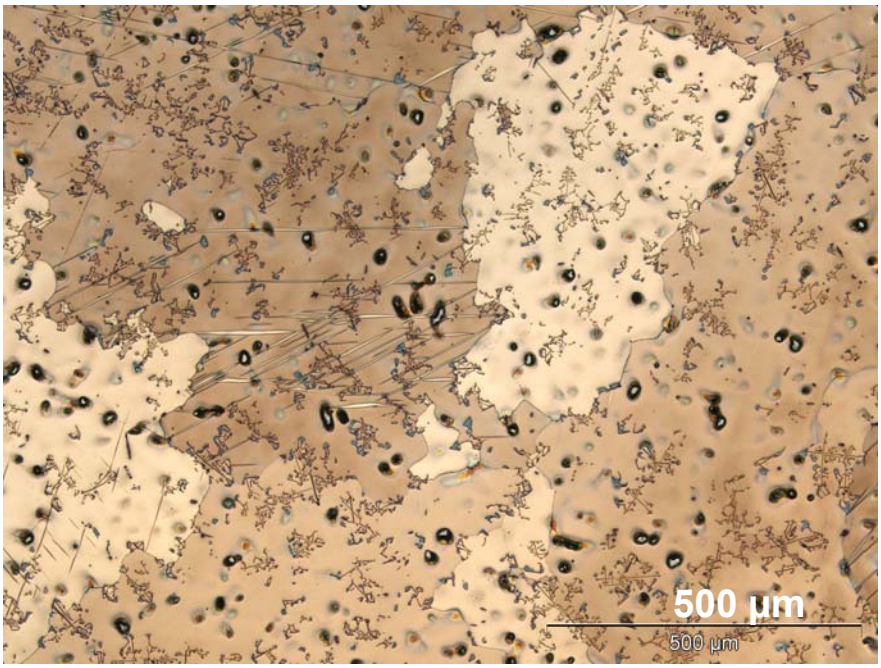

Appendix J: Sample after BLR test at 10 kN/ 175 °C showing twins

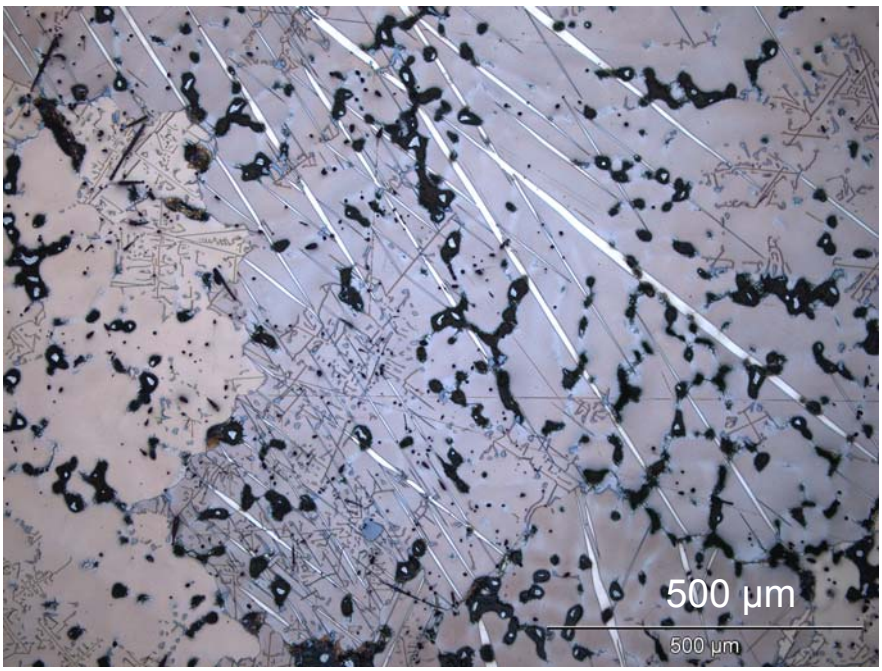

Appendix K: BLR of permanent mould AS41 at 125 °C

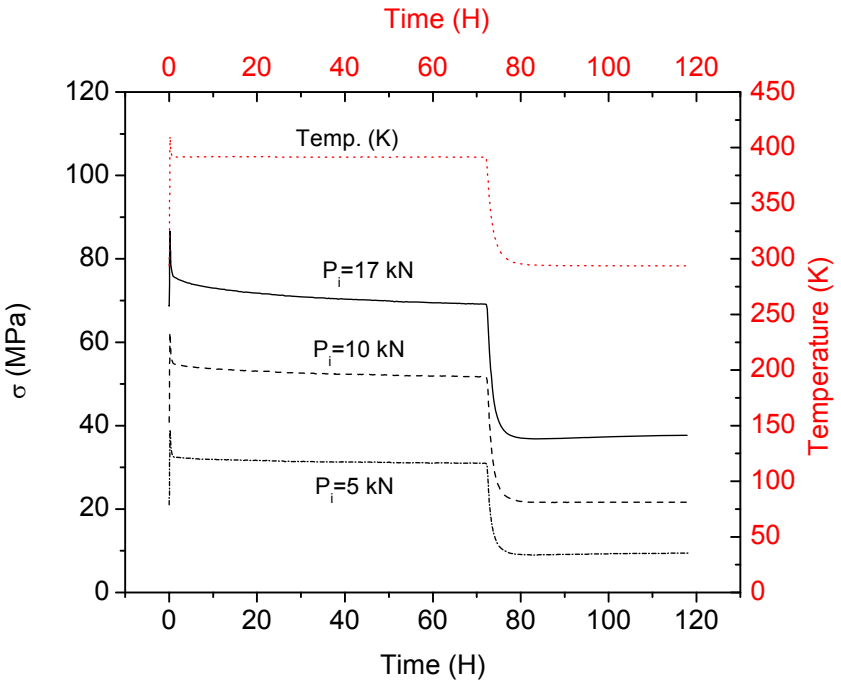

Appendix L: BLR of permanent mould AS41 at 175 °C

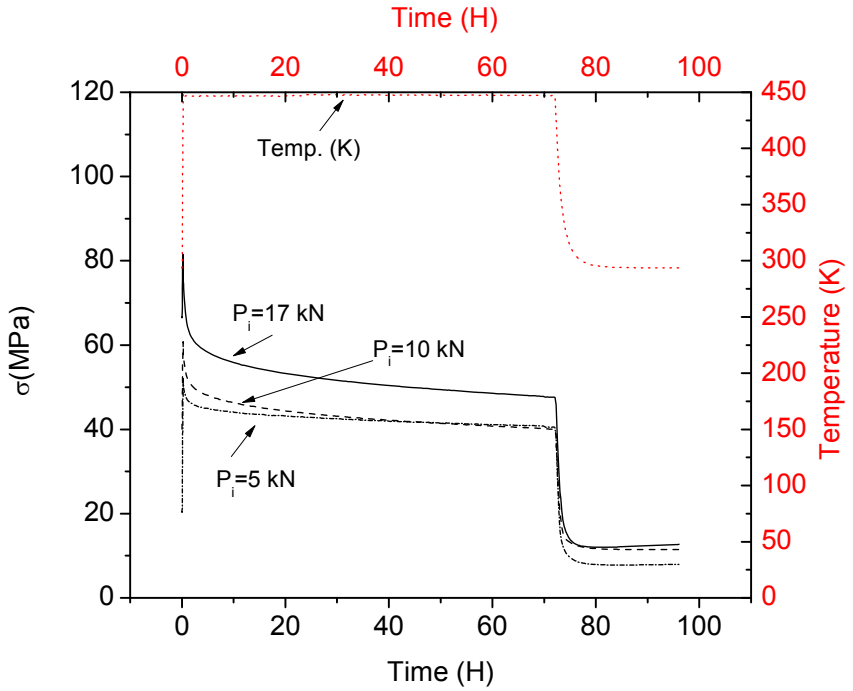

Curriculum vitae

Personal details	
Name:	Okechukwu Anopuo
Date of birth:	06. November 1971 in Lagos
Marital status:	Married
Education	
08/1978 – 07/1984	Asa Road Primary School
08/1984 – 12/1990	Holy Ghost College Owerri
01/1991 – 06/1992	Preparation course
08/1992 – 07/1998	Enugu State University of Science and Technology Material Science and Engineering, Bachelor (B. Eng.)
01/1999 – 01/2000	National Youth Service Corps
10/2002 – 02/2006	Technische Universität Hamburg-Harburg Material Science, Masters (M. Sc)
Work experience	
09/2003 – 11/2003	Intern at Romira Technische Kunststoffe GmbH, Pinneberg Production of polymer test samples, quality control of products and production of colour masterbatches, worked with injection moulding and double screw extruding machines
05/2004 – 02/2006	Research assistant at GKSS Forschungszentrum Geesthacht GmbH, Geesthacht Material characterization and corrosion analysis of Mg-Sn-Ca and Mg-Sn-Si alloy series
04/2006 – 12/2008	Wissenschaftlicher Mitarbeiter in DFG Project „Universal Kornfeinung von Mg-Al legierungen durch Keramic Partikle“
01/2009 – 03/2010	Wissenschaftlicher Mitarbeiter in GKSS Forschungszentrum Geesthacht GmbH